Targeting Functional Centers of the Ribosome

Chen Davidovich

Doctoral Thesis accepted by the Weizmann Institute of Science, Rehovot, Israel

Supervisor's foreword

Ribosomes, the key players in the translation process, are universal ribozymes performing two main tasks: decoding the genetic information and polymerizing amino acids. Hundreds of thousands of ribosomes operate is each living cell since the constant programmed cell death, which implies constant proteins degradation, requires simultaneous production of proteins. Fast replicating cells, e.g. liver cells, may contain a few millions ribosomes. Even bacterial cells may contain to 100,000 ribosomes during their log period. Other players are the mRNA chains, produced by the transcription of the segments of the DNA that should be translated, which carry the genetic information to the ribosomes, and tRNA molecules bring the cognate amino acids to the ribosome. For increasing efficiency, a large number of ribosomes act simultaneously as polymerases, synthesizing proteins by one-at-a-time addition of amino acids to a growing peptide chain, while translocating along the mRNA template, producing proteins on a continuous basis in an incredible speed, namely up to 20 peptide bonds per second.

Ribosomes are giant assemblies composed of many different proteins (r-proteins) and long ribosomal RNA (rRNA) chains. Among these, the RNA moieties perform the two ribosomal main functions. The ratio of rRNA to r-proteins (~2:1) is maintained throughout evolution, except in mitochondrial ribosome (mitoribosome) in which ~ half of the bacterial rRNA is replaced by r-proteins. Nevertheless, the active regions are almost fully conserved in all species. In all organisms ribosomes are built of two subunits, which associate to form the functionally active ribosomes. In prokaryotes, the small subunit, denoted as 30S, contains an RNA chain (16S) of ~1500 nucleotides and ~20 different proteins. The large subunit (50S in prokaryotes) has two RNA chains (23S and 5S RNA) of about 3000 nucleotides in total, and different >31 proteins. The available three dimensional structures of the bacterial ribosome and their subunits show that in each of the two subunits the ribosomal proteins are entangled within the complex rRNA conformation, thus maintaining a striking dynamic architecture that is ingeniously designed for their functions: precise decoding; substrate mediated peptide-bond formation and efficient polymerase activity.

While the elongation of the nascent chain proceeds, the two subunits perform cooperatively while the tRNA molecules are the non-ribosomal entities combine the two subunits. The small subunit provides the path along which the mRNA progresses, the decoding center and the mechanism

controlling translation fidelity. Translation initiation is the rate-limiting step of the entire process. It starts by the correct selection and placement of the mRNA reading frame, and proceeds through a tightly regulated decoding at the P-site. The large subunit contains the site for the main ribosomal catalytic function, namely polymerization of the amino acids and provides the dynamic protein exit tunnel. Simultaneously with the advancement of the mRNA along the path in the small subunit, peptide bonds are being formed. This inherently dynamic process requires small and large-scale motions of the ribosomal substrates coupled to conformational rearrangements of its components and substrates. The nascent proteins progress along a dynamic tunnel and emerge from the large subunit into a shelter formed by ribosome-bound trigger-factor, acting as a chaperone preventing aggregation and misfolding. The current consensus view is consistent with ribosomal positional catalysis, namely providing suitable stereochemistry for peptide bond formation accompanied by appropriate geometrical means for substrate mediated catalysis, and not by acid/base mechanism.

Chen Davidovich joined our group after the molecular structures of the two bacterial ribosomal subunits have been determined and their functional regions have been identified and localized. In his PhD thesis Chen aimed at revealing the structural basis for the catalytic function of the ribosome as a polymerase, namely as the cellular machine that forms peptide bonds successively, thus elongating the nascent chains. When he started, this approach was rather neglected since most ribosomologists assumed that understanding the formation of a single peptide bond is sufficient in order to describe the ribosomal function, and hence disregarded the processivity and elongation.

He investigated in detail the mode of function, inhibition, and evolution of the Peptidyl Transferase Center (PTC) by a combination of X-ray crystallography, biochemistry, molecular biology and theoretical studies. Among his major tools was the determination of the crystal structures of complexes of ribosomal particles with antibiotics that target the PTC and are clinically useful, despite the extremely high conservation of this region in all kingdom of life. Dr Davidovich revealed the modes of action of these antibiotics, thus shedding light on the discrimination principles between ribosomes of eubacterial pathogens and the eukaryotic hosts that are based on remote interaction networks and induced fit. In parallel, he investigated the mechanisms acquiring resistance to antibiotics. Furthermore, by thorough comparative structural and genetic analyses, he determined the structural basis for cross-resistance between all of the clinically useful PTC-binding antibiotics.

Chen also attempted shedding light on the origin of the ribosome. He was focusing on the ribosomal substructure that may represent the minimal entity capable of performing peptide bond formation, namely the proto-ribosomes. Remarkably, despite the ribosome asymmetric structure, in all of the so far determined structures the PTC and its environs are situated within a highly conserved region of internal structural symmetry that connects all ribosomal functional centers involved in amino-acid polymerization, hence can serve as the central signaling feature. The high level of conservation of the symmetrical region suggests that the modern ribosome evolved from a simpler entity that can be described as a proto-ribosome that was formed by gene fusion or gene duplication and contained a pocket confined by two self folded RNA chains, which associated to form a pocket like dimer with functional capabilities. As RNAs can act as gene-like molecules coding for their own reproduction, it is conceivable that the surviving pockets became the templates for the ancient ribosomes. In later stage these RNA genes underwent initial optimization to produce a more defined rather stable pocket, in which each of the two halves was further optimized for its task in distinction between the amino acid and the growing peptidyl sites, so that their sequences evolved differently. Indeed, the preservation of the three-dimensional structure of the two halves of the ribosomal frame regardless of their sequence demonstrates the superiority of rigorous functional requirements over sequence preservations.

As two symmetry-related RNA entities seem to have not only the capability to self fold, but also can undergo self dimerization, assuming that dimerization is the minimal requirement for formation of catalytic active pocket, Chen designed and synthesized RNA chains corresponding to the sequence of this pocket in the contemporary ribosome and determined their tendency to dimerize. He found, surprisingly, a marked preference of specific sequences to dimerize, whereas other, very similar RNA chains did not. This sequence preference for self dimerization, indicate that principles as survival of the fittest may have played a major role on the molecular level, although these terms are usually used for species, hence suggesting pre Darwinian Darwinisim.

Chen's thesis has already led to attempts at improving the PTC antibiotics, performed locally as well as by companies. Additionally, a significant effort is made by two graduate students and a postdoctoral fellow, who are trying to design a functional construct mimicking a functional proto-ribosome.

Ada Yonath, August 2010

Parts of this thesis have been published in the following journal articles:

1. **C. Davidovich**, M. Belousoff, I. Wekselman, T. Shapira, M. Krupkin, E. Zimmerman, A. Bashan, A. Yonath. "The Proto-Ribosome: An Ancient Nano-machine for Peptide Bond Formation" *Isr. J. Chem.,* (2010) 50 (1), pp. 29-35.

2. M.J. Belousoff, **C. Davidovich**, E. Zimmerman, Y. Caspi, I. Wekselman, L. Rozenszajn, T. Shapira, O. Sade-Falk, L. Taha, A. Bashan, M.S. Weiss, A. Yonath. "Ancient machinery embedded in the contemporary ribosome." *Biochem. Soc. Trans.,* (2010) 38 (2), pp. 422-7.

3. T. Auerbach, I. Mermershtain, **C. Davidovich**, A. Bashan, M. Belousoff, I. Wekselman, E. Zimmerman, L. Xiong, D. Klepacki, K. Arakawa, H. Kinashi, A. Mankin and A. Yonath, "The structure of ribosome-lankacidin complex reveals ribosomal sites for synergistic antibiotics", *Proc Natl Acad Sci U S A,*(2010) Epub since Jan 11.

4. **C. Davidovich**, M. Belousoff, A. Bashan and A. Yonath, "The evolving ribosome: from non-coded peptide bond formation to sophisticated translation machinery", *Res. Microbiol.,* (2009) 160 (7), pp. 487-92.

5. T. Auerbach, I. Mermershtain, A. Bashan, **C. Davidovich**, H. Rosenberg, D. H. Sherman, and A. Yonath, "Structural basis for the antibacterial activity of the 12-membered-ring mono-sugar macrolide methymycin", *Biotechnologia,* (2009) 84, pp. 24-35.

6. **C. Davidovich**, A. Bashan, A. Yonath, "Structural basis for cross-resistance to ribosomal PTC antibiotics", *Proc Natl Acad Sci U S A*, (2008) 105 (52), pp. 20665-70.

7. I. Wekselman*, **C. Davidovich***, I. Agmon, E. Zimmerman, H. Rosenberg, A. Bashan, R. Berisio and A. Yonath, "Ribosome's mode of function: myths, facts and recent results", *J Pept Sci,* (2008) 15 (3), pp. 122-30.

8. **C. Davidovich**, A. Bashan, T. Auerbach-Nevo, R.D. Yaggie, R.R. Gontarek, A. Yonath, "Induced-fit tightens pleuromutilins binding to ribosomes and remote interactions enable their selectivity", *Proc Natl Acad Sci U S A*, (2007) 104 (11), pp. 4291-96.

* Equal contribution.

Table of Contents

7

1. Introduction

The ribosome is a universal cellular organelle that translates the genetic code into proteins. It is an assembly of ribosomal proteins (r-proteins) and ribosomal RNA (rRNA) chains that facilitates the reaction of amino acid polymerization into proteins, according to specific genetic information that is encoded in the cell genome and transferred to the ribosome by messenger RNA (mRNA). The ribosome is responsible for the identification of the correct genetic reading frame and translation initiation. It ensures robust fidelity when translating the genetic code by selecting the proper transfer RNA (tRNA) molecules that carry the cognate amino acids to be incorporated into the elongating polypeptide chain. It provides the framework for peptide bonds formation and smooth elongation of the newly synthesized proteins, including co-translational folding, chaperoning by ribosome-associated factors and the exit tunnel. When stop cordon arrive at the decoding site, the ribosome utilizes recycling and release factors to execute translation termination (reviewed in (Marshall et al, 2008; Ramakrishnan, 2008; Steitz, 2008; Yonath, 2009; Yonath & Bashan, 2004)).

The ribosome is composed of two counterparts; a large subunit, with a typical sedimentation coefficient of 50S in prokaryotes, and a small subunit, with a typical sedimentation coefficient of 30S in prokaryotes. The two subunits associate to initiate the process of protein biosynthesis and dissociate as the process terminates. Throughout protein biosynthesis the associated ribosomal subunits facilitate different tasks: the small subunit is responsible for initiation, identification of the correct reading frame and encoding of the genetic code. The main chemical reaction of protein biosynthesis, peptide bond formation, occurs in the large subunit, which ensures smooth polymerization, channeling of the nascent chain through the exit tunnel and facilitate folding by the aid of associating factors.

The first phase in protein biosynthesis is the formation of the initiation complex: small ribosomal subunit, mRNA, initiator tRNA (in bacteria fMet-tRNA^{fMet}) that binds to the AUG start codon and the initiation factors. Next, association of the two subunits results with an active ribosomal complex. The amino acids are carried into the ribosome

by tRNA molecules, aminoacylated to its 3' end (aminoacyl tRNA), which consist of a universally conserved CCA sequence. The ribosome contains three tRNA binding sites: A (aminoacyl tRNA), P (peptidyl tRNA) and E (exit) (see **figure F1**). The first aminoacyl tRNA 3' end binds to the large subunit at the P-site. This is followed by the accommodation of the A-site tRNA so that both anticodon loops maintain the Watson Crick and Wobble base pairs for codon-anticodon interactions with the mRNA codon that is bound at the P- and the A-site at the decoding center, within the 30S subunit. While the proper stereochemistry is achieved between both substrates peptide bond is being formed within the PTC void, following translocation of the tRNA from the A- to the P-site and the ribosome is ready to receive new amino acylated tRNA substrate. The deacylated P-site tRNA acts as a leaving group and moves towards the E-site, on its way out from the ribosome. The newly synthesized protein is growing into the exit tunnel at the 50S subunit, adjacent to the PTC.

Efforts for ribosomes crystallization began three decades ago (Yonath et al, 1980), but these enormously complicated crystallographic studies became fruitful only at the end of the last decade, yielding the three dimensional structures of ribosomal particles from three microorganisms. These include the high resolution structures of the small ribosomal subunit (30S) of the thermophilic bacteria *T. thermophilus* (T30S) (Schluenzen et al, 2000; Wimberly et al, 2000), the large ribosomal subunit (50S) of the halophilic archaeon *H. marismortui* (H50S) (Ban et al, 2000), the mesophilic eubacterium *D. radiodurans* (D50S) (Harms et al, 2001). Half a decade later the structures of the empty 70S ribosome from *E. coli* (E70S) (Schuwirth et al, 2005) and of the 70S ribosomal complexes from *T. thermophilus* (T70S) with mRNA and tRNA molecules (Korostelev et al, 2006; Selmer et al, 2006).

Based on the structure of H50S it has been proposed that three specific rRNA nucleotides within the PTC provide chemical catalysis for peptide bond formation (Nissen et al, 2000). Later it was shown that the PTC and its upper rim provides the means for accurate positioning of the tRNA, in an orientation required for the nucleophilic attack on the P-site carbonyl carbon (Agmon et al, 2005; Bashan et al, 2003). Based on this finding, together with results of genetic, biochemical and theoretical studies (reviewed in (Bashan & Yonath, 2008; Bashan et al, 2003b; Gregory & Dahlberg,

2004; Wekselman et al, 2009; Yonath, 2009; Zimmerman & Yonath, 2009)) it has been suggested that the ribosome provides positional catalysis to facilitate peptide bond formation.

A reliable structural approach to gain knowledge regarding ribosomal function and structure is by using x-ray crystallography techniques on ribosomal particles complexed with different antibiotics. Ribosomal antibiotics typically bind to functional centers and hamper ribosomal activity. These relatively small compounds enable feasible soaking protocols or co-crystallization procedures that were found to yield well diffracting crystals of the ribosome/antibiotic complex. Such studies shed light on the role of the small ribosomal subunit (Carter et al, 2001; Pioletti et al, 2001; Ramakrishnan, 2008), revealed some of the fundamental characteristics of the PTC (Auerbach et al, 2009; Blaha et al, 2008; Hansen et al, 2003; Harms et al, 2004; Ippolito et al, 2008; Schluenzen et al, 2001) and the polypeptide exit tunnel (Amit et al, 2005; Berisio et al, 2003; Hansen et al, 2002; Schluenzen et al, 2003; Schluenzen et al, 2001; Tu et al, 2005; Voss et al, 2006).

Furthermore, careful analysis of complexes of the large subunit with substrate analogs revealed a universal sizable symmetrical region of 180 nucleotides within the otherwise asymmetric ribosome. This symmetrical region is located in and around the PTC, at the heart of the ribosome. This region provides the structural elements allowing for peptide bond formation and tRNA translocation. It connects, directly or via its extensions, all the ribosomal functional sites involved in amino acid polymerization (Bashan et al, 2003). Its key role in protein biosynthesis led to the suggestion that the ribosome evolved by gene fusion or gene duplication (Agmon et al, 2005).

1.1 Ribosomal antibiotics: function, activity and selectivity

Having a fundamental role in cell viability and although being highly conserve, the ribosome has some diverge genetic characteristics that distinguish between bacteria and eukaryotes. Thus, the ribosome is a major target for clinically useful antibiotics. By targeting functional centers of the ribosome, these drugs compete with substrates and factors binding.

Crystal structures of ribosome-antibiotic complexes revealed different conformational states of functional sites, thus are described as a "snapshot" of a "frozen" conformation. For instance, the antibiotic Synercid® composed of two synergistically active streptogramin compounds dalfopristin (S_A) and quinupristin (S_B), each of which is a poor antibiotic agent. They bind to the PTC and the macrolide binding site close to the tunnel entrance, respectively (Harms et al, 2004). Quinupristin partially blocks the exit tunnel and dalfopristin stabilizes a swung conformation of U2585 (nucleotides are numbered according to *E. coli* system throughout, unless otherwise mentioned), which is flipped by 180° with respect to its location in the D50S apo structure. Such enormous conformational rearrangement reflects the high flexibility of this nucleotide that was suggested to serve as an anchor for the tRNA A- to P-site rotatory motion (Agmon et al, 2004). This simple example emphasizes the possible usage of ribosome inhibitors as a valuable tool for functional studies.

Ribosomal antibiotics must not only bind with high affinity, but their clinical usage requires high selectivity, namely; having the ability to target and inhibit the bacterial ribosome, without hampering the ribosome of the eukaryotic host. This is usually achieved as a result of minor differences between ribosomal functional sites in bacteria and eukaryotes. An example is the macrolide class of antibiotics, which all share interactions with nucleotide A2058 (Schluenzen et al, 2001). This nucleotide is a conserved adenine in eubacteria and a conserved guanine in archaea and eukaryotes (Cannone et al, 2002), hence provides selectivity for these compounds. Indeed, the mutation A2058G in bacteria leads to macrolides resistance (Douthwaite & Aagaard, 1993) while the mutation G2058A in the archaeon *H. marismortui* permits macrolides binding to the ribosome of this microorganism (Tu et al, 2005), which naturally is not sensitive to these antibiotics.

1.2 Pleuromutilins: a class of PTC ribosomal antibiotics for clinical use

As a result of the dramatic increase in antibiotic resistance among pathogenic strains, which causes a major clinical threat in recent years, the arsenal of efficient antibacterial drugs decreases. A promising strategy for reducing the magnitude of this

11

problem is the introduction of antibiotics from novel classes that so far have not been used clinically and have a unique mode of action. An example is the pleuromutilin family.

Pleuromutilin was discovered in 1951 as a natural product of the fungi *Pleurotus mutilus* (nowadays *Clitopilus scyphoides*) (Kavanagh et al, 1951) (see **figure F2** for chemical formula). Although the natural drug exhibited reasonable, however not excellent in-vitro activity against *Staphylococcus aureus*, there was no advantage in using it rather than any other available antibiotic; hence it was abandoned for the next two decades. The discovery made in the seventies, that semi-synthetic pleuromutilin derivatives may show elevated activity over a broad spectrum (Egger & Reinshagen, 1976) paved the way for further development of this new class of antibacterial agents, initially used as veterinary drugs, namely tiamulin and valnemulin (see **figure F2** for chemical formula). During the early 1980s, extensive efforts were made in order to formulate azamulin (TDM-85,530**)** (see **figure F2** for chemical formula)**,** a pleuromutilin derivative for clinical use in human (Hildebrandt et al, 1983; Hoegenauer & Brunowsky, 1983; Von Graevenitz & Bucher, 1983). Although this compound is active against a large variety of clinical isolates, including erythromycin- and tetracycline-resistant strains, it strongly inhibits cytochrome P-450 (Schuster et al, 1983), thus was not suitable for clinical use and never progressed beyond phase I clinical trials (Ulrich et al, 1983). However, continuous efforts to further develop pleuromutilin antibiotics yielded several novel semisynthetic compounds, some of which with increased activity and reduced metabolism. Among these, a few derivatives are currently in the industries' pipelines, and the most advanced – retapamulin (SB-275833) (Champney & Rodgers, 2007; Goldstein et al, 2006; Jones et al, 2006; Kosowska-Shick et al, 2006; Pankuch et al, 2006; Ross & Jones, 2005; Yan et al, 2006), was already issued for clinical use in human (Scangarella-Oman et al, 2009; Shawar et al, 2009; Yang & Keam, 2008a; Yang & Keam, 2008b).

The first potent group of semisynthetic pleuromutilin is of the C(14)-sulfanyl-acetate derivatives. This group includes the recently formulated drug retapamulin, the commonly used veterinary drugs tiamulin and valnemulin, and other potent compounds, such as azamulin and SB-280080 (see **figures F2** for chemical formula). This group of compounds is characterized by high antibacterial activity against various clinically

relevant Gram negative bacterial strains (for review see (Hunt, 2000)). However, C(14)-sulfanyl-acetate derivatives undergo rapid metabolism by cytochrome P-450 (Brooks et al, 2001; Hunt, 2000), thus characterized by limited oral bioavailability.

An additional group of pleuromutilins with good antibacterial activity are the C(14)-acyl-carbamate derivatives. This group, which includes SB-571519 and SB-264128 **(figure F2),** are slightly less potent than the sulfanyl-acetate derivatives, but it is characterized as having a reduced metabolism with elimination rate of down to tenth in respect to the C(14)-sulfanyl-acetate derivatives (Brooks et al, 2001). As this is a major advantage from a clinical point of view, these compounds were originally aimed for oral treatment.

Pleuromutilins block peptide bond formation by interfering with substrate binding both at the A- and the P-sites of the ribosomal PTC (Hodgin & Hogenauer, 1974; Schluenzen et al, 2004). It was found that the drug competes with 3'-terminues tRNA analogues, like puromycin and CpCpA oligonucleotide, and with the antibiotic chloramphenicol (Hogenauer, 1975) that binds at the PTC A-site (Schluenzen et al, 2001). However, once elongation process has begun; translation will not be effected by the drug (Dornhelm & Hogenauer, 1978). Consistently, the detailed crystal structure of the large ribosomal subunit from *D. radiodurans* in complex with the pleuromutilin class antibiotic tiamulin indicates binding to the PTC (Schluenzen et al, 2004), overlapping the binding sites of the A- and P-substrates.

Yet, until the point where my study was launched, no extensive comparative structural analysis of pleuromutilin antibiotics has been conducted, and the only structural information describing this class of antibiotics was heavily relayed on, and biased by, a single antibiotic designated for veterinary use, namely tiamulin. Under these circumstances; general mechanisms for drug binding and antibiotic resistance describing this class were vague and details providing hints for further drug design were lacking. Moreover, to that point no mechanism for drug selectivity was known. Within my research, as describes herein, I carried out the first comparative structural study of this class of antibiotics. Herein I describe general and detailed structural mechanisms for binding, resistance and selectivity of pleuromutilin antibiotics.

1.3 Structural basis for cross-resistance between ribosomal PTC antibiotics

Among the various classes of clinically useful antibiotics that target the ribosome, five classes target the PTC, namely phenicols, lincosamines, streptogramins A, pleuromutilins and oxazolidinones. These drugs bind to the PTC of bacterial ribosomes with high affinity and great specificity, thus hamper ribosomal activity, resulting in the loss of bacterial cell vitality, without significant effect on the eukaryotic host.

Cross-resistance appears when two or more drugs share binding sites with overlapping positions. According to crystal structures of the large ribosomal subunits from the eubacteria *D. radiodurans* (D50S) and the archaeon *H. marismortui* (H50S) that were complexed with various PTC binding antibiotics (Davidovich et al, 2007; Hansen et al, 2003; Harms et al, 2004; Ippolito et al, 2008; Schluenzen et al, 2004; Schluenzen et al, 2001) this is the case for all the five classes of antibiotics mentioned above.

All of these antibiotics were shown to bind with overlapping sites in the PTC A-site, in the vicinity of nucleotide U2504. The only exception was the case of chloramphenicol that was shown in two different locations in D50S and H50S. While in D50S the drug was shown in the A-site, with overlapping positions with all other PTC antibiotics, the H50S/chloramphenicol complex indicating a controversial binding site at the tunnel entrance, possibly because of the extremely high antibiotic concentration of 20 mM that was used in that experiment and the "lower affinity of the archaeal ribosome A-site crevice for chloramphenicol consistent with archaeal ribosomes being resistant to inhibition by chloramphenicol" (Hansen et al, 2003).

In recent years few indications accumulated indicating cross-resistance between some PTC antibiotics (Kehrenberg et al, 2005; Long et al, 2006; Miller et al, 2008). In addition, nucleotide U2504 was suggested to be an impotent intermediate that carries conformational changes induced by mutations in remote nucleotides and amino acids that are involved in tiamulin resistance (Pringle et al, 2004). By performing a comprehensive structural study on pleuromutilin antibiotics (Davidovich et al, 2007) and comparing with crystal structure of tiamulin/D50S complex (Schluenzen et al, 2004), we have suggested

that similar mutations are likely to affect other members of this class. This finding was based on the discovery that all the studied pleuromutilins derivatives bind with their common tricyclic core at overlapping positions in a tight binding pocket that includes nucleotide U2504. Similar mechanism for resistance and selectivity was later suggested based on the analysis of the locations of resistance mutations to the archeal and eukaryotic antibiotic anisomycin (Blaha et al, 2008).

While PTC antibiotics from five different classes can be used clinically and although in the recent years valuable information regarding resistance mechanism for each class of these drugs was obtained by structural and biochemical studies, not much has been done in order to derive general properties of these classes. Such analysis can predict common patterns for resistance mechanisms. As this issue has great value in light of the emergence evidences for cross-resistance between PTC antibiotics of different classes (Kehrenberg et al, 2005; Long et al, 2006; Miller et al, 2008; Smith & Mankin, 2008; Toh et al, 2007), I conducted a cooperative study. Herein I present a comprehensive structural analysis aimed at reveling common characteristics that govern the mechanism of drug resistance in the PTC. This was done by analyzing the spatial distribution of nucleotides that affect resistance to PTC antibiotics, as well by suggesting a structure based mechanism by which remote mutations alter the binding site of these drugs.

1.4 Oligonucleotides as ribosomal inhibitors and as tools for structural and functional study

Long before the emergence of the high resolution crystal structures of the ribosome short oligonucleotides were used to structurally and functionally characterize it. Short DNA oligonucleotides, down to six bases long, were used to probe rRNA accessibility. Nucleotides of this length are sufficient to hybridize into DNA-RNA double strands, hence can target accessible functional sites in the 16S rRNA during initiation complex formation (Weller & Hill, 1991). Such nucleotides were also exploited to probe 16S region involved in ribosomal subunits association (Tapprich & Hill, 1986), to map the decoding center in the presence and the absence of polyU and tRNA[Phe] (Weller &

Hill, 1991), and to probe the interactions of tRNA with the 23S rRNA (Hill et al, 1990; Marconi & Hill, 1989). In another study a DNA probe was used to locate a known RNA sequence in the low resolution EM map of the ribosome, using 12 bases long oligonucleotide with a terminal modification designed for immune electron microscopy (Lasater et al, 1990). This probe was designed to hybridize to the 16S rRNA sequence 520-531, near the decoding site (**figure F1**). The correct identification of the decoding center within these EM maps was confirmed when the high resolution structures of the small ribosomal subunit appeared ten years later (Schluenzen et al, 2000; Wimberly et al, 2000). Another technique exploited DNA antisense oligonucleotides that were chemically modified with a photo-sensitive affinity label. Such probe enabled site specific cross-linking, thus identified specific neighborhoods. This method showed cross-linking of an antisense DNA complementary to bases 2497-2505 of domain V of the 23S rRNA to r-protein L3 (Muralikrishna & Cooperman, 1991), an observation that was later confirmed by the x-ray structure of the eubacterial large ribosomal subunit (Harms et al, 2001).

While the majority of these studies concentrated on rRNA sequences that are currently known to reside on accessible regions of the ribosomal subunits, a similar study concentrated on the PTC cavity (Marconi et al, 1990). In this study, a ^{32}P labeled DNA probes, 6 to 15 bases long, were used to probe rRNA accessibility in the presence of the ribosomal antibiotic chloramphenicol. This study demonstrated DNA oligonucleotides binding to ribosomal functional centers located in deep ribosomal cavities, as is currently known for the PTC.

The idea that short antisense oligonucleotide sequences can selectively inhibit the bacterial ribosome has already been confirmed. One of the first attempts for a rational design of oligonucleotide ribosomal inhibitor was based on the Shine-Dalgarno (SD) sequence. The SD sequence is a short sequence (AGGAGG) within the mRNA that signals for initiation of protein biosynthesis in bacteria (Shine & Dalgarno, 1974). It is located upstream of the first coding AUG, and its complimentary sequence (ACCUCCU) is located at the 3' end of the 16S rRNA in the small subunit of the bacterial ribosome. The idea that specific recognition between a short mRNA sequence and the 16S rRNA is directly responsible for mRNA binding to the ribosome led to the suggestion that such short oligonucleotide sequence may selectively inhibit the bacterial ribosome (Jayaraman

et al, 1981). In that work, Jayaraman and coworkers used short (3 to 7 bases) nonionic oligonucleotides (deoxy ribo oligonucleoside methylphosphonates) that were complimentary to the anti-SD sequence at the 16S rRNA. The most potent sequences were of 6 and 7 bases long that mimicked the SD sequence (AGGAGG and AGGAGGT, respectively). These two oligonucleotides sequences inhibited protein synthesis of in vitro transcription translation system with IC_{50}, namely the inhibitor concentration required to inhibit the system down to 50% of its observed inhibitor-free activity, of between 25 μM to 12.5 μM. Such IC_{50} values are lower than those previously measured for the standard ribosomal antibiotic tetracycline (30 μM), and just slightly higher than the IC_{50} values of the ribosomal antibiotics chloramphenicol (5 μM) and linezolide (2.5 μM) (Murray et al, 2001). However, these oligonucleotides failed to inhibit the growth of intact *E. coli*, due to low permeability. A subject for similar studies was the α-sarcin domain of the 23S rRNA (2646-2674). This stem-loop contains 12 universally conserved nucleotides, and is among the most conserved sequences in the 23S rRNA. A hydrolysis of the rRNA backbone after nucleotide G2661 by the highly specific RNase α-sarcin blocks all elongation factor dependent reactions (Hausner et al, 1987). An antisense DNA oligonucleotide sequence complimentary to this region was found to inhibit ribosome activity both in eukaryotes (Saxena & Ackerman, 1990) and prokaryotes (Meyer et al, 1996). However, effective inhibition of poly(Phe) synthesis was achieved only at low temperature of 25 °C.

In another study a set of 12 overlapping antisense 2'-O-methyl 10-mer oligoribonucleotides were designed to target nucleotides 1485-1516 in the A-site of the small ribosomal subunit (Abelian et al, 2004). The binding and inhibition properties of these oligonucleotides were tested, and some of them were found to bind ribosomes with K_d of down to 30 nM, as well as with the ability to inhibit in-vitro transcription-translation system with IC_{50} of as low as 10 μM. The approach of using predefined length antisense oligonucleotides as antisense probes is suitable for targeting relatively short and defined rRNA regions, but it can become more extensive if considering longer rRNA target sequences, and oligomers with various length.

In the studies described above, the antisense oligonucleotides were designed either according to the target rRNA sequence, or based on considerations regarding the

two dimensional rRNA structure. In some cases, as described above, these attempts were successful. However, not all of them were of the same efficiency, and some were totally inefficient.

During the past two decades several theoretical methods were developed in order to predict RNA secondary structure, and its hybridization with antisense oligonucleotides (e.g. (Ding & Lawrence, 2001; Mathews et al, 1999; Muckstein et al, 2006; Stark et al, 2003; Stull et al, 1992)). Such approaches may be suitable for single unbound RNA fragments, as mRNA, or in cases of well thermodynamically defined RNA structures, however are inappropriate for RNA-protein assembly as the ribosome, which includes a large inaccessible core, tens of incorporated proteins, and convoluted thermodynamics that is far from been understood.

Neither of the early antisense oligonucleotides that have been proved to serve as effective ribosome inhibitors (Abelian et al, 2004; Jayaraman et al, 1981; Meyer et al, 1996; Saxena & Ackerman, 1990) and ribosome targeting probes (Hill et al, 1990; Marconi & Hill, 1989; Marconi et al, 1990) designed based on three dimensional structural information. On the other hand, coordinates of high resolution crystal structures of ribosomal complexes are available. Yet, when I started no three dimensional structure based strategy has been developed to derive effective antisense sequences that will bind to exposed RNA elements of molecules or complexes with known structure, as the ribosome. Hence, I initiated a process for the development of a novel approach for structure-based design of antisense oligonucleotide sequences capable of binding to ribosomal exposed functional centers. Such oligonucleotides can potentially be used as inhibitors and also serve as the basis for future antibacterial drugs.

1.5 Minimal ribosomal components with PTC structure and function

Since the discovery made in the 1960s that the ribosome can catalyze the formation of peptide bonds between minimal substrates, e.g. puromycin and fMet-tRNA (Bretscher & Marcker, 1966) or CAACAA-formyl-methionine (Monro & Marcker, 1967), in a biochemical reaction called the "fragment reaction", efforts were made in order to search for the smallest set of ribosomal components that are capable of carrying

out such reaction. During the early 1980s Schulze and Nierhaus found that the large ribosomal subunit *per-se* possesses peptidyl transferase activity even in the presence of only the 23S rRNA and 15 r-proteins, out of its "34 distinct components" (Schulze & Nierhaus, 1982).

A decade later Noller showed that the large ribosomal subunit has catalytic activity after vigorous treatment with proteinase K and SDS (Noller et al, 1992). Partial activity was also observed in reconstituted large subunits from T7 RNA polymerase transcribed 23S and 5S rRNA and r-proteins that were extracted from 50S subunit (Khaitovich et al, 1999). The smallest active sub-ribosomal particle that obtained in those studies included both 5S and 23S rRNA and 8 ribosomal proteins (Khaitovich et al, 1999a). Yet, while the combination of several intact ribosomal component were shown to maintain some level of ribosomal activity, trials to obtain peptidyl transferase activity by designing minimal construct that will include only small portion of 23S rRNA from the vicinity of the PTC were unsuccessful (Anderson et al, 2007; Nitta et al, 1998a; Nitta et al, 1999a; Nitta et al, 1998b; Nitta et al, 1999b).

The PTC, i.e. the core catalytic center and the site of peptide bond formation, is composed solely of highly conserved ribosomal RNA (rRNA). It is located at the heart of the contemporary ribosome in the midst of a symmetrical 'pocket-like' structure (Agmon et al, 2006; Agmon et al, 2005; Agmon et al, 2009; Bashan et al, 2003) (**figure F3**). This is an unusual feature within the otherwise asymmetric ribosome. This region exists in all known high resolution crystal structures of ribosomal complexes (Ban et al, 2000; Harms et al, 2001; Korostelev et al, 2006; Schuwirth et al, 2005; Weixlbaumer et al, 2008) and its inner part displays resistance to mutations (Sato et al, 2006). Its 180 nucleotides are divided into two distinct regions that are related by a pseudo two fold structural symmetry, irrespective of the nucleotide sequences.

This symmetrical 'pocket-like' region hosts the two ribosome's substrates, namely the amino acylated and the peptidyl tRNA molecules. The elaborate architecture of this structural element provides the framework for the ribosome catalytic activity, as it positions the ribosome's substrates in favorable stereochemistry for peptide bond formation (Agmon et al, 2006; Agmon et al, 2005; Agmon et al, 2009; Bashan et al, 2003; Bieling et al, 2006; Gregory & Dahlberg, 2004; Moore & Steitz, 2003; Weinger &

Strobel, 2007) and for substrate-mediated catalysis (Bashan & Yonath, 2008; Weinger et al, 2004; Yonath, 2003; Youngman et al, 2004). Additionally, by encircling the PTC it confines the void required for the motions involved in the translocation of the tRNA 3′ end, which, in turn, is necessary for successive peptide bond formation, enabling the amino acid polymerase activity of the ribosome (Agmon et al, 2006; Agmon et al, 2005; Agmon et al, 2009; Bashan & Yonath, 2008). The rRNA entities of the symmetrical region possess the common stem-elbow-stem (SES) structural motif, and are hypothesized to be capable of self-assembly and dimerization (Agmon et al, 2006; Agmon et al, 2009).

Based on the above observations we have proposed that the ancient machinery that could form peptide bonds was made exclusively from RNA molecules that self assembled to create the ribosomal active site, which is still implanted in the modern ribosome. I therefore initiated an experimental study aimed at revealing RNA chains dimerize for acquiring a conformation resembling the PTC and that can bind substrates and catalyze the formation of peptide bonds. Herein I discuss biochemical evidence supporting the existence of an ancestral dimeric proto-ribosome, as well as of compounds that could serve as its substrates. These include the development of structural tools for approaching one of the key questions in origin of life, namely: did the ancient translation apparatus survive selection pressure and are its vestiges are embedded within the modern ribosome?

2. Methods

2.1 Structural study of pleuromutilin antibiotics

2.1.1 Crystallization and data collection

D50S crystals were obtained as previously described (Auerbach-Nevo et al, 2005). Individual crystals were soaked in harvesting solution at room temperature with 0.01 mM retapamulin (SB-275833) or SB-280080 for 12 h, or 0.1 mM SB-571519 for 8 h and than transferred into an anti-freeze solution (Auerbach-Nevo et al, 2005) for 10 min

in the presence of the pleuromutilin antibiotics at adequate concentrations. This was followed by flash cooling in liquid nitrogen. X-ray diffraction data were collected at 85 K. A few crystals were needed for yielding complete datasets of D50S complexes with SB-275833 and SB-280080. Importantly, a complete set with significant redundancy could be collected from a single crystal of the SB-571519 complex (**table 1**).

2.1.2 Data processing, structure solution and refinement

Data were processed with HKL2000 (Otwinowski & Minor, 1997) and CCP4 package suite (Bailey, 1994). The pleuromutilin derivatives binding sites were unambiguously located in a sigmaa-weighted difference electron density maps using the apo structure of D50S (PDB ID code 1NKW) as reference, after refinement by CNS (Brunger et al, 1998). Because no crystal structure of any isolated pleuromutilin derivative is available, initial models were generated from tiamulin coordinates (PDB ID code 1XBP) modified by using insight II (Accelrys, San Diego, CA) and CORINA (www.molecular-networks.com/software/category/gen3dcoord.html), followed by energy minimization with no x-ray terms. The maps were traced interactively using O (Jones et al, 1991) and COOT (Emsley & Cowtan, 2004), followed by subsequent restraint CNS minimization for the entire complex. The same randomly selected 5% of the data were omitted for cross validation of all refinement procedures. The resulting coordinates have been deposited at the Protein Data Bank with PDB ID codes 2OGM, 2OGN, and 2OGO.

2.2 Comparative structural analysis to reveal the structural basis for cross-resistance between PTC antibiotics

To perform general structural and statistical analysis, we generated a database holding information on the nucleotides involved in resistance or reduced susceptibility to PTC antibiotics (**table T2**). This database includes information for each nucleotide, the antibiotics families affected by it, and the distance spans between this nucleotide to the most proximal atom of the bound antibiotic. Precisely, this distance represented the minimum value within a set of distances spans between all possible pairs of two atoms (excluding hydrogens); one in the relevant nucleotide and the other within the

corresponding antibiotic molecule. Structural analysis was based on crystal structures of complexes of D50S with various antibiotics, including the phenicol chloramphenicol, the lincosamide clindamycin, the streptogramin$_A$ dalfopristin, the pleuromutilin tiamulin, and the oxazolidinone linezolid. Crystal structures of D50S with other pleuromutilins, methymycin, and lankacidin were not included as currently no resistance data are available for them. Biochemical data on antibiotic resistance in the archaeon *H. halobium*, and crystallographic data obtained for complexes of PTC antibiotics with the large ribosomal subunit from the archaeon *H. marismortui*, were also included. As these archaeons may resemble eukaryotes and since known pathogens are typically eubacteria, distances and data analyses were performed separately for eubacteria and for archaea. Calculations and database analysis were performed by MATLAB (MathWorks, Inc., Natick, MA). *In silico* mutagenesis and structural analysis were performed by COOT (Emsley & Cowtan, 2004) and PyMol (DeLano Scientific, Palo Alto, CA, USA). PyMol was also used for image rendering. PDB ID codes are shown when relevant.

2.3 Antisense oligonucleotides for targeting functional ribosomal centers

2.3.1 Database construction

The 23S rRNA of the large ribosomal subunit of eubacteria was selected as a model for initial study. First, we constructed a database that contained structural and thermodynamical information (MathWorks, Inc., Natick, MA). The parameters that were incorporated into the database are as follows:

1. **Mutation sites:** Includes mutations in nucleotides that were previously related with one of the following categories: (i) antibiotic resistance or antibiotic enhancement, (ii) slow bacterial growth or reduce ribosomal activity and (iii) lethality. A total number of 132 mutations obeying at least one of these categories were selected out of the rRNA mutations database of Kathleen Triman (ribosome.fandm.edu).

2. **Stacking distance:** Including distances between the bases of each two sequent nucleotides (i.e. nucleotides i and i+1), using N3 as a reference atom. The

22

distances were calculated according to the coordinates of the large ribosomal subunit from *D. Radiodurans* (1NKW). A small $N3_i$ to $N3_{i+1}$ distance is a rough assessment for a stacking interaction between nucleobases, while a long distance indicates poor stacking.

3. **Base pairing:** Indicates Watson-Crick and Wobble pairs, as appeared in the 3D structure, detected by X3DNA (Lu & Olson, 2003).

4. **Surface accessibility:** Was calculated for each nucleotide separately; for the entire residue and for the backbone only (phosphate and ribose). Calculation done in the presence of all the large ribosomal subunit components (23S, 5S and r-proteins), using a probe radius of 1.4 Å (Crystallography & NMR System (CNS), (Brunger et al, 1998)).

5. **Thermodynamics parameters:** Done by our collaborator, Joseph Sofaer, from the research group of Tamar Schlick, Faculty of Chemistry, NYU, using the computer program OligoWalk (Mathews et al, 1999). These parameters were calculated for all the possible 5 to 25 bases long antisense DNA oligonucleotides for the 23S rRNA of *E. coli*: a total sum of 60,690 theoretical antisense sequences. The following parameters were derived for each of them:

   a. **Target structure energy:** The energy associated with braking the 2D structure of the target rRNA. The 2D structure of the 23S rRNA used to generate this parameter.

   b. **Intramolecular energy:** calculated for secondary structures that might be formed by the antisense itself.

   c. **Intermolecular energy:** considered antisense-antisense interactions.

   d. **Duplex formation energy:** The energy gain of binding an antisense to the target sequence.

   e. **Total binding energy:** Incorporating all of the thermodynamic parameters mentioned above to yield the overall binding energy.

   f. **Tm of the duplex:** An estimate for the temperature by which 50% of the target sequences are bound to antisense oligonucleotides. This calculation

neglected the structures of the target and of the antisense oligonucleotide, and assumed an excess of the antisense over the target. Tm calculated for antisense concentration of 1 μM.

2.3.2 In-vitro transcription-translation system for ribosome activity assay

In order to characterize IC_{50} values for the selected antisense oligonucleotides we constructed an in-vitro transcription-translation system of *E. coli*, with firefly luciferase as a reporter gene. The procedure for in-vitro transcription-translation system was used as previously described (Abelian et al, 2004; Zubay, 1973), with some modifications:

2.3.2.1 E. coli cell extract preparation

E. coli BL21(DE3) strain (Stratagene) fermented in LB medium (250 rpm at 37 °C). Induction with 1 mM IPTG, for expression of T7 RNA polymerase, performed at 0.5 OD_{600}, followed by additional four hours of incubation (250 rpm at 37 °C) before harvesting (15 min under 4000 RCF at 4 °C). Next, 20 g of bacterial paste were washed twice in 1 L and 500 ml buffer A (60 mM AcOK, 10 mM Tris-OAc pH 8.2, 14 mM $Mg(OAc)_2$, 155 μg/ml DTT, 0.5 μl/ml β-mercaptoethanol), followed by centrifugation (SPA-3000 rotor, 6000 rpm, 15 min, 4 °C). The pellet was resuspended with 20 ml of buffer B (60 mM AcOK, 10 mM Tris-OAc pH 8.2, 14 mM $Mg(OAc)_2$, 155 μg/ml DTT). Cells were lysed using a French Press (American Instrument Company, Silver Spring, MA) at 8000 psi. The bacterial lysate was centrifuged to remove cell debris (SS-34 rotor, 11,600 rpm, 30 min, 4 °C). The supernatant was re-centrifuged under the same conditions, and then dialyzed with SnakeSkin® 3.5 kDa molecular weight cut-off (MWCO) regenerated cellulose membrane (Pierce Biotechnology, Rockford, IL) against buffer B (750 ml x 4 times, 1 to 1.5 hours each, 4 °C). The solution was centrifuged (SS-34 rotor, 5,800 rpm, 10 min, 4 °C) followed by incubation of 30 minutes at 37 °C to reduce amounts of endogenous mRNA. Cell extract was divided into 500 μl aliquots, flash-frozen in liquid nitrogen, and stored at -80 °C.

2.3.2.2 Transcription-translation reaction

Reaction mixtures included: 0.22 v/v *E. coli* cell extract, 1.8 ng/ul pIVEX2.6d plasmid carrying firefly luciferase under T7 promoter (donated by Roy Bar-Ziv, Weizmann Institute of Science), 900 μM of each amino acid (Sigma), 230 μg/ml Creatine Kinase from rabbit muscle (Roche), 150 μg/ml *E. coli* tRNA mixture (Sigma), 50 mM Hepes-KOH (pH 7.5), 9% PEG 8000, 180 mM KGlu, 1.6 mM DTT, 1.1 mM ATP, 0.8 mM GTP, 0.8 mM CTP and 0.8 mM UTP, 0.6 mM cAMP, 70 mM Creatine Phosphate, 30 μg/ml folinic acid, 25 mM NH_4OAc and 16 mM $Mg(OAc)_2$.

30 μl reaction mixtures were incubated for 60 min at 37° C in the presence of different concentrations of the various ODNs. Reactions stopped instantly with the addition of erythromycin solution to final concentration of 5 μM.

2.3.2.3 Luciferase activity assay for translation quantification

50 μl Luciferase Assay System (Promega) were added to 10 μl of the incubated reaction mixture in a black 96 well plate (Nunc, Roskilde, Denmark), and photoluminescence was instantly measured using SpectraFluor Plus plate reader (Tecan, Maennedorf, Switzerland). Dose response curves were fitted to the experimental data with MATLAB (MathWorks, Inc., Natick, MA) to produce IC_{50} values.

2.3.3 Antisense oligonucleotides nomenclature

Antisense oligonucleotides were named according to their length and their first target nucleotide in *E. coli* numbering (e.g. antisense 463-10 is a 10 bases antisense that targets nucleotides 463 to 472 in *E. coli*).

2.4 Minimal ribosomal components with PTC structure and function

2.4.1 In vitro RNA transcription

DNA constructs were prepared using gene synthesis (purchased from GenScript, NJ) and were obtained in varies scales from few micrograms to few milligrams (Plasmid

Mini, Midi, Maxi and Giga Kits, Qiagen). Plasmids were linearized with HgaI or BsaI (New England Biolabs, Madison, WI). RNA transcription and purification curried out from microgram to milligram scales, as described elsewhere (Christopher, 1998), using a recombinant His-tagged T7 RNA polymerase (RNAP). T7 RNAP was overexpressed following standard protocols (*E. coli* BL21 strain carrying the gene in pQE8 expression vector was kindly donated by Dr. Irit Sagi and Dr. Barak Akabayov, Weizmann Institute). Mutations in RNA sequences were incorporated either by transcription from custom synthesized single strand DNA templates carrying the desired mutation (Sigma) or were incorporated to plasmids carrying the wild-type sequence using QuikChange Site-Directed Mutagenesis Kit (Stratagene), following manufacturer instructions.

2.4.2 Study of dimerization tendency

RNA samples were dissolved in double distilled water and annealed for 1 minute at 90 ℃ then flash cooled on ice. Incubation buffer was added to a final concentration of 89 mM tris-borate (TB) pH 7.5 and 15 mM MgCl. Unless otherwise indicated, final RNA concentration in samples was 2 μM. Samples were incubated at 37 ℃ for 30 minutes and then placed on ice for additional 15 minutes. For non-denaturing gels 10X glycerol loading dye (50% glycerol, 0.25% w/v bromophenol blue and 0.25% w/v xylene cyanol) was added and the samples were immediately loaded on ice-chilled 12% or 15% polyacrylamide (19:1 polyacrylamide:bisacrylamide) mini gel buffered with 89 mM TB pH 7.5 and 15 mM MgCl. For magnesium-free assays, $MgCl_2$ was replaced with 2 mM EDTA in both samples and gels. Non-denaturing gels were run overnight in icebox, under constant voltage of 40 V (Mini-PROTEAN®, BioRad). For denaturing gels 2X formamide loading dye (90% v/v deionized formamide, 0.25 % w/v bromophenol blue, 0.25 % w/v xylene cyanol, 2 mM EDTA, 100 mM Tris-HCl, pH 7.3) was added to RNA samples following 10 minutes incubation at 65 ℃. Next, samples were briefly chilled on ice and loaded on denaturing 12% or 15% polyacrylamide gel with 7 M urea, buffered with 89 mM tris-borate pH 8.3 and 2.5 mM EDTA (TBE). Denaturing gels were run up to 2 hours under constant voltage of 150 V (Mini-PROTEAN®, BioRad). Gels were stained with 0.5 μg/ml ethidium bromide (EtBr) and imaged using Bio-Rad Molecular Imager Gel Doc XR system, controlled by the Quantity One software (Bio-Rad).

2.4.3 Electrophoresis Mobility Shift Assay (EMSA)

The studied RNA was dephosphorylated using calf intestinal alkaline phosphatase (New England Biolabs) and 5′-end labeled with [33]P (gamma-^{33}P-ATP, Institute of Isotope Co., Ltd., Budapest, Hungary) or [32]P (gamma-^{32}P-ATP, PerkinElmer Inc.) using T4 polynucleotide kinase (New England Biolabs) as described elsewhere (Christopher, 1998) or by KinaseMax[TM] Kit (Ambion) according to manufacturer instructions. For homodimer Kd assessments non-labeled RNA of the same sequence in various concentrations was mixed with trace amount of ^{33}P or ^{32}P labeled RNA, and then was subjected to dimerization assay followed by non-denaturing polyacrylamide gel electrophoresis, as described above. For heterodimerization, labeled and unlabeled RNA of different sequences were used. Gels were transferred to Whatman 3M paper and were dried under a vacuum at 80 °C for 2 hours using BioRad gel drying apparatus. Dried gels were exposed to a phosphorimager cassette (Molecular Dynamics) for periods ranging from overnight to one week, scanned (Phosphorimager Storm 820, Amersham Pharmacia Biotech) and analyzed (Quantity One software, Bio-Rad).

2.4.4 Size Exclusion Chromatography (SEC) for the separation between dimer and monomer

SEC based separation between the dimer and the monomer was based on previous publications (Kim et al, 2007; Lukavsky & Puglisi, 2004; McKenna et al, 2007) with some modifications. Briefly, samples of the studied RNA were annealed as described above for non-denaturing gels. 10 μg to 100 μg RNA samples were loaded on Superdex 200 10/300 GL column (Amersham Pharmacia Biosciences) equilibrated with 20 mM Tris-HCl pH 7.8, 40 mM KCl and 8 mM $MgCl_2$. Load volume was not exceeding 15 μl. Chromatography was performed at 0.5 ml/min at 4 ºC to 7 ºC and fractions were collected manually into ice-chilled tubes.

2.4.5 Radiolabeling of substrates for Peptidyl Transferase activity assay

CC-puromycin (CCPmn) or C-puromycin (CPmn) substrates (Dharmacon) were labeled with ^{33}P or ^{32}P as described above for 5' RNA labeling. 2X formamide loading dye (FD) added to labeled substrates prior to separation from unincorporated radiolabeled ATP by polyacrylamide gel electrophoresis (PAGE), using 12 % acrylamide:bis-acrylamide ratio 29:1 gels buffered with 1X TBE and 7 M urea as denaturing agent. Gels run 1.5 hours at 80 V (Mini-PROTEAN®, BioRad) in a tank containing 0.5X TBE. Under these conditions CCPmn labeled substrate co-migrated with the xylene cyanol dye. CCPmn and CPmn containing bends were sliced and eluted into Milli-Q water overnight at 4 ^{O}C and quantified by scintillation counting.

2.4.6 Assay for Peptidyl Transferase activity

Peptidyl transferase activity for various dimers performed as previously described (Schmeing et al, 2002) with some modifications. Briefly, RNA constructs were resuspended in Milli-Q water, annealed 1 min at 90 ^{O}C and cooled down to room temperature before adding incubation buffer to final concentration of 120 mM KCl, 15 mM MgCl$_2$, 40 mM of either 2-(*N*-morpholino) ethanesulfonic acid (MES) pH 6.0, TRIS pH 6.8, HEPES pH 7.5 or HEPES pH 8.0. Substrates added to final concentration of 1 mM CCA-phenylalanine-caproic acid-biotin (Dharmacon) and >2000 cpm ^{33}P or ^{32}P labeled CCPmn or CPmn. Samples contained 2 uM RNA. Control samples were incubated in the absence of RNA and the presence or absence of 1 uM 50S ribosomal subunit from *E. coli.* To check possible positive contribution of alcohol to peptidyl transferase activity, as was previously observed for similar reactions using larger substrates (Bretscher & Marcker, 1966; Monro & Marcker, 1967), samples were incubated in the presence or absence of 30% methanol. 10 ul reactions were incubated for periods varying from 2 hours to 24 hours at room temperature, 37 ^{O}C or 50 ^{O}C. Reactions were quenched with the addition of 18.1 ul of 2X FD following with the addition of 8.1 ul of 5 mg/ml streptavidin (GenScript) aqueous in 150 mM NaCl and 10 mM potassium phosphate, pH 7.2. Samples were loaded on 7% acrylamide:bis-acrylamide 29:1 gels buffered with 1X TBE and 7 M urea as denaturing agent. Gels run 1 hour at 80 V in a

tank containing 0.5 X TBE (Mini-PROTEAN®, BioRad), dried and scanned as described above.

2.4.7 RNA two-dimensional structure prediction

Two-dimensional structure prediction performed using mFold (Zuker, 1989), version 3.2, using the default settings.

2.5 Numbering, Sequence Alignment, and Images.

Nucleotides are numbered according to *E. coli* numbering system throughout, unless otherwise mentioned. Multiple sequence alignment was performed by ClustalW (Thompson et al, 1994) and presented by JalView (Clamp et al, 2004). Figures of three dimensional structures were generated by Pymol (DeLano, 2002).

3. Results

3.1 The structures of D50S/Pleuromutilins comlexes

Complete crystallographic data sets of complexes of D50S with SB-571519, SB-280080, and retapamulin (SB-275833) (**figure F2**) yielded electron density maps at 3.50, 3.56, and 3.66 Å resolution, respectively (**table T1**), in which the location and conformation of each of the three bound compounds were unambiguously resolved (**figure F4**). Grouped occupancy refinement yielded a value of approximately 1.0 for all three compounds, confirming that the they are quantitatively bound, in accord with the high binding affinity observed (**table T3**) in a competitive ribosome-binding assay by using a radiolabeled pleuromutilin derivative (Yan et al, 2006).

The electron density maps of each of the three pleuromutilins complexes (**figure F4, panels a–c**) indicate that all of these pleuromutilins are located at the PTC, similar to tiamulin (Schluenzen et al, 2004), in the vicinity of the location that should have been occupied by the transition state intermediate of peptide bond formation (Gindulyte et al,

2006). Their tricyclic cores are almost fully superposed on that observed for tiamulin (**figure F5**). All interact with the 23S RNA domain V (**figure F4, panels d–f**) by hydrophobic interactions and hydrogen bonds, formed with surrounding nucleotides, namely A2503, U2504, G2505, U2506, C2452, and U2585. The C11 hydroxyl group of all of the compounds is located in a position suitable for hydrogen bonding to G2505 phosphate. In SB-280080 and SB-571519, it can be involved in an additional H-bond with the O2′ hydroxyl of A2503 (**figure F4, panels d and f**). The additional hydroxyl group of SB-571519 C2 (R_2 in **figure F2**) may be involved in polar interactions or an H-bond with O3′ or O5′ phosphoester of G2505 (**figure F4, panel d**), because the distances between its oxygen and G2505 phosphoester oxygens are 3.2 and 3.0 Å, respectively.

As observed for tiamulin (Schluenzen et al, 2004), the essential (Egger & Reinshagen, 1976) C21 keto group (**figure F2**) of the C14 extension of all three compounds is involved in two to three hydrogen bonds with G2061. This H-bond network is similar for all three compounds, including the carbamate derivative SB-571519 that utilizes its additional carbonyl as an alternative H-bond acceptor (**figure F4, panels d–f**). Apart from these H-bonds with G2061, it seems that the pleuromutilins' C14 extension is involved only in minor hydrophobic contacts with ribosomal nucleotides.

Among the conformational rearrangements of the rRNA observed upon binding of all three studied pleuromutilins (**figure F4, panels g–i**), the most notable is the 40° rotation of U2506 base toward the tricyclic core, a motion that closes tightly the binding pocket on the bound compound. An additional conformational rearrangement, of the flexible base of U2585 (Agmon et al, 2004; Bashan et al, 2003), was also detected. In eubacteria, in the absence of substrates or inhibitors, this flexible nucleotide (Bashan et al, 2003) is located in a position (Harms et al, 2001; Schuwirth et al, 2005; Selmer et al, 2006) that should interfere or interact with C14 extension of all studied pleuromutilins, including tiamulin. Consequently, to avoid steric hindrance, in the presence of pleuromutilins U2585 undergoes a slight shift, which allows for interactions between its base and that of U2506, thus stabilizing the conformations of both nucleotides in the bound state (**figure F4, panels d–f**). In the SB-571519- and SB-280080-bound forms, U2585 forms a single hydrogen bond with U2506, whereas in the retapamulin complex the distance between the two bases allows for van der Waals or similar interactions.

It was previously suggested that mutations in ribosomal protein L3 reduce bacterial susceptibility to pleuromutilins by indirect influence of the binding pocket conformation (Bosling et al, 2003; Pringle et al, 2004; Schluenzen et al, 2004). I could unambiguously trace protein L3 Arg-144 (*D. radiodurans* numbering) owing to the high quality of the electron density map of SB-571519/D50S complex, as it was constructed from a complete dataset that was collected form a single crystal with significant redundancy (**table T1**). This map shows that L3 Arg-144 extends toward the PTC, and interacts electrostatically with U2506 phosphate, but does not make any contacts with the pleuromutilin compound (**figure F6, panel a**). In addition, no significant conformational rearrangements were detected in protein L3 in all studied pleuromutilin derivatives as well as tiamulin (Schluenzen et al, 2004).

3.2 Structural basis for cross resistance between ribosomal PTC antibiotics

The spatial distributions of nucleotides associated with resistance to PTC antibiotics identified by various non crystallographic methods (**table T2**) mapped onto D50S crystal structure (**figure F7 and figure F8**), indicate that almost all of the nucleotides mediating resistance are clustered in a distinct region, although the PTC surroundings offer various nucleotides for antibiotics binding, some of which can be mutated without losing cell vitality (Sato et al, 2006). This region is located farthest from the intersubunit interface and stretches into the entrance to the nascent protein exit tunnel (**figure F7** and **figure F8**). The only outlier is the highly flexible nucleotide A2062, which is located closer to the subunit interface and was detected in different orientations in complexes of various antibiotics, namely chloramphenicol (Schluenzen et al, 2001), streptogramin$_A$ (Harms et al, 2004), lankacidin (Auerbach et al, 2010) and methymycin (Auerbach et al, 2009).

For describing the locations of the nucleotides mediating antibiotics resistance, the PTC was divided by an artificial plane into two regions: one contains components participating in resistance mutations, and the other consists of nucleotides that are not involved in resistance. This artificial plane is defined by two perpendicular imaginary axes, namely the postulated 2-fold symmetry axis (Agmon et al, 2005; Bashan et al,

2003) and the line connecting the bases of nucleotides G2553 and G2251 (**figure F8**), which are located at the boundaries of the space consumed by the rotatory motion of the translocating tRNA 3′ end from the A to the P site, and are engaged in Watson–Crick base pairing with both tRNAs (**figure F8**). Thus, the translocation of the tRNA required for nascent chain elongation is performed by two correlated motions: sideways progression of most of the tRNA molecule together with the mRNA by one codon at a time, and a rotatory motion of the aminoacylated 3′ end of the A site tRNA around the bond connecting it to the rest of the tRNA molecule. This bond coincides with the rotation axis of a pseudo-symmetrical region, comprising 180 nucleotides and located in and around the PTC (Agmon et al, 2005; Bashan et al, 2003) within the otherwise asymmetric ribosome. When viewing from the subunit interface, the PTC wall associated with PTC antibiotics resistance is located behind the site of peptide bond formation (called the PTC "rear wall"). It is the main constituent of PTC region that navigates and guides the translocation of the tRNA 3′ end from the A to the P site, by creating extensive transient interactions of its backbone.

Plot P1, panel a, shows that for clinically relevant complexes, half of the nucleotides mediating resistance to PTC antibiotics are located at distances of 6–12 Å from the affected antibiotic. For instance, pleuromutilins resistance is acquired by mutations of remotely located nucleotides of the 23S RNA as well as of residues of r-protein L3 (Ippolito et al, 2008; Pringle et al, 2004; Schluenzen et al, 2004). **Plot P1, panel b,** shows that approximately half of the nucleotides involved in resistance to PTC antibiotics affect two or more different families of antibiotics. In some cases resistance to drugs from up to five different antibiotic families are associated with same nucleotide (**table T2 and plot P1, panel b**).

Confining the resistance space to a single region in the PTC (**figure F7 and figure F8**) regardless of the bacterial species and the used methodology, indicates a functional distinction between the two sides of the PTC. Limiting the mutations to the PTC rear wall is consistent with the finding that in most cases the rear wall backbone, rather than its bases, plays a crucial functional role in guiding the translocation of A site tRNA 3′ end from A to P site during peptide bond formation (Agmon et al, 2005; Bashan et al, 2003).

3.3 Oligonucleotides as ribosomal inhibitors and as tools for structural and functional study

Twenty one target sites were selected from the 23S rRNA of the *E. coli* ribosome, based on structural, thermodynamical and genetic information, according to the following guidelines:

1. All target sites were limited to known functional centers, namely subunits interface, L7/12 and L1 stalks, the exit tunnel and the vicinity of the PTC.

2. A target site was preferred if it contained a mutation site that was previously related to antibiotic resistance, slow growth or lethality.

3. Tm (melting temperature) was set to be no less than 37 ºC in the presence of 1 μM ODN.

4. Intermolecular and intramolecular energy were set to be higher than -5.1 kcal/mol and -0.8 kcal/mol, respectively.

5. A target site was preferred if its total binding energy was relatively low.

6. Most exposed or most buried sites were selected.

7. ODNs length varied from 10 to 22 bases.

ODNs capability to inhibit protein translation of *E. coli* cell free system was assayed as described in methodology section above. The IC_{50} values were varied from 11 ± 2 uM to 148 ± 32 uM (**table T4**).

3.3.1 Correlation between IC_{50} and various ODN parameters

Analysis of the magnitude of inhibition of all 21 oligonucleotides in cell free system showed statistically significant correlation between IC_{50} and ODN length (r = -0.48685, p = 0.025206), as well as with the potential number of h-bonds (r = -0.50586, p

= 0.019304), i.e. the sum of 2*(sum(A)+sum(T)) + 3*(sum(G)+sum(C)), where r is the Pearson correlation coefficient, p is the observed significance level of the test (P-value, namely the probability of obtaining the observed correlation coefficient providing that the value of r is actually 0), sum(X) is the number of nucleotides of the type X in a given ODN. Other parameters (such as describing sequence conservation, calculated energy require for unwinding rRNA secondary structure, calculated energy gained by antisense binding, surface accessibility, number of hydrogen bonds between rRNA elements as observed crystallographically at the ribosomal target site etc.) resulted in correlation coefficients that are not statistically significant.

3.3.2. Effect of ODN length

Since the correlation observed between the extent of inhibition and ODN length, and with additional parameters linked to ODN length (e.g. 'number of potential h-bonds', namely the total number of donors and acceptors for Watson-Crick base pairing) the effect of ODN length was further examined. The oligonucleotides were split into two groups and correlation was recalculated for each group separately. One group included the relatively short sequences (length <= 14, n = 9) while the other group included the relatively long sequences (length > 14, n = 12). The cutoff at length of 14 bases was selected in order to obtain two groups with a similar number of ODNs (n).

3.4 Minimal ribosomal components with PTC structure and function

3.4.1 Construct design

Constructs were designed in order to create a mimic of the minimal rRNA construct that resembles the surrounding of the PTC and is capable of performing of peptide bond formation. Constructs were designed based on nucleotides sequence within parts or all of the symmetrical region within the 23S rRNA of *T. thermophilus*, which is identical to *D. radiodurans* (see **figure F9** and **table T5**).

Minimal constructs contained two helices, corresponding to the 23S rRNA H74 and H89 (named P1) or H90 and H93 (named A1) and the elbows connecting them. These two pairs of helices form the major part of the 2-fold symmetrical region, in which H74 and H89 are symmetrically related to H90 and H93 (Agmon et al, 2003; Agmon et al, 2005). The first nucleotide in P1 corresponds to nucleotide 2058. This nucleotides is a conserved A in eubacteria. In the construct it was replaced to G in order to meet the requirement for a leading guanosine in T7 RNAP transcript (Christopher, 1998). This alteration is not expected to result in a negative effect since this nucleotide is a conserved G in eukaryotes and archaea. Short sequences of up to six nucleotides were inserted in order to form a stable hairpins within positions where original rRNA helixes, which are longer in the contemporary ribosome, were truncated to form minimal constructs that include only the symmetrical region (Agmon et al, 2005). These inserted loops were designed based on the stable hexamer hairpin 5'-CUUCGG-3' (Cheong et al, 1990; Tuerk et al, 1988), a pattern found in various mRNA sequences in the center of palindrome-like patterns that were predicted to form stem loops (Tuerk et al, 1988). This pattern is also found in the 16S rRNA (starting in positions 207, 419, 1028, 1449) (Tuerk et al, 1988) and the 23S rRNA (starting at nucleotide 1691), where it folds as loops at the tips of a well defined rRNA helices in all ribosome crystal structures.

In the contemporary ribosome H80 and H97 carry the P-loop and the A-loop, respectively. These highly conserved loops reside within the symmetrical region, and form Watson-Crick base-pairs with the 3' CCA end of tRNA substrates within the contemporary ribosome. Sequences of these loops, together with rRNA sequences of the corresponding helices that carry them, were incorporated into the sequence of P1 and A1 to form larger constructs, namely P2 and A2 respectively, each bearing the entire nucleotides sequence of either the full A- or P-regions within the contemporary ribosome (**figure F9**, **table T5**). Additional constructs were designed based on the sequence of the entire 2-fold symmetrical region in the absence or presence of H80 and H90 and named AP1 and AP2, respectively (**figure F9**, **table T5**).

In the contemporary ribosome the interactions between the two parts of the symmetrical region involve an A-minor interaction (Nissen et al, 2001) between GNRA tetraloop, where N is any nucleotide and R is purine, in H93 at the A-region (including

the GNRA tetraloop sequence GUGA) and a receptor located at H74 in the P-region (**figure F10**). The sequence of H74 already included in both RNA constructs P1 and P2. Therefore, I have incorporated the GUGA sequence into these constructs, at the location corresponding to H89, instead of the hyper stable hairpin CUUCGG (constructs named P1c and P2c). This design was applied in order to enable the formation of P1 or P2 homodimers with enhanced affinity between monomers and probability for improved organization of a tightly packed dimer forming a pocket, rather than extended arrangement, based on symmetrical considerations. As it was impossible to predict if the inclusion of the GUGA tetra-loop per-se is sufficient and optimal to promote correct fold and dimerization, another two constructs were derived from P1c and P2c to carry the GUGA together with the addition of three adjacent base pairs from H93, named P1d and P2d (**table T5**).

3.4.2 Study of dimerization tendency

In order to test the hypothesis that the 2-fold symmetrical region surrounding the PTC evolved by gene fusion or gene duplication, I tested its tendency to form dimers, the prerequisite for obtaining the conformation required for supporting peptide bond formation by the two components, namely the A1 and P1 RNA constructs. Accordingly, mixtures of the two constructs, A1 and P1, were subjected to gel electrophoresis under denaturing and non-denaturing conditions. A single band was detected for A1 in both denaturing and non-denaturing gels, indicating for no dimerization under the experimental conditions (**figure F11**). However, For P1, one band was detected in denaturing gel but two bands appeared in the non-denaturing gel, hence indicating for P1 dimerization.

I have further verified this observation by Size Exclusion Chromatography (SEC) Chromatogram obtained following injection of 100 μg P1 RNA in 300 μM concentration indicated for coexistence of monomer, dimer and some higher order aggregates (**figure F12, top panel**). Approximately 750 μl fractions of both dimer and monomer were collected in 1 μM concentration. Fractions were kept on ice for >30 minutes, and then were injected again to the same column without any further treatment in order to evaluate

the quality of the separation and to assess the thermodynamic stability of the dimer and monomer for the time required for optional further enzymatic characterization (Knapp, 1989). Under such experimental conditions the enzymatic reaction can be immediately performed, before equilibrium between dimer and monomer is achieved, and hence detect even metastable RNA structures (Linnstaedt et al, 2006). Both chromatograms indicated a significant excess of the desired mer over the alternative entity, with a remarkably reduced amount of aggregates (**figure F12, bottom panel**), indicating that both dimer and monomer were thermodynamically stable under the experimental conditions.

The detection of two bands on non-denaturing gel can be an indication for two RNA conformers, rather than for a dimer and monomer. Therefore, using EMSA P1 was incubated at elevating RNA concentrations (10 nM to 160 μM), and then subjected to non-denaturing gel electrophoresis. The concentration-dependence of the slow migrating band that was observed indicates a homo-dimer formation with a Kd of ~10^{-5} M (**figure F13**). This result supports the hypothesis that the 2-fold symmetry region could have been potentially formed by the dimerization of one of its asymmetrical components.

Based on these results I focused on constructs designed according to P1 sequence. In an attempt to increase the tendency to dimerize, I incorporated a GNRA tetra-loop into the helix corresponding to H89 to form the RNA construct P1c (**figure F10, right panels**). P1c formed a dimer with higher affinity then P1, as can be seen by the increased intensity of the slaw migrating band that represents the dimer, in respect to the fast migrating band of the monomer (on non-denaturing PAGE in the presence of magnesium) (**figure F10, left panel**). In order to verify the contribution of the GNRA tetra-loop to dimer formation I introduced to P1c a "point mutation" G53U, thus abolishing the GNRA motif by converting the GUGA tetra-loop sequence to GUUA (**figure F14, right panel**). As a result, the "mutant" failed to form a dimer (**figure F14, left panel**), indicating that the GNRA sequence contributes to dimer formation, presumably through A-minor interactions.

Notably, the "mutation" G53U in P1c did not shifted the thermodynamic equilibrium between dimer and monomer to the reduced level observed in case of P1, but completely abolished dimerization to below detection limit. The minor sequence alteration between P1c and P1 at the helix corresponding to H89 in the contemporary

ribosome (see **figure F10** and text above) is limited to nucleotides designed to be located on the opposite side of this helix with respect to the presumed catalytic site. Therefore, a plausible scenario upon GNRA motif abolishment would predict that affinity between both monomers will be similar to the affinity observed between monomers in case of P1, rather than completely eliminated. As this is not the case the complete loss of dimerization of P1c "mutant" G53U, may indicate a more general role of the remote end of this helix in promoting dimerization also in case of P1. The contribution of the corresponding region of P1 to dimer formation is well supported by the loss of dimerization observed when either insertion or deletion of a designed single base-pair were introduced to the corresponding location of P1 (namely the remote end of H89 in the contemporary ribosome) (**figure F15**).

I tested the ability of RNA constructs A1, P1 and P1c to form heterodimers by EMSA (**figure F16**). While A1 failed to form heterodimers with either P1 or P1c, the latter two confirmed to form a stable heterodimer presumably via A-minor interactions between the receptor in P1 to the GNRA tetra-loop in P1c. An explanation for failure of A1 to form either hetero or homo dimers can be the misfolding of the RNA construct, although it was designed based on rRNA sequence that is naturally folded and stabilized within the contemporary ribosome. This hypothesis can be supported by inaccurate two-dimensional diagram that was predicted for A1 by mFold (Zuker, 1989) (**figure F17**), with compared to the structure observed for the corresponding region within the contemporary ribosome. In contrast to A1 folding prediction, both P1 and P1c were predicted to fold into a structure resembling their corresponding rRNA structure used for its design (**figure F17**).

Within the contemporary ribosome, the A- and P-loops are part of the symmetrical region that surrounds the PTC, but these loops are not involved in the actual positioning of very short substrates, such as puromycin derivatives (used for the fragment reaction), which may resemble the initial substrates. Based on this observation we have hypothesized that incorporation of the P-loop into either P1 or P1c constructs will not prevent their dimerization, assuming that these constructs indeed fold and dimerize into a structure resembling rRNA at the surroundings of the contemporary PTC. Accordingly, I incorporated nucleotides sequence of the P-loop, including H80 that carries it (**figures F9**

and F18), into the sequence of A1, P1 and P1c, resulting with RNA constructs A2, P2 and P2c, respectively (**table T5**). Non-denaturing PAGE confirmed that both P2 and P2c formed homodimers (**figure F18**), as could be expected in case of a properly folded and assembled dimers. Another RNA constructs that were tested are P1d and P2d. These were derived from P1c and P2c by incorporation of ten nucleotides sequence from H93 in the contemporary ribosome to P1 and P1c RNA sequence within the region designed to form a helix corresponding to H89 in the contemporary ribosome. This sequence included the GUGA tetraloop and three nucleotides up and down stream of it. No significant evidence for remarkable dimerization observed under the experimental condition tested for these two constructs, apart for a very pale band for dimer observed in case of P2d (**figure F18**).

3.4.3 Functional characterization: Assay for peptidyl transferase activity

In order to test the functional capabilities of RNA constructs that formed dimers I performed a serial of peptidyl transferase assays using minimal substrates (see **figure F19** for typical experiment results). Based on results obtained from the dimerization assays, I tested the following pairs of RNA constructs (final concentration of 1 uM each): P1:P1, P1c:P1c, P1:P1c, P2:P2, P2:P2c, P2c:P2c and P2c:P2d. In addition, I tested 1 uM of the constructs AP1 and AP2. Each experiment included a control containing 1 uM of *E. coli* 50S ribosomal subunit instead of RNA constructs.

I tested various incubation conditions, with pH ranging from 6.0 to 8.0, at room temperature, 37 ^{O}C or 50 ^{O}C, in the presence or absence of 30% methanol, using incubation periods of up to 24 hours. In none of these experiments a detectable catalytic activity was observed. In all experiments the *E. coli* 50S subunits control showed catalytic activity, indicating that product detection was experimentally valid. While it is impossible to exclude the possibility that lack of catalytic activity could potentially result from insufficient variation of experimental conditions, yet another plausible explanation could be deficient or inaccurate fold, dimer formation and/or substrates binding and positioning. Any of these potential problems could have emerged because these RNA constructs carry rRNA sequence from the contemporary ribosome. It is possible that

these sequences were evolved to fulfill their present task within the context of the ribosome. Therefore, when presented as an isolated entity it is possible that slight or extensive sequence alterations are required for enabling activity. Also, it is likely that the substrates used so far do not mimic the original substrates. Therefore, experiments with additional substrates will follow within the group.

4. Discussion

4.1 Pleuromutilins

4.1.1 Induced-fit mechanism for pleuromutilin binding

U2506 and U2585 undergo the most significant rRNA structural rearrangements upon binding of all three pleuromutilins. The conformational alterations of U2506 close tightly the binding pocket on the bound tricyclic core of all pleuromutilins (**figure F4, panels g–i**). The altered conformation of U2506 is stabilized by its hydrophobic interactions with the bound compound as well as by its interactions with U2585, which shifts away from the C14 extension. These interactions may account for the protection of N3 in U2506 and U2585 detected by chemical footprinting experiment done by 1-cyclohexyl-3-(2-morpholinoethyl) carbodiimide metho-*p*-toluenesulfonate (CMCT) in *E. coli* and *B. hyodysenteriae* in the presence of tiamulin, valnemulin, pleuromutilin, and the carbamate derivative SB-264128 (**figure F2**) (Bosling et al, 2003; Long et al, 2006; Poulsen et al, 2001; Pringle et al, 2004). It is worth noting that U2506 and U2585 motions are not conditional for pleuromutilins binding because slightly different location of the compound can partially compensate for it, as observed for tiamulin, an additional C14-sulfanyl acetate derivative (Schluenzen et al, 2004).

U2506 and U2585 nucleotides were identified as essential for ribosomal function biochemically (Youngman et al, 2004) and by systematic genetic selection (Hirabayashi et al, 2006). Both nucleotides are highly flexible, as noticed due to the differences of their orientations in crystals kept in environments that are close (Harms et al, 2001) or far (Ban et al, 2000) from physiological conditions. Consistently, conformational rearrangements of both nucleotides were observed in several crystal structures of complexes of the large ribosomal subunit with substrate analogs (Schmeing et al, 2005). In particular, U2585

flexibility was suggested to provide means for the 3′ end tRNA A- to P-site rotatory motion (Bashan et al, 2003), for D-amino acid rejection (Agmon et al, 2004), and for facilitating the synergistic action of the streptogramins (Harms et al, 2004). Hence, it appears that the binding of pleuromutilins utilizes the intrinsic flexibility of the ribosome, and thereby undergoes induced fit for binding of a large ensemble of compounds. Such induced-fit mechanism is consistent with kinetic data showing a prolonged retapamulin off-rate from *S. aureus* ribosomes, as well as with data suggesting that retapamulin inhibits P-site substrate binding independently of substrate concentration (Yan et al, 2006).

4.1.2 C14 extension is located in the PTC void.

In all cases, the C14 extension is located in the PTC and is held mainly by a two-to three–hydrogen-bond network between G2061 and the essential C21 keto of the bound compound (Egger & Reinshagen, 1976). In addition, in all cases U2585 is shifted away from the bound compound, to allow pleuromutilins binding. However, although in its altered location U2585 is in close proximity to C14 extension, it does not interact with it (**figure F4, panels d–f**), regardless of the chemical nature of the C14 extension. The most prominent alteration of U2585 has been observed in the presence of the rigid C14 extension of SB-571519, where U2585 is shifted >3 Å away from its native conformation (**figure F4 g**).

In all three cases, the C14 extensions are located at the PTC, between the acetylated and the peptidylated tRNA CCA ends (**figure F5, panel b**) (Nissen et al, 2000). All amino acids, of varying chemical characteristics, can be equally accommodated in this space. As this region contain only a few candidates for interactions, by its nature it should tolerate binding of various chemical moieties (Yonath, 2003b). This explains why all C14 extensions of the bound compounds hardly interact with PTC components. Instead, longer extensions may interact with distal rRNA nucleotides, as observed crystallographically for tiamulin (Schluenzen et al, 2004) or suggested, based on biochemical evidences, for valnemulin (Nissen et al, 2000). The small number of interactions of the C14 extensions rationalizes the similar activity of the

different C14 pleuromutilin derivatives (Berry et al, 1999) and permits more flexibility in the design of this moiety.

Comparing the present findings with previous results (Brooks et al, 2001; Egger & Reinshagen, 1976; Yan et al, 2006) indicated that conditional to pleuromutilins activity is the H-bond network of C14 with G2061. Of importance is the C21 carbonyl group (**figure F2**) that exists also in the pleuromutilin mother compound and forms an H-bond with G2061 in all of the structurally studied pleuromutilins. Consistently, attempts to eliminate this group resulted in significantly lower or no activity (Brooks et al, 2001; Egger & Reinshagen, 1976). An example for a successful modification of C14 extension is the C14-acyl-carbamate pleuromutilin derivatives, here represented by SB-571519. The slightly decreased binding affinity of the acyl-carbamate derivative in comparison to the sulfanyl acetate derivatives **(table T3)** may result from less optimal H-bond formed by the rigid acyl-carbamate group with G2061. This may lead to a slightly lower affinity of SB-571519 in respect to the studied sulfanyl acetate derivatives **(table T3)**. Importantly, it was shown that this slight decrease in activity can be tolerated clinically, in view of the low metabolism rates of the acyl-carbamates (Brooks et al, 2001; Hunt, 2000) compared with the C14-sulfanyl-acetate derivatives, which are rapidly eliminated by cytochrome P450 (Schuster et al, 1983).

4.1.3 Pleuromutilins resistance

The slow stepwise manner of the appearance of pleuromutilin resistance is consistent with the finding that several pleuromutilin resistant strains include more than one mutation (Pringle et al, 2004). Furthermore, the majority of the nucleotides that are mutated for acquiring resistance do not directly interact with the bound compound, consistent with the essentiality of the interacting nucleotides for ribosomal function. It appears, therefore, that the strategy for acquiring resistance to antibiotics targeting the vicinity of the PTC is mutating nonconserved ribosomal components that do not belong to the essential portion of the PTC, but are involved in an interaction network with PTC nucleotides in a manner crucial for the organization of its functional conformation. Thus,

it appears that these mutations reshape the conformation of this region, and/or alter its functional flexibility, in a fashion similar to allosteric rearrangements.

Likewise, the nonconserved region of L3 protein, residing in the vicinity of the PTC highly conserved nucleotides, enables such mechanism by mediating fine tuning of the PTC key nucleotides. Crystal structures of ribosome bound pleuromutilins confirm that the majority of pleuromutilin-rRNA interactions are between the tricyclic core and the binding pocket, and that most of these contacts are formed regardless of the chemical nature of their C14 extension **(figure F4, panels d–f)**. Furthermore, the addition of hydroxyl group at C2 in SB-571519 did not result in remarkably different binding orientation. Hence, it is not surprising that many pleuromutilin resistance mutations, identified in animal pathogens, involve nucleotides residing in the vicinity of the mutilin core, namely G2032, C2055, G2447, C2499, A2572, and U2504 (Pringle et al, 2004). A similar effect has been previously observed for several mutations in the nearby protein L3.

Although somewhat different in sequence, in all known structures of the large ribosomal subunit (Ban et al, 2000; Harms et al, 2001; Schuwirth et al, 2005; Selmer et al, 2006) protein L3 penetrates deeply toward the PTC (**figure F6, panels a–c**). Several mutations that cluster in a loop-like region of L3 at the proximity of the PTC induce resistance or reduce susceptibility to pleuromutilins (Pringle et al, 2004) (**figure F6, panel b**), presumably by altering the rRNA conformation or flexibility in the vicinity of the binding site (Bosling et al, 2003; Schluenzen et al, 2004). Similar resistance mechanisms were observed in yeasts (Fried & Warner, 1981; Jimenez et al, 1975), where mutations in the corresponding L3 residues 255 to 257 (Meskauskas et al, 2005) are responsible for anisomycin resistance.

In D50S/SB-571519 complex, Arg-144 (*D. radiodurans* numbering) of L3 interacts electrostatically with the phosphate of U2506 (**figure F6, panel a**), a nucleotide playing a key role in defining pleuromutilins binding surface, thus showing that this L3 region is capable of interacting with PTC nucleotides involved in pleuromutilin binding. These particular electrostatic interactions may be specific to *D. radiodurans*, as the entire six amino acids loop-like region of L3 hosting Arg-144 displays rather high sequence diversity (**figure F6, panel b**). Nevertheless, the principle of reshaping a functional

region composed of highly conserve nucleotides by using a nonconserved protein segment, is likely to be of a general character.

4.1.4 Pleuromutilins selectivity acquired by remote interactions

The key for clinical usage of antibiotics is their selectivity, namely the distinction between pathogens and their eukaryotic hosts. As the pleuromutilins bind to the highly or universally conserved PTC nucleotides (Cannone et al, 2002), their selectivity is attributed to differences in the shape of the boundaries of the binding pocket induced by the non conserved nucleotides residing in its vicinity. Thus, pleuromutilins seem to discriminate between eubacteria and higher organisms in a fashion similar to that used for acquiring resistance, exploiting interactions between nucleotides that do not interact with the bound compounds.

An example for kingdom-related differences in the orientation of a major element in the binding pocket is nucleotide U2504. In the structure of the eubacterial large ribosomal subunit from *D. radiodurans* (Harms et al, 2001), in its complex with pleuromutilin (Schluenzen et al, 2004), and in the eubacterial *E. coli* (Schuwirth et al, 2005) and *T. thermophilus* (Korostelev et al, 2006; Selmer et al, 2006) 70S ribosomal complexes, this nucleotide points toward the pleuromutilin binding pocket (**figure F6, panel d**), whereas in the large ribosomal subunit of the Archaeon *Haloarcula marismortui* (Ban et al, 2000) this nucleotide is tilted away from the binding site, presumably owing to its interactions with C2055. The difference in the identity of this nucleotide, namely cytosine in eubacteria but adenine in archaea (>80%) and eukarya (>96%) (Cannone et al, 2002) seems to indirectly alter the binding site conformation, and consequently the affinity of pleuromutilins. In support of this hypothesis is the C2055A mutation that decreases the susceptibility of *Brachyspira* species to pleuromutilins (Pringle et al, 2004). An additional component that may promote drug discrimination is the significant sequence variability of protein L3 loop-like region that may trigger rRNA conformational differences among the pleuromutilin-binding pocket of ribosomes from different species.

4.2 Structural basis for cross resistance between ribosomal PTC antibiotics

4.2.1 Resistance to PTC antibiotics is frequently acquired by mutating remote nucleotides

Because the PTC is highly conserved, the mechanisms for acquiring resistance are based on altering the conformation and the flexibility of nucleotides residing remotely. This trend is represented by **plot P1, panel a**, which shows that approximately half of the nucleotides mediating antibiotic resistance reside at distances >6 Å from the affected bound drug. Because such distances are too long for direct interactions with the drugs, resistance mechanisms to PTC antibiotics appear to be assisted by additional nucleotides capable of forming remote interactions that, in turn, alter the conformation and the flexibility of the binding pocket surface.

Because altering the identity of PTC nucleotides in the immediate vicinity of the bound antibiotics is unfavorable, a common mechanism for acquiring resistance to PTC antibiotics is mediated by altering remote nucleotides (**plot P1, panel a**). Indeed, proximity limitations would have severely limited the nucleotides pool, which in principle can be increased significantly (e.g., by approximately the power of three) with respect to the distance between the altered nucleotide and the antibiotic binding site. However, because of the requirement to trigger progressive conformational rearrangements, there is an upper limit for the nucleotides that can be included in the pool. Therefore, nucleotides residing at relatively large distances (>10Å) from the binding site are less likely to significantly alter its conformation. Hence, the advantage of increasing the pool of potential nucleotides by including nucleotides residing far from the binding site is compromised by their minute contribution to resistance, consistent with the existence of relatively fewer such cases. This effect can be somewhat compensated by altering more than a single nucleotide, as observed for pleuromutilins (Pringle et al, 2004).

Resistance acquired by remote mutations has also been observed in other antibiotics families. For example, erythromycin resistance can result from mutations in r-proteins L4 and L22 (Gregory & Dahlberg, 1999; Zaman et al, 2007) which do not interact directly with the bound drug (Schluenzen et al, 2001). However, because

resistance to macrolides can be acquired by alterations of nucleotides that interact with the drug, such as A2058, it seems that remotely acquired resistance to macrolides is an alternative mechanism, contrary to resistance to PTC antibiotics that is typically mediated by remote interactions.

4.2.2 U2504 at the crossroad of remote mutations networks that hamper binding of PTC antibiotics.

U2504, which plays pivotal roles in resistance to PTC antibiotics, is part of the binding pockets of phenicols (Schluenzen et al, 2001), lincosamides (Hansen et al, 2003; Schluenzen et al, 2001), pleuromutilins (Davidovich et al, 2007; Schluenzen et al, 2004) and oxazolidinones (Ippolito et al, 2008; Wilson et al, 2008) (**figure F20 and F21, panels a-r**). Mutations of U2504 were shown to promote resistance to pleuromutilin in the veterinary pathogens *Brachyspira pilosicoli* and *Brachyspira hyodysenteriae* (Pringle et al, 2004) and to linezolid in the archaeon *H. halobium* (Kloss et al, 1999). However, because it resides close to the PTC center, in the first layer of the PTC nucleotides that define the binding pocket surface, its alteration is expected to cause serious problems or be impossible. Consequently, altering neighboring nucleotides that can remotely affect 2504 may circumvent its essentiality. A mechanism by which U2504 is being perturbed by mutations of proximal nucleotides was suggested for tiamulin resistance (Pringle et al, 2004). This mechanism was later extended to be the general mechanism for resistance and selectivity of the pleuromutilin family, based on comparative crystallographic studies (Davidovich et al, 2007). Likewise, linezolid resistance was shown to be acquired by a mutation in nucleotide G2576 (G2576U) (Miller et al, 2008; Prystowsky et al, 2001) that is located >6 Å away from the bound drug (Ippolito et al, 2008), but can affect the conformation of nucleotide U2504.

Notably, in many cases, albeit not in all eubacteria, U2504 is a pseudouridine (Del Campo et al, 2005; Ofengand & Bakin, 1997). Nevertheless, regardless of being uridine or pseudouridine, in all known structures of eubacterial ribosomes, U2504 makes similar interactions with its neighboring nucleotides (e.g., 2447) (Ban et al, 2000; Harms et al, 2001; Korostelev et al, 2006; Schuwirth et al, 2005; Selmer et al, 2006). Interestingly, although this posttranscriptional modification is not necessary for smooth function of

eubacterial ribosomes, it was linked to resistance to PTC antibiotics, because *E. coli* strains deficient of it are more susceptible to tiamulin, clindamycin, and linezolid (Toh & Mankin, 2008). The elevated susceptibility by the loss of posttranscriptional modification can be attributed, in part, to the centrality of this nucleotide in the binding pocket of PTC antibiotics. The same rationale, namely, the centrality of nucleotide U2504, explains why the key role played by this nucleotide in PTC resistance mechanism is independent of the presence or absence of the additional potential interactions that may accomplish by pseudouridine compared with unmodified nucleotide.

4.2.3 Second layer nucleotides

The conformation and flexibility of nucleotide 2504 is dictated by five nucleotides residing within the second layer from the PTC wall, namely U2500, A2453, C2055, A2572 and G2447. The base pair U2500:A2453 forms a planar barrier that prevents U2504 from tilting away from the PTC (Harms et al, 2001; Selmer et al, 2006) (**figure F20** and **figure F21, panel b**). Thus, disruption of this pairing should release this planar barrier and enable U2504 to flip away from the PTC, in accord with the appearance of resistance to linezolid in clinical *S. aureus* isolates carrying a mutation U2500A (Meka et al, 2004) and in *H. halobium* strains carrying either of the induced mutations U2500C, A2453G, or A2453C (Kloss et al, 1999), all of which are predicted to destabilize the U2500:A2453 base pair.

G2447 is an additional nucleotide residing in the second layer that forms close contacts (approximately 3Å) with U2504 (**figure F20, panels c and d, and figure F21, panels c-h**). In D50S its interactions with U2504 involve a hydrogen bond between O4 carbonyl of the uracil base of U2504 and N3 of G2447 (**figure F20, panel c, and figure F21, panel e**). In the structures of *Thermus thermophilus* ribosomes (T70S) (Korostelev et al, 2006; Selmer et al, 2006) (**figure F20, panel c, and figure F21, panel e**) and of *E. coli* (E70S) (Schuwirth et al, 2005) O4 of U2504 faces the carbonyl O6 of G2447 base. In all structures G2447 stacks to U2500 (**figure 4, panel d, and figure F21, panel f**) and thus restrains its conformation and indirectly facilitates further stabilization of U2504 by U2500. Hence, it is not surprising that although G2447 does not interact with any PTC

antibiotics, its mutation G2447U (**figure F21, panel h**) confers resistance to linezolid in *E. coli* (Xiong et al, 2000) and *Mycobacterium smegmatis* (Sander et al, 2002), as well as to tiamulin in *E. coli* (Miller et al, 2008) and *B. hyodysenteriae* (Pringle et al, 2004). Furthermore, *E. coli* and *Bacillus stearothermophilus* ribosomes carrying the mutation G2447A (**figure F21, panel g**) are not impaired by chloramphenicol in peptide bond formation in vitro (Thompson et al, 2001), as positions 1 and 6 in this purine undergos a polar inversion in which both H bond donors become acceptors and vice versa. The conversion from purine to pyrimidine, followed the mutation G2447U, should result in exclusion of all interactions between these two nucleotides (**figure F21, panel h**), as well as lose the stacking interaction with U2500.

Whereas U2500, A2453, and G2447 limit potential motions of U2504 base, both C2055 and A2572, located approximately 3 Å away from it, block its ribose sugar from shifting away from the PTC (**figure F21, panels i and j**). The involvement of C2055 and A2572 in restraining U2504 conformation and flexibility is further supported by the tiamulin-resistant isolate of *B. hyodysenteriae* that carries both the mutations A2572U and C2055A (Pringle et al, 2004) (**figure F21, panel j**), although they are located 6 to 8 Å away from the bound drug. The purine to pyrimidine conversion after A2572U mutation releases the sterical hindrance of U2504 ribose sugar. In contrast, pyrimidine to purine conversion caused by the mutation C2055A can provide stacking interface that stabilizes U2504 in an altered conformation, with its base tilted away from the PTC, as observed for H50S (Ban et al, 2000), where nucleotide 2055 is an adenine. Thus, the different environments of U2504 in the eubacteria D50S and the archaea H50S, which is closer to eukaryotes in this aspect, explain the selectivity of pleuromutilins (Davidovich et al, 2007).

4.2.4 Third Layer Nucleotides

Alteration in the PTC surface can be performed also by third layer nucleotides. Among them nucleotide 2032, a highly conserved guanine in bacteria (>94%), is involved in resistance to PTC antibiotics of four different families although it reside 6 to 8 Å from each of the bound drugs. Thus, the mutation G2032A (**figure F20, panels e–**

g and figure F21, panels n-r) confers resistance to the antibiotics chloramphenicol, clindamycin (Douthwaite, 1992), and linezolid (Xiong et al, 2000) in *E. coli* but not in *T. thermophilus* (Gregory et al, 2005b). The same mutation in *B. hyodysenteriae*, together with L3 r-protein mutation Asn148Ser, confers resistance to tiamulin (Pringle et al, 2004). In addition, elevated minimum inhibitory concentrations (MICs) of linezolid were observed for *E. coli* strains carrying the mutations G2032U and G2032C (Xiong et al, 2000).

The base of G2032 in T70S is tilted by 90° with respect to the corresponding nucleotide in D50S (**figure F20, panel g, and figure F21, panel m**). In T70S carbonyl O6 of G2032 forms a hydrogen bond with O2′ hydroxyl of nucleotide A2453 and its secondary amine N1 forms a hydrogen bond with O4′ of A2572 (**figure F21, panel n**). G2032A mutation should lead to hydrogen bond acceptor imine at position N1 of adenine instead of the donor amine at position N1 of guanine. Additionally, the acceptor O6 carbonyl will be replaced by a primary amine that can act as a donor (**figure F21, panel o**). These two polar inversions are likely to result in local repulsions that will force nucleotides A2453 and A2572 to adopt a slightly altered U2504 conformation. In D50S the secondary amine N1 of G2032 is located within a short distance of 2.5 Å from the pyrimidine ring carbonyl oxygen of the proximal C2055 (**figure F21, panel p**). Hence, in the G2032A mutant the secondary amine hydrogen in position 1 of the guanine base is replaced by the imine lone pair of electrons located at the same position in adenine (**figure F21, panel q**). This substitution can result in repulsion between the imine nitrogen of the mutated A2032 and the carbonyl oxygen of C2055 pyrimidine ring. These interactions are likely to indirectly perturb the conformation and flexibility of the proximal U2504.

C2499, a 100% conserved nucleotide in eubacteria, is also located in the third layer. Assuming that the conformation of 2032 in *B. hyodysenteriae* resembles its conformation in D50S, the C2499A mutation should stabilize the mutated nucleotide A2032 (originally guanine) by a favorable polar attraction between the primary amine at position 6 of A2032 and the imine nitrogen of the nearby mutated A2499 (originally cytosine) (**figure F21, panel r**). The need for mutation in 2499 for the stabilization of 2032 in a conformation capable of pushing 2055 toward the PTC is further supported by

49

the difference in the conformations of 2032 in T70S and D50S (**figure F20, panel g, and figure F21, panel m**). It suggests that the unfavorable interactions with 2055, caused by the mutation G2032A without the compensating mutation C2499A, may stabilize 2032 in the T70S conformation. Therefore, the role of 2499 in resistance involves stabilizing the mutated 2032 in a conformation enabling repulsion of 2055, which ought to push 2504 toward the PTC and restrain its flexibility. Mutations in 2032 were observed in eubacteria, together with mutations of 2504 or 2499, as well as mutation in L3 Asn148Ser (Pringle et al, 2004). Whereas G2032A/U2504G double mutation should lead to resistance, mainly because of U2504G mutation, G2032A/C2499A should stimulate the mechanism proposed above (Pringle et al, 2004). The contribution of G2032A and C2499A double mutation for drug resistance in the later case is further supported by the reduced MIC of an identical bacterial strain that carries the same mutation in L3 protein but not the G2032A/C2499A double mutation (Pringle et al, 2004). The single example for mutation in 2032 causing linezolid resistance without the involvement of 2499 also fits with the general trait of resistance mediated by remote nucleotides.

The strategic position of U2504 at the A site and the cleft formed between it and the PTC rear wall serve as a hot spot for antibiotic binding (**figure F20, panel a, and figure F21, panel a**), but is less suitable to mediate resistance owing to its high conservation. However, U2504 possesses a significant level of flexibility, which seems to be used for acquiring pleuromutilin selectivity via remote interactions with less conserved components (Davidovich et al, 2007). The similarities in the binding modes of all PTC antibiotics suggest that this mechanism can be extended to contribute to the selectivity of all five classes of clinically useful PTC antibiotics, in accord with the findings showing that the conformation of nucleotide 2504 affects the binding and resistance of PTC antibiotics even when the drugs are not in direct contact with it. Further support for this suggestion is the finding that 2504 acquires bacterial-like conformation in H50S when binding linezolid, despite the huge differences (three orders of magnitudes) in drug concentrations required for obtaining crystallographically suitable complexes of H50S (Ippolito et al, 2008) compared with D50S (Wilson et al, 2008).

An additional nucleotide that can affect U2504 is its covalently attached neighbor A2503 (m^2A in *E. coli*) (Kowalak et al, 1995), which is prone to methylation in

eubacterial strains carrying the resistance Cfr gene (Kehrenberg et al, 2005; Long et al, 2006; Toh et al, 2007). Supporting the suggestion that A2503 induces resistance indirectly is the finding that although chloramphenicol does not interact with A2503, alterations of A2503 lead to resistance probably through altered conformations of U2504 and G2061, in line with the finding that nucleotides that shape the antibiotics binding pockets determine the usefulness of bound antibiotics (Bommakanti et al, 2008; Yonath, 2004; Yonath, 2005).

Although most of the resistance mechanisms mediated by indirect contacts seem to hinge on U2504, in a few cases PTC antibiotics are hindered remotely by other nucleotides. Among these are the mutation G2576U that was suggested to hamper linezolid binding indirectly by nucleotides U2505 and U2506 (Ippolito et al, 2008; Miller et al, 2005) in addition to U2504, as well as the resistance to the streptogramin$_A$ virginiamycin M$_1$ in the archaeon *H. halobium* by mutation in nucleotide A2059 (Porse & Garrett, 1999a'). An open issue is the case of chloramphenicol, for which resistance by nucleotides 2057, 2058, and 2062, located at the exit tunnel, was reported (Douthwaite, 1992; Ettayebi et al, 1985; Mankin & Garrett, 1991) similar to chloramphenicol location in the ribosome of archaeon *H. marismortui* (Hansen et al, 2003) that possesses sequence-resembling ribosomes from eukaryote, contrary to chloramphenicol binding site in the PTC of the pathogen model *D. radiodurans* (Schluenzen et al, 2001).

4.2.5 Resistance to various PTC antibiotics mediated by the same nucleotides

The involvement of the same nucleotides in resistance to several antibiotic families of different chemical natures (**table T2**, **figures F22, F7 and F8 and plot P1 panel b**) occurs presumably because of the overlapping binding sites of these drugs. As only a limited pool of nucleotides belonging to the PTC rear wall and the tunnel entrance is used for acquiring resistance, the probability of inducing resistance to more than a single antibiotic family by altering a given nucleotide is fairly high. This effect is further enhanced by the potential flexibility and the central location of U2504, which amplifies

its possible involvement in resistance to various PTC antibiotics by indirect perturbation of its conformation and flexibility.

Resistance and/or reduced susceptibility to different antibiotics include (*i*) *E. coli* carrying the mutation C2032A that confers resistance to chloramphenicol and clindamycin (Douthwaite, 1992); (*ii*) G2057A in other *E. coli* strains that causes resistance to chloramphenicol and erythromycin (Ettayebi et al, 1985); (*iii*) A2058G and A2058U in *E. coli* acquiring reduced susceptibility to chloramphenicol and resistance to clindamycin and erythromycin (Thompson et al, 2001); (*iv*) A2062C that appears together with the mutation Ser20Asn in L4 r-protein confirmed resistance to both streptogramins and macrolides in an isolate of *S. pneumoniae* (Mankin & Garrett, 1991).

Cross-resistance in the PTC was observed for linezolid and tiamulin in *S. aureus* following the mutation G2576U in all copies of 23S genes (Miller et al, 2008). An example for potential clinical threat of cross-resistance in the PTC is the multidrug resistance phenotype mediated by the *cfr* rRNA methyltransferase. This gene encodes a methyltransferase that modifies the PTC nucleotide A2503, and is responsible for resistance to phenicols, lincosamides, oxazolidinones, pleuromutilins, and streptogramin A antibiotics, namely the PhLOPS$_A$ group (Kehrenberg et al, 2005; Long et al, 2006). Remarkably, a clinical isolate of *S. aureus* was shown to carry this gene together with the *ermB* gene on the same chromosome (Toh et al, 2007) and in the same operon (Smith & Mankin, 2008). The expression of this operon, designated *mlr* for modification of large ribosomal subunit, resulted in a strain resistant to all clinically relevant antibiotics that target the large ribosomal subunit.

To conclude, cross-resistance is of great importance in light of the increasing use of diverse antibiotics families hitting the same, or a similar, target. Structural studies on resistance mechanisms to various clinically useful families of PTC antibiotics revealed that all share overlapping positions in the vicinity of the PTC rear wall and nucleotide U2504. Common traits of resistance to several antibiotic families showed that almost all of the 23S nucleotides mediating resistance cluster within a defined small region of the PTC confined by its rear wall. Furthermore, approximately half of the nucleotides implicated in PTC antibiotic resistance are not directly interacting with the bound drugs,

but reshape the binding pocket indirectly via networks of remote interactions, most of which through the flexible nucleotide U2504.

The significant number of nucleotides associated with multiple resistance phenotypes for PTC antibiotics indicates a linkage between structure, function, and resistance to several antibiotics, some with immense clinical value. Hence, the common traits of resistance revealed by this study may be useful in the design of preferred chemical moieties. Thus, it is likely that rather than being confined to the PTC rear wall, designing new PTC antibiotics with capabilities to dock to additional PTC components provides a feasible strategy for decreasing the probability for cross-resistance between PTC antibiotics.

4.3 Oligonucleotides as ribosomal inhibitors and as tools for structural and functional studies

The results suggested that the preferred target sites for short and long ODNs are characterized by different properties. It appears that short ODN displays lower IC_{50} when targeting rRNA sequences with relatively large accessible surface (r = -0.65145, p = 0.057327) and long 'base to base distance' (r = -0.72791, p = 0.026194), namely a rough measure for stacking, indicating the distance between N1 in pyrimidines and N9 in purines of two adjacent bases. These two parameters characterize accessible and poorly stacked rRNA. The results indicate that short oligonucleotides are preferred when target less conserved sequences, as was shown quantitatively by relatively low R_{seq} (Schneider et al, 1986) (r = 0.5244, p = 0.14724). Such sites can be found on the periphery of the ribosome. These results indicating that short ODNs bind preferably to relatively exposed sites where they do not have to compensate for the high energetic penalty of perturbing the 3D structure in order to approach the target site. In case of short ODNs, this penalty may not be rewarded back upon hybridization. This can be further supported by the fact that most of the active short ODNs were designed to bind target sites that are clustering in the L7/12 stalk (**figure F23**). This ribosomal moiety is highly flexible and rather accessible in comparison with the majority of the well packed internal 23S rRNA.

IC$_{50}$ in presence of the group of longer ODNs has poor correlation with r < 0.5 and p > 0.1 for all parameters, except for base to base distance (r = 0.53119, p = 0.075546). Thus, as of now solid conclusions regarding this group of ODNs, are not readily derived. However, the existence of statistically significant correlation between some of the tested parameters and the activity of long ODNs cannot be excluded. Hence, in order to derive such correlation coefficients, more observations are required (i.e. more ODNs to be tested).

A statistically valid (see **table T6**) multiple linear model making chemical and biological sense could not be constructed when all ODNs were considered. The only valid models could be derived only if ODNs with length ≤ 15 were considered. Any attempt to include ODNs with higher length resulted with non valid models. This is in agreement with the diversity between the short and the long ODNs and with the relatively weak correlation between the long ODNs and the various parameters.

A total of 8191 possible models were tested, considering all of the possible combinations of the best correlating parameters (n=13). The selected model contains four parameters (see **table T6** for full description and **plot P2** for predicted vs. observed IC$_{50}$). According to this model, an ODN is predicted to have a low IC$_{50}$ if its target site is characterized by a relatively long base to base distances, high sequence conservation, low duplex formation energy and high target structure energy, namely the energy required to unwind the secondary structure of the rRNA at the target site. The model accords with chemical and biological sense. In addition it is mostly compatible with the trends observed when correlations were calculated for each parameter individually. The only parameter that appeared with different trend in the model is sequence conservation (mean R$_{seq}$ (Schneider et al, 1986)). When tested individually, this parameter was positively correlated with IC$_{50}$ but when placed within the global model it displays a negative regression coefficient. This is presumably because the parameter serving as indicator for ribosomal periphery was first tested individually but pointed for highly functional centers when presented in the model.

4.4 Minimal ribosomal components with PTC structure and function

It is assumed that in the early terrestrial environment, the genetic information that was embedded in RNA sequences could lead to self replication and to phenotypes with catalytic properties (Eigen et al, 1989; Ferris, 2002; Lincoln & Joyce, 2009; Pino et al, 2008; Smith & Szathmáry, 1995; Woese, 1973; Woese, 2001; Yarus, 2002). In the case of the proto-ribosome, it is likely that the more efficient and more stable RNA dimers with pocket like structure that functioned as proto-ribosomes by positioning the substrates in a spatial arrangement facilitating peptide bond formation, had a better chance to be replicated. Thus, the surviving ancient pockets could become the templates for the ancient ribosomes. In a later stage these molecular entities underwent optimization from non-genetic peptide bond formation towards performing genetically driven translation.

The transition from a molecule forming peptide bonds to an elaborate apparatus capable of decoding genetic information seems to be coupled with the evolving genetic code and the proto-ribosome substrates. A higher level of efficiency could have been achieved by the creation of a supporting environment alongside the elongation of the substrates form the minimal mono- or oligonucleotide/amino acid conjugates, towards the modern tRNA. The conversion into longer compounds with a contour that can complement the inner surface of the reaction pocket occurred concurrently with proto-ribosome size increase, by the mutational optimization, aimed at accurate substrate positioning, which in the modern ribosome is governed by remote interactions between the RNA and the cavity leading to the PTC (Bashan et al, 2003; Yonath, 2003b). This scenario accords with the fact that in the contemporary ribosome the symmetry is related to the backbone fold and not to the nucleotide sequence, thus emphasizing the superiority of functional requirement over sequence conservation.

A substantial increase in the catalytic rate could be obtained by the inclusion of peripheral elements, as observed for other ribozymes (Voytek & Joyce, 2007). These additionally recruited structural elements could have been RNA chains or elongated oligopeptides that interacted with the proto-ribosome and its surroundings in a manner resembling the protein-RNA interactions in the modern ribosome. These could contribute to the suitability of the apparatus to act as an efficient machine and to support the

emergence of genetic code translation. Mutational optimization that facilitated distinction between the two sides of the active site allowed differentiation between the two substrates, namely the acylated and the peptidyl tRNA. Besides functional optimization the nucleotide identities and conformations evolved for enhancing the stability of the symmetrical region. Consequently, the orientation of some RNA bases of the contemporary symmetrical region violate the internal symmetry (**figure F24**). Thus, with selection pressure for increased stability and efficiency, the proto-ribosome evolved into an entity that can provide all the activities required for nascent protein elongation in the modern ribosome. As such, the modern ribosome could have evolved gradually around the symmetrical region until it acquired its final shape and could perform programmed translation, either hierarchically (Bokov & Steinberg, 2009) or by another mechanism (e.g. (Fox & Naik, 2004)).

The emergence of Life required an apparatus for synthesizing polypeptides capable of performing catalytic or other life supporting tasks, i.e. the ribosome. The proto-ribosome, which served as the precursor for the modern translation machinery by its capacity to autonomously catalyze peptide bonds forming non-coded amino acid oligo- or polymers, is suggested to have appeared by spontaneous dimeric assembly of two self-folding RNA chains. These pocket-like dimers offered a catalytic site for favorable positioning of the substrates involved in peptide bond formation and simple elongation. Assuming the existence of a proto ribosome my studies suggest that it is likely that it is still embedded in the core of the modern ribosome, and that the tendency for dimerization of the proto-ribosome, a prerequisite for obtaining the catalytic center, is intrinsically linked to its sequence thus indicating functional selection at the molecular level in the prebiotic era.

5. References

Abelian A, Walsh AP, Lentzen G, Aboul-Ela F, Gait MJ (2004) Targeting the A site RNA of the Escherichia coli ribosomal 30 S subunit by 2'-O-methyl oligoribonucleotides: a quantitative equilibrium dialysis binding assay and differential effects of aminoglycoside antibiotics. *Biochem J* **383**(Pt 2)**:** 201-208

Agmon I, Amit M, Auerbach T, Bashan A, Baram D, Bartels H, Berisio R, Greenberg I, Harms J, Hansen HA, Kessler M, Pyetan E, Schluenzen F, Sittner A, Yonath A, Zarivach R (2004) Ribosomal crystallography: a flexible nucleotide anchoring tRNA translocation, facilitates peptide-bond formation, chirality discrimination and antibiotics synergism. *FEBS Lett* **567**(1)**:** 20-26.

Agmon I, Auerbach T, Baram D, Bartels H, Bashan A, Berisio R, Fucini P, Hansen HA, Harms J, Kessler M, Peretz M, Schluenzen F, Yonath A, Zarivach R (2003) On peptide bond formation, translocation, nascent protein progression and the regulatory properties of ribosomes. *Eur J Biochem* **270**(12)**:** 2543-2556

Agmon I, Bashan A, Yonath A (2006) On Ribosome Conservation and Evolution. *Isr J Ecol Evol* **52:** 359-379

Agmon I, Bashan A, Zarivach R, Yonath A (2005) Symmetry at the active site of the ribosome: structural and functional implications. *Biol Chem* **386**(9)**:** 833-844

Agmon I, Davidovich C, Bashan A, Yonath A (2009) Identification of the prebiotic translation apparatus within the contemporary ribosome. *http://precedingsnaturecom/documents/2921/version/1*

Amit M, Berisio R, Baram D, Harms J, Bashan A, Yonath A (2005) A crevice adjoining the ribosome tunnel: hints for cotranslational folding. *FEBS Lett* **579**(15)**:** 3207-3213

Anderson RM, Kwon M, Strobel SA (2007) Toward ribosomal RNA catalytic activity in the absence of protein. *J Mol Evol* **64**(4)**:** 472-483

Auerbach T, Mermershtain I, Bashan A, Davidovich C, Rosenberg H, Sherman DH, Yonath A (2009) Structural basis for the antibacterial activity of the 12-membered-ring mono-sugar macrolide methymycin. *Biotechnolog* **84:** 24-35

Auerbach T, Mermershtain I, Davidovich C, Bashan A, Belousoff M, Wekselman I, Zimmerman E, Xiong L, Klepacki D, Arakawa K, Kinashi H, Mankin AS, Yonath A (2010) The structure of ribosome-lankacidin complex reveals ribosomal sites for synergistic antibiotics. *Proc Natl Acad Sci U S A* **107**(5)**:** 1983-1988

Auerbach-Nevo T, Zarivach R, Peretz M, Yonath A (2005) Reproducible growth of well diffracting ribosomal crystals. *Acta Crystallogr D Biol Crystallogr* **61:** 713-719

Bailey S (1994) The CCP4 suite - programs for protein crystallography. *Acta Crystallogr D Biol Crystallogr* **50:** 760-763

Ban N, Nissen P, Hansen J, Moore PB, Steitz TA (2000) The complete atomic structure of the large ribosomal subunit at 2.4 A resolution. *Science* **289**(5481)**:** 905-920

Bashan A, Agmon I, Zarivach R, Schluenzen F, Harms J, Berisio R, Bartels H, Franceschi F, Auerbach T, Hansen HAS, Kossoy E, Kessler M, Yonath A (2003) Structural basis of the ribosomal machinery for peptide bond formation, translocation, and nascent chain progression. *Mol Cell* **11:** 91-102

Bashan A, Yonath A (2008) Correlating ribosome function with high-resolution structures. *Trends Microbiol* **16**(7)**:** 326-335

Bashan A, Zarivach R, Schluenzen F, Agmon I, Harms J, Auerbach T, Baram D, Berisio R, Bartels H, Hansen HA, Fucini P, Wilson D, Peretz M, Kessler M, Yonath A (2003b) Ribosomal crystallography: Peptide bond formation and its inhibition. *Biopolymers* **70**(1)**:** 19-41.

Berisio R, Harms J, Schluenzen F, Zarivach R, Hansen HA, Fucini P, Yonath A (2003) Structural insight into the antibiotic action of telithromycin against resistant mutants. *J Bacteriol* **185**(14)**:** 4276-4279.

Berry V, Dabbs S, Frydrych CH, Hunt E, Woodnutt G, Sanderson FD (1999) Pleuromutilin derivatives as antimicrobials. *Patent number WO9921855*

Bieling P, Beringer M, Adio S, Rodnina MV (2006) Peptide bond formation does not involve acid-base catalysis by ribosomal residues. *Nat Struct Mol Biol* **13**(5)**:** 424-428

Blaha G, Gurel G, Schroeder SJ, Moore PB, Steitz TA (2008) Mutations Outside the Anisomycin-Binding Site Can Make Ribosomes Drug-Resistant. *J Mol Biol* **379**(3)**:** 505-519

Bokov K, Steinberg SV (2009) A hierarchical model for evolution of 23S ribosomal RNA. *Nature* **457**(7232)**:** 977-980

Bommakanti AS, Lindahl L, Zengel JM (2008) Mutation from guanine to adenine in 25S rRNA at the position equivalent to E. coli A2058 does not confer erythromycin sensitivity in Sacchromyces cerevisae. *RNA* **14**(3)**:** 460-464

Bosling J, Poulsen SM, Vester B, Long KS (2003) Resistance to the peptidyl transferase inhibitor tiamulin caused by mutation of ribosomal protein l3. *Antimicrob Agents Chemother* **47**(9)**:** 2892-2896.

Bretscher MS, Marcker KA (1966) Polypeptidyl-sigma-ribonucleic acid and amino-acyl-sigma-ribonucleic acid binding sites on ribosomes. *Nature* **211**(5047)**:** 380-384

Brooks G, Burgess W, Colthurst D, Hinks JD, Hunt E, Pearson MJ, Shea B, Takle AK, Wilson JM, Woodnutt G (2001) Pleuromutilins. Part 1. The identification of novel mutilin 14-carbamates. *Bioorg Med Chem* **9**(5)**:** 1221-1231

Brunger AT, Adams PD, Clore GM, DeLano WL, Gros P, Grosse-Kunstleve RW, Jiang JS, Kuszewski J, Nilges M, Pannu NS, Read RJ, Rice LM, Simonson T, Warren GL (1998) Crystallography & NMR system: A new software suite for macromolecular structure determination. *Acta Crystallogr D Biol Crystallogr* **54**(Pt 5)**:** 905-921

Cannone JJ, Subramanian S, Schnare MN, Collett JR, D'Souza LM, Du Y, Feng B, Lin N, Madabusi LV, Müller KM, Pande N, Shang Z, Yu N, Gutell RR (2002) The Comparative RNA Web (CRW) Site: an online database of comparative sequence and structure information for ribosomal, intron, and other RNAs. *BMC Bioinformatics* **3**(2)**:** 1-31

Carter AP, Clemons WM, Jr., Brodersen DE, Morgan-Warren RJ, Hartsch T, Wimberly BT, Ramakrishnan V (2001) Crystal structure of an initiation factor bound to the 30S ribosomal subunit. *Science* **291**(5503)**:** 498-501

Champney WS, Rodgers WK (2007) Retapamulin Inhibition of Translation and 50S Ribosomal Subunit Formation in Staphylococcus aureus Cells. *Antimicrob Agents Chemother* **51**(9)**:** 3385-3387

Cheong C, Varani G, Tinoco I, Jr. (1990) Solution structure of an unusually stable RNA hairpin, 5'GGAC(UUCG)GUCC. *Nature* **346**(6285)**:** 680-682

Christopher WS (1998) *RNA:Protein interactions: A Practical approach*, 1st edn.: Oxford University Press.

Clamp M, Cuff J, Searle SM, Barton GJ (2004) The Jalview Java alignment editor. *Bioinformatics* **20**(3)**:** 426-427

Davidovich C, Bashan A, Auerbach-Nevo T, Yaggie RD, Gontarek RR, Yonath A (2007) Induced-fit tightens pleuromutilins binding to ribosomes and remote interactions enable their selectivity. *Proc Natl Acad Sci U S A* **104**(11)**:** 4291-4296

Del Campo M, Recinos C, Yanez G, Pomerantz SC, Guymon R, Crain PF, McCloskey JA, Ofengand J (2005) Number, position, and significance of the pseudouridines in the large subunit ribosomal RNA of Haloarcula marismortui and Deinococcus radiodurans. *RNA* **11**(2)**:** 210-219

DeLano WL. (2002) The PyMOL Molecular Graphics System. San Carlos California USA.

Ding Y, Lawrence CE (2001) Statistical prediction of single-stranded regions in RNA secondary structure and application to predicting effective antisense target sites and beyond. *Nucleic Acids Res* **29**(5)**:** 1034-1046

Dornhelm P, Hogenauer G (1978) The effects of tiamulin, a semisynthetic pleuromutilin derivative, on bacterial polypeptide chain initiation. *Eur J Biochem* **91**(2)**:** 465-473

Douthwaite S (1992) Interaction of the antibiotics clindamycin and lincomycin with Escherichia coli 23S ribosomal RNA. *Nucleic Acids Res* **20**(18)**:** 4717-4720

Douthwaite S, Aagaard C (1993) Erythromycin binding is reduced in ribosomes with conformational alterations in the 23 S rRNA peptidyl transferase loop. *J Mol Biol* **232**(3)**:** 725-731

Egger H, Reinshagen H (1976) New pleuromutilin derivatives with enhanced antimicrobial activity.II.Structure-activity correlations. *J Antibiot (Tokyo)* **29**(9)**:** 923-927.

Eigen M, Lindemann BF, Tietze M, Winkler-Oswatitsch R, Dress A, von Haeseler A (1989) How old is the genetic code? Statistical geometry of tRNA provides an answer. *Science* **244**(4905)**:** 673-679

Emsley P, Cowtan K (2004) Coot: model-building tools for molecular graphics. *Acta Crystallogr D Biol Crystallogr* **60**(Pt 12 Pt 1)**:** 2126-2132

Ettayebi M, Prasad SM, Morgan EA (1985) Chloramphenicol-erythromycin resistance mutations in a 23S rRNA gene of Escherichia coli. *J Bacteriol* **162**(2)**:** 551-557

Ferris JP (2002) Montmorillonite catalysis of 30-50 mer oligonucleotides: laboratory demonstration of potential steps in the origin of the RNA world. *Orig Life Evol Biosph* **32**(4)**:** 311-332

Fox GE, Naik AK (2004) The Evolutionary History of the Ribosome. In *The Genetic Code and the Origin of Life*, Ribas de Poplana L (ed), pp 92-105. Landes Bioscience

Fried HM, Warner JR (1981) Cloning of yeast gene for trichodermin resistance and ribosomal protein L3. *Proc Natl Acad Sci U S A* **78**(1)**:** 238-242

Gindulyte A, Bashan A, Agmon I, Massa L, Yonath A, Karle J (2006) The transition state for formation of the peptide bond in the ribosome. *Proc Natl Acad Sci U S A* **103**(36)**:** 13327-13332

Goldstein EJ, Citron DM, Merriam CV, Warren YA, Tyrrell KL, Fernandez HT (2006) Comparative in vitro activities of retapamulin (SB-275833) against 141 clinical isolates of Propionibacterium spp., including 117 P. acnes isolates. *Antimicrob Agents Chemother* **50**(1)**:** 379-381

Gregory ST, Carr JF, Rodriguez-Correa D, Dahlberg AE (2005b) Mutational Analysis of 16S and 23S rRNA Genes of Thermus thermophilus. *J Bacteriol* **187**(14)**:** 4804-4812

Gregory ST, Dahlberg AE (1999) Erythromycin resistance mutations in ribosomal proteins L22 and L4 perturb the higher order structure of 23 S ribosomal RNA. *J Mol Biol* **289**(4)**:** 827-834

Gregory ST, Dahlberg AE (2004) Peptide bond formation is all about proximity. *Nature Structural & Molecular Biology* **11:** 586 -587

Hansen JL, Ippolito JA, Ban N, Nissen P, Moore PB, Steitz TA (2002) The structures of four macrolide antibiotics bound to the large ribosomal subunit. *Mol Cell* **10**(1)**:** 117-128

Hansen JL, Moore PB, Steitz TA (2003) Structures of five antibiotics bound at the peptidyl transferase center of the large ribosomal subunit. *J Mol Biol* **330**(5)**:** 1061-1075

Harms J, Schluenzen F, Fucini P, Bartels H, Yonath A (2004) Alterations at the peptidyl transferase centre of the ribosome induced by the synergistic action of the streptogramins dalfopristin and quinupristin. *BMC Biol* **2**(1)**:** 4;1-10

Harms J, Schluenzen F, Zarivach R, Bashan A, Gat S, Agmon I, Bartels H, Franceschi F, Yonath A (2001) High resolution structure of the large ribosomal subunit from a mesophilic eubacterium. *Cell* **107**(5)**:** 679-688

Hausner TP, Atmadja J, Nierhaus KH (1987) Evidence that the G2661 region of 23S rRNA is located at the ribosomal binding sites of both elongation factors. *Biochimie* **69**(9)**:** 911-923.

Hildebrandt J, Berner H, Laber G, Schuetze E, Turnowsky F (1983) TDM 85.530 - a pleuromutilin derivative and its spectrum of antibacterial activity in vitro. *Proc Int Congr Chemother* **13th 5:** 108/124-108/128

Hill WE, Tassanakajohn A, Tapprich WE (1990) Interaction of tRNA with domain II of 23S rRNA. *Biochim Biophys Acta* **1050**(1-3)**:** 45-50

Hirabayashi N, Sato NS, Suzuki T (2006) Conserved loop sequence of helix 69 in Escherichia coli 23 S rRNA is involved in A-site tRNA binding and translational fidelity. *J Biol Chem* **281**(25)**:** 17203-17211

Hodgin LA, Hogenauer G (1974) The mode of action of pleuromutilin derivatives. Effect on cell-free polypeptide synthesis. *Eur J Biochem* **47**(3)**:** 527-533

Hoegenauer G, Brunowsky W (1983) Mode of action of TDM 85-530. *Proc Int Congr Chemother* **13th 5:** 108/133-108/137

Hogenauer G (1975) The mode of action of pleuromutilin derivatives. Location and properties of the pleuromutilin binding site on Escherichia coli ribosomes. *Eur J Biochem* **52**(1)**:** 93-98.

Hunt E (2000) Pleuromutilin antibiotics. *Drugs of the Future* **25**(11)**:** 1163-1168

Ippolito JA, Kanyo ZF, Wang D, Franceschi FJ, Moore PB, Steitz TA, Duffy EM (2008) Crystal Structure of the Oxazolidinone Antibiotic Linezolid Bound to the 50S Ribosomal Subunit. *J Med Chem* **51**(12)**:** 3353-3356

Jayaraman K, McParland K, Miller P, Ts'o PO (1981) Selective inhibition of Escherichia coli protein synthesis and growth by nonionic oligonucleotides complementary to the 3' end of 16S rRNA. *Proc Natl Acad Sci U S A* **78**(3)**:** 1537-1541

Jimenez A, Sanchez L, Vazquez D (1975) Simultaneous ribosomal resistance to trichodermin and anisomycin in Saccharomyces cerevisiae mutants. *Biochim Biophys Acta* **383**(4)**:** 427-434

Jones RN, Fritsche TR, Sader HS, Ross JE (2006) Activity of retapamulin (SB-275833), a novel pleuromutilin, against selected resistant gram-positive cocci. *Antimicrob Agents Chemother* **50**(7)**:** 2583-2586

Jones TA, Zou JY, Cowan SW, Kjeldgaard (1991) Improved methods for building protein models in electron density maps and the location of errors in these models. *Acta Crystallogr A* **47**(Pt 2)**:** 110-119

Kavanagh F, Hervey A, Robbins WJ (1951) Antibiotic substances from basidiomycetes. VIII. Pleurotus mutilus (Fr.) Sacc. & Pleurotus passeckerianus Pilat. *Proc Natl Acad Sci U S A* **37:** 570-574

Kehrenberg C, Schwarz S, Jacobsen L, Hansen LH, Vester B (2005) A new mechanism for chloramphenicol, florfenicol and clindamycin resistance: methylation of 23S ribosomal RNA at A2503. *Mol Microbiol* **57**(4)**:** 1064-1073

Khaitovich P, Mankin AS, Green R, Lancaster L, Noller HF (1999a) Characterization of functionally active subribosomal particles from Thermus aquaticus. *Proc Natl Acad Sci U S A* **96**(1)**:** 85-90

Khaitovich P, Tenson T, Kloss P, Mankin AS (1999) Reconstitution of functionally active Thermus aquaticus large ribosomal subunits with in vitro-transcribed rRNA. *Biochemistry* **38**(6)**:** 1780-1788

Kim I, McKenna SA, Viani Puglisi E, Puglisi JD (2007) Rapid purification of RNAs using fast performance liquid chromatography (FPLC). *Rna* **13**(2)**:** 289-294

Kloss P, Xiong L, Shinabarger DL, Mankin AS (1999) Resistance mutations in 23 S rRNA identify the site of action of the protein synthesis inhibitor linezolid in the ribosomal peptidyl transferase center. *J Mol Biol* **294**(1)**:** 93-101

Knapp G (1989) Enzymatic approaches to probing of RNA secondary and tertiary structure. *Methods Enzymol* **180:** 192-212

Korostelev A, Trakhanov S, Laurberg M, Noller HF (2006) Crystal Structure of a 70S Ribosome-tRNA Complex Reveals Functional Interactions and Rearrangements. *Cell* **126:** 1065-1077

Kosowska-Shick K, Clark C, Credito K, McGhee P, Dewasse B, Bogdanovich T, Appelbaum PC (2006) Single- and multistep resistance selection studies on the activity of retapamulin compared to other agents against Staphylococcus aureus and Streptococcus pyogenes. *Antimicrob Agents Chemother* **50**(2)**:** 765-769

Kowalak JA, Bruenger E, McCloskey JA (1995) Posttranscriptional modification of the central loop of domain V in Escherichia coli 23 S ribosomal RNA. *J Biol Chem* **270**(30)**:** 17758-17764

Lasater LS, Montesano-Roditis L, Cann PA, Glitz DG (1990) Localization of an oligodeoxynucleotide complementing 16S ribosomal RNA residues 520-531 on the small

subunit of Escherichia coli ribosomes: electron microscopy of ribosome-cDNA-antibody complexes. *Nucleic Acids Res* **18**(3)**:** 477-485

Lincoln TA, Joyce GF (2009) Self-Sustained Replication of an RNA Enzyme. *Science* **323**(5918)**:** 1229-1232

Linnstaedt SD, Kasprzak WK, Shapiro BA, Casey JL (2006) The role of a metastable RNA secondary structure in hepatitis delta virus genotype III RNA editing. *Rna* **12**(8)**:** 1521-1533

Long KS, Poehlsgaard J, Kehrenberg C, Schwarz S, Vester B (2006) The Cfr rRNA Methyltransferase Confers Resistance to Phenicols, Lincosamides, Oxazolidinones, Pleuromutilins, and Streptogramin A Antibiotics. *Antimicrob Agents Chemother* **50**(7)**:** 2500-2505

Lu XJ, Olson WK (2003) 3DNA: a software package for the analysis, rebuilding and visualization of three-dimensional nucleic acid structures. *Nucleic Acids Res* **31**(17)**:** 5108-5121

Lukavsky PJ, Puglisi JD (2004) Large-scale preparation and purification of polyacrylamide-free RNA oligonucleotides. *Rna* **10**(5)**:** 889-893

Mankin AS, Garrett RA (1991) Chloramphenicol resistance mutations in the single 23S rRNA gene of the archaeon Halobacterium halobium. *J Bacteriol* **173**(11)**:** 3559-3563

Marconi RT, Hill WE (1989) Evidence for a tRNA/rRNA interaction site within the peptidyltransferase center of the Escherichia coli ribosome. *Biochemistry* **28**(2)**:** 893-899

Marconi RT, Lodmell JS, Hill WE (1990) Identification of a rRNA/chloramphenicol interaction site within the peptidyltransferase center of the 50 S subunit of the Escherichia coli ribosome. *J Biol Chem* **265**(14)**:** 7894-7899

Marshall RA, Aitken CE, Dorywalska M, Puglisi JD (2008) Translation at the Single-Molecule Level. *Annu Rev Biochem* **77:** 177-203

Mathews DH, Sabina J, Zuker M, Turner DH (1999) Expanded sequence dependence of thermodynamic parameters improves prediction of RNA secondary structure. *J Mol Biol* **288**(5)**:** 911-940

McKenna SA, Kim I, Puglisi EV, Lindhout DA, Aitken CE, Marshall RA, Puglisi JD (2007) Purification and characterization of transcribed RNAs using gel filtration chromatography. *Nat Protoc* **2**(12)**:** 3270-3277

Meka VG, Pillai SK, Sakoulas G, Wennersten C, Venkataraman L, DeGirolami PC, Eliopoulos GM, Moellering RC, Jr., Gold HS (2004) Linezolid resistance in sequential Staphylococcus aureus isolates associated with a T2500A mutation in the 23S rRNA gene and loss of a single copy of rRNA. *J Infect Dis* **190**(2)**:** 311-317

Meskauskas A, Petrov AN, Dinman JD (2005) Identification of functionally important amino acids of ribosomal protein L3 by saturation mutagenesis. *Mol Cell Biol* **25**(24)**:** 10863-10874

Meyer HA, Triana-Alonso F, Spahn CM, Twardowski T, Sobkiewicz A, Nierhaus KH (1996) Effects of antisense DNA against the alpha-sarcin stem-loop structure of the ribosomal 23S rRNA. *Nucleic Acids Res* **24**(20)**:** 3996-4002

Miller K, Dunsmore CJ, Fishwick CW, Chopra I (2008) Linezolid and Tiamulin Cross-Resistance in Staphylococcus Aureus Mediated by Point Mutations in the Peptidyl-Transferase Center. *Antimicrob Agents Chemother* **52**(5)**:** 1737-1742

Miller VM, Paulson HL, Gonzalez-Alegre P (2005) RNA interference in neuroscience: progress and challenges. *Cell Mol Neurobiol* **25**(8)**:** 1195-1207

Monro RE, Marcker KA (1967) Ribosome-catalysed reaction of puromycin with a formylmethionine-containing oligonucleotide. *J Mol Biol* **25**(2)**:** 347-350

Moore PB, Steitz TA (2003) The structural basis of large ribosomal subunit function. *Annu Rev Biochem* **72:** 813-850.

Muckstein U, Tafer H, Hackermuller J, Bernhart SH, Stadler PF, Hofacker IL (2006) Thermodynamics of RNA-RNA binding. *Bioinformatics* **22**(10)**:** 1177-1182

Muralikrishna P, Cooperman BS (1991) A photolabile oligodeoxyribonucleotide probe of the peptidyltransferase center: identification of neighboring ribosomal components. *Biochemistry* **30**(22)**:** 5421-5428

Murray RW, Melchior EP, Hagadorn JC, Marotti KR (2001) Staphylococcus aureus cell extract transcription-translation assay: firefly luciferase reporter system for evaluating protein translation inhibitors. *Antimicrob Agents Chemother* **45**(6)**:** 1900-1904

Nissen P, Ippolito JA, Ban N, Moore PB, Steitz TA (2001) RNA tertiary interactions in the large ribosomal subunit: the A-minor motif. *Proc Natl Acad Sci U S A* **98**(9)**:** 4899-4903

Nissen P, Kjeldgaard M, Nyborg J (2000) Macromolecular mimicry. *Embo J* **19**(4)**:** 489-495

Nitta I, Kamada Y, Noda H, Ueda T, Watanabe K (1998a) Reconstitution of peptide bond formation with Escherichia coli 23S ribosomal RNA domains. *Science* **281**(5377)**:** 666-669

Nitta I, Kamada Y, Noda H, Ueda T, Watanabe K (1999a) Peptide bond formation: retraction. *Science* **283**(5410)**:** 2019-2020

Nitta I, Ueda T, Watanabe K (1998b) Possible involvement of Escherichia coli 23S ribosomal RNA in peptide bond formation. *Rna* **4**(3)**:** 257-267

Nitta I, Ueda T, Watanabe K (1999b) Retraction. *Rna* **5**(5)**:** 707

Noller HF, Hoffarth V, Zimniak L (1992) Unusual resistance of peptidyl transferase to protein extraction procedures. *Science* **256**(5062)**:** 1416-1419

Ofengand J, Bakin A (1997) Mapping to nucleotide resolution of pseudouridine residues in large subunit ribosomal RNAs from representative eukaryotes, prokaryotes, archaebacteria, mitochondria and chloroplasts. *J Mol Biol* **266**(2)**:** 246-268

Otwinowski Z, Minor W (1997) Processing of X-ray Diffraction Data Collected in Oscillation Mode, Methods in Enzymology. In *Macromolecular Crystallography*, Carter JCW, Sweet RM (eds), Vol. 276, pp 307-326.

Pankuch GA, Lin G, Hoellman DB, Good CE, Jacobs MR, Appelbaum PC (2006) Activity of retapamulin against Streptococcus pyogenes and Staphylococcus aureus evaluated by agar dilution, microdilution, E-test, and disk diffusion methodologies. *Antimicrob Agents Chemother* **50**(5)**:** 1727-1730

Pino S, Ciciriello F, Costanzo G, Di Mauro E (2008) Nonenzymatic RNA ligation in water. *J Biol Chem* **283**(52)**:** 36494-36503

Pioletti M, Schluenzen F, Harms J, Zarivach R, Gluehmann M, Avila H, Bashan A, Bartels H, Auerbach T, Jacobi C, Hartsch T, Yonath A, Franceschi F (2001) Crystal structures of complexes of the small ribosomal subunit with tetracycline, edeine and IF3. *Embo J* **20**(8)**:** 1829-1839

Porse BT, Garrett RA (1999a') Sites of interaction of streptogramin A and B antibiotics in the peptidyl transferase loop of 23 S rRNA and the synergism of their inhibitory mechanisms. *J Mol Biol* **286**(2)**:** 375-387

Poulsen SM, Karlsson M, Johansson LB, Vester B (2001) The pleuromutilin drugs tiamulin and valnemulin bind to the RNA at the peptidyl transferase centre on the ribosome. *Mol Microbiol* **41**(5)**:** 1091-1099

Pringle M, Poehlsgaard J, Vester B, Long KS (2004) Mutations in ribosomal protein L3 and 23S ribosomal RNA at the peptidyl transferase centre are associated with reduced susceptibility to tiamulin in Brachyspira spp. isolates. *Mol Microbiol* **54**(5)**:** 1295-1306.

Prystowsky J, Siddiqui F, Chosay J, Shinabarger DL, Millichap J, Peterson LR, Noskin GA (2001) Resistance to linezolid: characterization of mutations in rRNA and comparison of their occurrences in vancomycin-resistant enterococci. *Antimicrob Agents Chemother* **45**(7)**:** 2154-2156

Ramakrishnan V (2008) What we have learned from ribosome structures. *Biochem Soc Trans* **36**(Pt 4)**:** 567-574

Ross JE, Jones RN (2005) Quality control guidelines for susceptibility testing of retapamulin (SB-275833) by reference and standardized methods. *J Clin Microbiol* **43**(12)**:** 6212-6213

Sander P, Belova L, Kidan YG, Pfister P, Mankin AS, Bottger EC (2002) Ribosomal and non-ribosomal resistance to oxazolidinones: species-specific idiosyncrasy of ribosomal alterations. *Mol Microbiol* **46**(5)**:** 1295-1304

Sato NS, Hirabayashi N, Agmon I, Yonath A, Suzuki T (2006) Comprehensive genetic selection revealed essential bases in the peptidyl-transferase center. *Proc Natl Acad Sci U S A* **103**(42)**:** 15386-15391

Saxena SK, Ackerman EJ (1990) Microinjected oligonucleotides complementary to the alpha-sarcin loop of 28 S RNA abolish protein synthesis in Xenopus oocytes. *J Biol Chem* **265**(6)**:** 3263-3269

Scangarella-Oman NE, Shawar RM, Bouchillon S, Hoban D (2009) Microbiological profile of a new topical antibacterial: retapamulin ointment 1%. *Expert Rev Anti Infect Ther* **7**(3)**:** 269-279

Schluenzen F, Harms JM, Franceschi F, Hansen HA, Bartels H, Zarivach R, Yonath A (2003) Structural basis for the antibiotic activity of ketolides and azalides. *Structure (Camb)* **11**(3)**:** 329-338.

Schluenzen F, Pyetan E, Fucini P, Yonath A, Harms J (2004) Inhibition of peptide bond formation by pleuromutilins: the structure of the 50S ribosomal subunit from Deinococcus radiodurans in complex with tiamulin. *Mol Microbiol* **54**(5)**:** 1287-1294

Schluenzen F, Tocilj A, Zarivach R, Harms J, Gluehmann M, Janell D, Bashan A, Bartels H, Agmon I, Franceschi F, Yonath A (2000) Structure of functionally activated small ribosomal subunit at 3.3 angstroms resolution. *Cell* **102**(5)**:** 615-623.

Schluenzen F, Zarivach R, Harms J, Bashan A, Tocilj A, Albrecht R, Yonath A, Franceschi F (2001) Structural basis for the interaction of antibiotics with the peptidyl transferase centre in eubacteria. *Nature* **413**(6858)**:** 814-821

Schmeing TM, Huang KS, Strobel SA, Steitz TA (2005) An induced-fit mechanism to promote peptide bond formation and exclude hydrolysis of peptidyl-tRNA. *Nature* **438**(7067)**:** 520-524

Schmeing TM, Seila AC, Hansen JL, Freeborn B, Soukup JK, Scaringe SA, Strobel SA, Moore PB, Steitz TA (2002) A pre-translocational intermediate in protein synthesis observed in crystals of enzymatically active 50S subunits. *Nat Struct Biol* **9**(3)**:** 225-230

Schneider TD, Stormo GD, Gold L, Ehrenfeucht A (1986) Information content of binding sites on nucleotide sequences. *J Mol Biol* **188**(3)**:** 415-431

Schulze H, Nierhaus KH (1982) Minimal set of ribosomal components for reconstitution of the peptidyltransferase activity. *Embo J* **1**(5)**:** 609-613

Schuster I, Fleschurz C, Hildebrandt J, Turnowsky F, Zsutty H, Kretschmer G, Spitzy KH, Karrer K (1983) Binding and degradation of TDM 85-530 by a microsomal Cyt P-

450 form from man, rat and mouse in vitro. *Proc Int Congr Chemother* **13th 5:** 108/142-108/146

Schuwirth BS, Borovinskaya MA, Hau CW, Zhang W, Vila-Sanjurjo A, Holton JM, Cate JHD (2005) Structures of the Bacterial Ribosome at 3.5 A Resolution. *Science* **310**(5749)**:** 827-834

Selmer M, Dunham CM, Murphy FVt, Weixlbaumer A, Petry S, Kelley AC, Weir JR, Ramakrishnan V (2006) Structure of the 70S ribosome complexed with mRNA and tRNA. *Science* **313**(5795)**:** 1935-1942

Shawar R, Scangarella-Oman N, Dalessandro M, Breton J, Twynholm M, Li G, Garges H (2009) Topical retapamulin in the management of infected traumatic skin lesions. *Ther Clin Risk Manag* **5**(1)**:** 41-49

Shine J, Dalgarno L (1974) The 3'-terminal sequence of Escherichia coli 16S ribosomal RNA: complementarity to nonsense triplets and ribosome binding sites. *Proc Natl Acad Sci U S A* **71**(4)**:** 1342-1346

Smith JM, Szathmáry E (1995) *The Major Transitions in Evolution*, New York.

Smith LK, Mankin AS (2008) Transcriptional and translational control of the mlr operon which confers resistance to seven classes of protein synthesis inhibitors. *Antimicrob Agents Chemother* **52**(5)**:** 1703-1712

Stark A, Brennecke J, Russell RB, Cohen SM (2003) Identification of Drosophila MicroRNA targets. *PLoS Biol* **1**(3)**:** E60

Steitz TA (2008) A structural understanding of the dynamic ribosome machine. *Nat Rev Mol Cell Biol* **9**(3)**:** 242-253

Stull RA, Taylor LA, Szoka FC, Jr. (1992) Predicting antisense oligonucleotide inhibitory efficacy: a computational approach using histograms and thermodynamic indices. *Nucleic Acids Res* **20**(13)**:** 3501-3508

Tapprich WE, Hill WE (1986) Involvement of bases 787-795 of Escherichia coli 16S ribosomal RNA in ribosomal subunit association. *Proc Natl Acad Sci U S A* **83**(3)**:** 556-560

Thompson J, Kim DF, O'Connor M, Lieberman KR, Bayfield MA, Gregory ST, Green R, Noller HF, Dahlberg AE (2001) Analysis of mutations at residues A2451 and G2447 of 23S rRNA in the peptidyltransferase active site of the 50S ribosomal subunit. *Proc Natl Acad Sci U S A* **98**(16)**:** 9002-9007

Thompson JD, Higgins DG, Gibson TJ (1994) CLUSTAL W: improving the sensitivity of progressive multiple sequence alignment through sequence weighting, position-specific gap penalties and weight matrix choice. *Nucleic Acids Res* **22**(22)**:** 4673-4680

Toh SM, Mankin AS (2008) An Indigenous Posttranscriptional Modification in the Ribosomal Peptidyl Transferase Center Confers Resistance to an Array of Protein Synthesis Inhibitors. *J Mol Biol* **380**(4)**:** 593-597

Toh SM, Xiong L, Arias CA, Villegas MV, Lolans K, Quinn J, Mankin AS (2007) Acquisition of a natural resistance gene renders a clinical strain of methicillin-resistant Staphylococcus aureus resistant to the synthetic antibiotic linezolid. *Mol Microbiol* **64**(6)**:** 1506-1514

Tu D, Blaha G, Moore PB, Steitz TA (2005) Structures of MLSBK Antibiotics Bound to Mutated Large Ribosomal Subunits Provide a Structural Explanation for Resistance. *Cell* **121:** 257-270

Tuerk C, Gauss P, Thermes C, Groebe DR, Gayle M, Guild N, Stormo G, d'Aubenton-Carafa Y, Uhlenbeck OC, Tinoco I, Jr., et al. (1988) CUUCGG hairpins: extraordinarily stable RNA secondary structures associated with various biochemical processes. *Proc Natl Acad Sci U S A* **85**(5)**:** 1364-1368

Ulrich G, Stephen A, Obenaus H, Baumgartner R, Walzl H, Brueggemann S, Schmid B, Racine R, Schatz F, Haberl H, Spitzy KH, Karrer K (1983) TDM 85-530: toxicity in laboratory animals, tolerance and pharmacokinetics after oral application to volunteers. *Proc Int Congr Chemother* **13th 5:** 108/153-108/157

Von Graevenitz A, Bucher C (1983) In vitro activity of TDM 85'530 against selected aerobic bacteria. *Proc Int Congr Chemother* **13th 5:** 108/103-108/105

Voss NR, Gerstein M, Steitz TA, Moore PB (2006) The geometry of the ribosomal polypeptide exit tunnel. *J Mol Biol* **360**(4)**:** 893-906

Voytek SB, Joyce GF (2007) Emergence of a fast-reacting ribozyme that is capable of undergoing continuous evolution. *Proc Natl Acad Sci U S A* **104**(39)**:** 15288-15293

Weinger JS, Parnell KM, Dorner S, Green R, Strobel SA (2004) Substrate-assisted catalysis of peptide bond formation by the ribosome. *Nat Struct Mol Biol* **11**(11)**:** 1101-1106

Weinger JS, Strobel SA (2007) Exploring the mechanism of protein synthesis with modified substrates and novel intermediate mimics. *Blood Cells Mol Dis* **38**(2)**:** 110-116

Wekselman I, Davidovich C, Agmon I, Zimmerman E, Rozenberg H, Bashan A, Berisio R, Yonath A (2009) Ribosome's mode of function: myths, facts and recent results. *J Pept Sci* **15**(3)**:** 122-130

Weller J, Hill WE (1991) Probing the initiation complex formation on E coli ribosomes using short complementary DNA oligomers. *Biochimie* **73**(7-8)**:** 971-981

Wilson DN, Schluenzen F, Harms JM, Starosta AL, Connell SR, Fucini P (2008) The oxazolidinone antibiotics perturb the ribosomal peptidyl-transferase center and effect tRNA positioning. *Proc Natl Acad Sci U S A* **105**(26)**:** 13339–13344

Wimberly BT, Brodersen DE, Clemons WM, Jr., Morgan-Warren RJ, Carter AP, Vonrhein C, Hartsch T, Ramakrishnan V (2000) Structure of the 30S ribosomal subunit. *Nature* **407**(6802)**:** 327-339

Woese CR (1973) The rotating ribosome: a gross mechanical model for translation. *J Theor Biol* **38**(1)**:** 203-204

Woese CR (2001) Translation: in retrospect and prospect. *RNA* **7**(8)**:** 1055-1067

Xiong L, Kloss P, Douthwaite S, Andersen NM, Swaney S, Shinabarger DL, Mankin AS (2000) Oxazolidinone resistance mutations in 23S rRNA of Escherichia coli reveal the central region of domain V as the primary site of drug action. *J Bacteriol* **182**(19)**:** 5325-5331.

Yan K, Madden L, Choudhry AE, Voigt CS, Copeland RA, Gontarek RR (2006) Biochemical characterization of the interactions of the novel pleuromutilin derivative retapamulin with bacterial ribosomes. *Antimicrob Agents Chemother* **50**(11)**:** 3875-3881

Yang LP, Keam SJ (2008a) Retapamulin: a review of its use in the management of impetigo and other uncomplicated superficial skin infections. *Drugs* **68**(6)**:** 855-873

Yang LP, Keam SJ (2008b) Spotlight on retapamulin in impetigo and other uncomplicated superficial skin infections. *Am J Clin Dermatol* **9**(6)**:** 411-413

Yarus M (2002) Primordial genetics: phenotype of the ribocyte. *Annu Rev Genet* **36:** 125-151

Yonath A (2003b) Ribosomal tolerance and peptide bond formation. *Biol Chem* **384**(10)**:** 1411-1419

Yonath A (2005) Antibiotics targeting ribosomes: resistance, selectivity, synergism, and cellular regulation. *Annu Rev Biochem* **74:** 649-679

Yonath A (2009) Large facilities and the evolving ribosome, the cellular machine for genetic-code translation. *J R Soc Interface* **6 Suppl 5:** S575-585

Yonath A, Bashan A (2004) Ribosomal Crystallography: Initiation, Peptide Bond Formation, and Amino Acid Polymerization are Hampered by Antibiotics. *Annu Rev Microbiol* **58:** 233-251

Yonath A, Muessig J, Tesche B, Lorenz S, Erdmann VA, Wittmann HG (1980) Crystallization of the large ribosomal subunit from B. stearothermophilus. *Biochem Int* **1:** 315-428

Youngman EM, Brunelle JL, Kochaniak AB, Green R (2004) The active site of the ribosome is composed of two layers of conserved nucleotides with distinct roles in Peptide bond formation and Peptide release. *Cell* **117**(5)**:** 589-599.

Zaman S, Fitzpatrick M, Lindahl L, Zengel J (2007) Novel mutations in ribosomal proteins L4 and L22 that confer erythromycin resistance in Escherichia coli. *Mol Microbiol* **66**(4)**:** 1039-1050

Zimmerman E, Yonath A (2009) Biological Implications of the Ribosome's Stunning Stereochemistry. *ChemBioChem* **10**(1)**:** 63-72

Zubay G (1973) In vitro synthesis of protein in microbial systems. *Annu Rev Genet* **7:** 267-287

Zuker M (1989) On finding all suboptimal foldings of an RNA molecule. *Science* **244**(4900)**:** 48-52

6. Figures, tables and plots
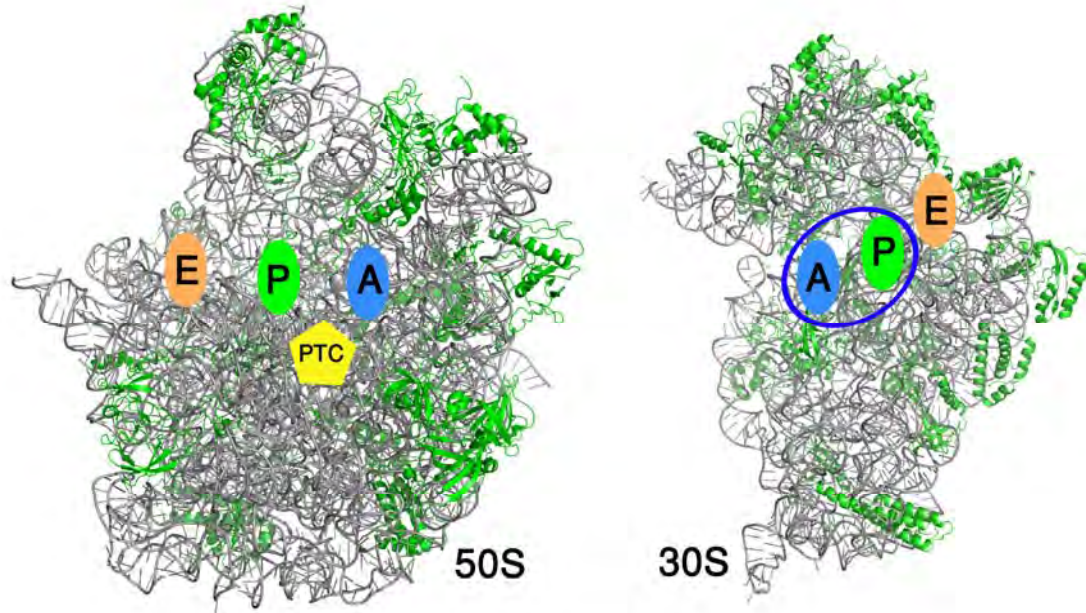
Figure F1 - **Front views (the subunit interfaces) of the two eubacterial ribosomal subunits.** Shown are the large ribosomal subunit from Deinococcus radiodurans (50S, left panel) and the small ribosomal subunit from Thermus thermophilus (30S, right panel). Ribosomal RNA is shown in gray, proteins colored green. Blue, green and orange ellipsoids marked A, P, and E, respectively, designate the three tRNA binding sites within the small subunit (namely, the approximate positions of the anticodon loops) and the large subunit (namely, the approximate positions of the tRNA acceptor stems). The yellow pentagon indicates the approximate location of the PTC in the large subunit and blue ellipsoid surrounding the A and P sites within the small ribosomal subunit indicating for the decoding center.
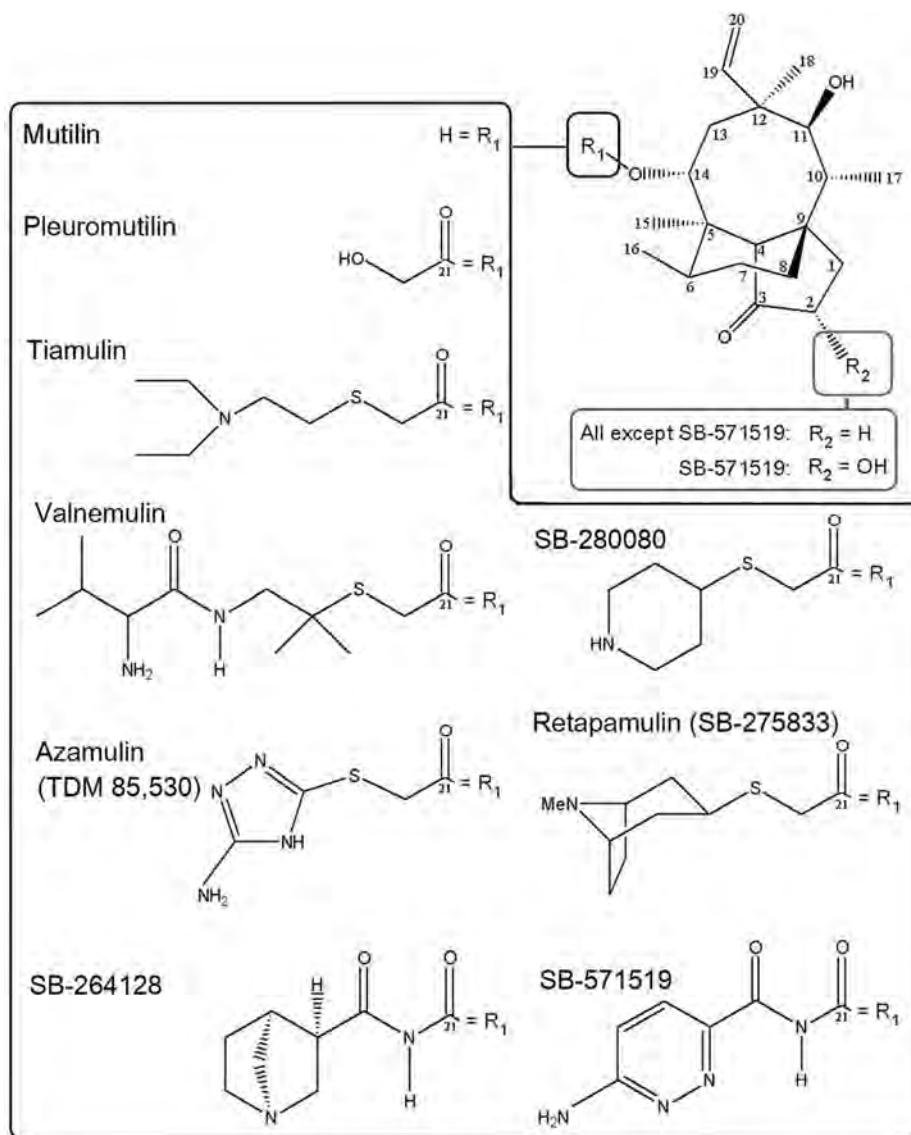
Figure F2 - **Chemical formula of selected pleuromutilin derivatives.** Typically, the tricyclic mutilin core is conserved among pleuromutilin derivatives. Notable is the variability of the C14 extension (R1 in the large box). **Large box**: previously studied pleuromutilins (**left**), pleuromutilins characterized within the present study (**right**), mutilin and the natural pleuromutilin (**upper left**), acyl-carbamate semisynthetic derivatives (**bottom**). Notable is the conserved C21 carbonyl that is crucial for pleuromutilins activity (see discussion). **Upper right, small box:** R2, the acyl-carbamate derivative SB-571519 includes an additional hydroxyl that substituted on C2.
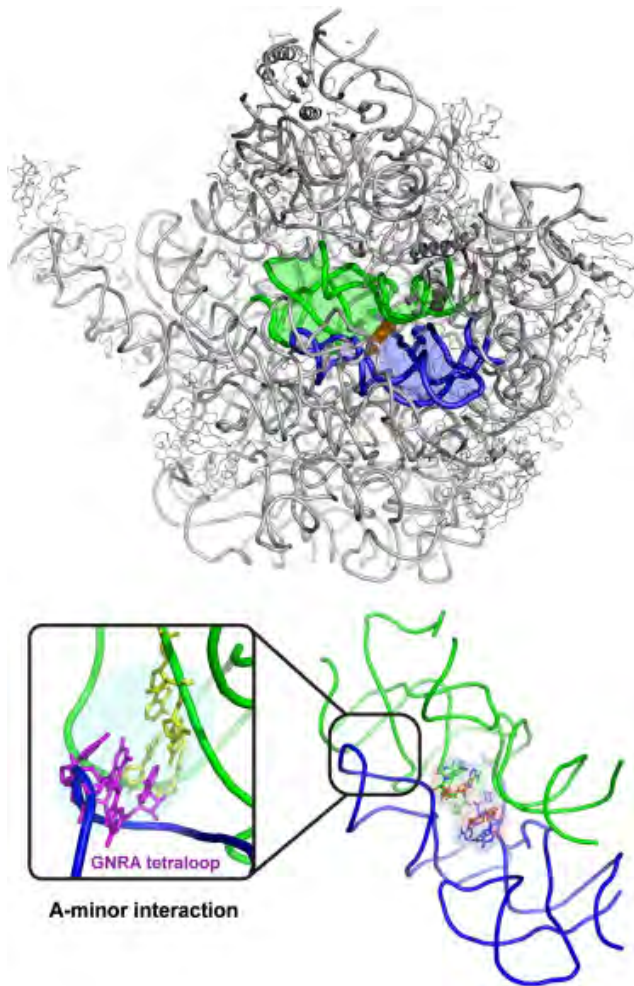
Figure F3 - The symmetrical region within the large ribosomal subunit. Top: The A-region is shown in blue, the P-region in green, and the substrate position is indicated by the orange object. **Bottom:** the GNRA tetraloop and the A-minor interaction between the A-region (blue) and the P-region (green).
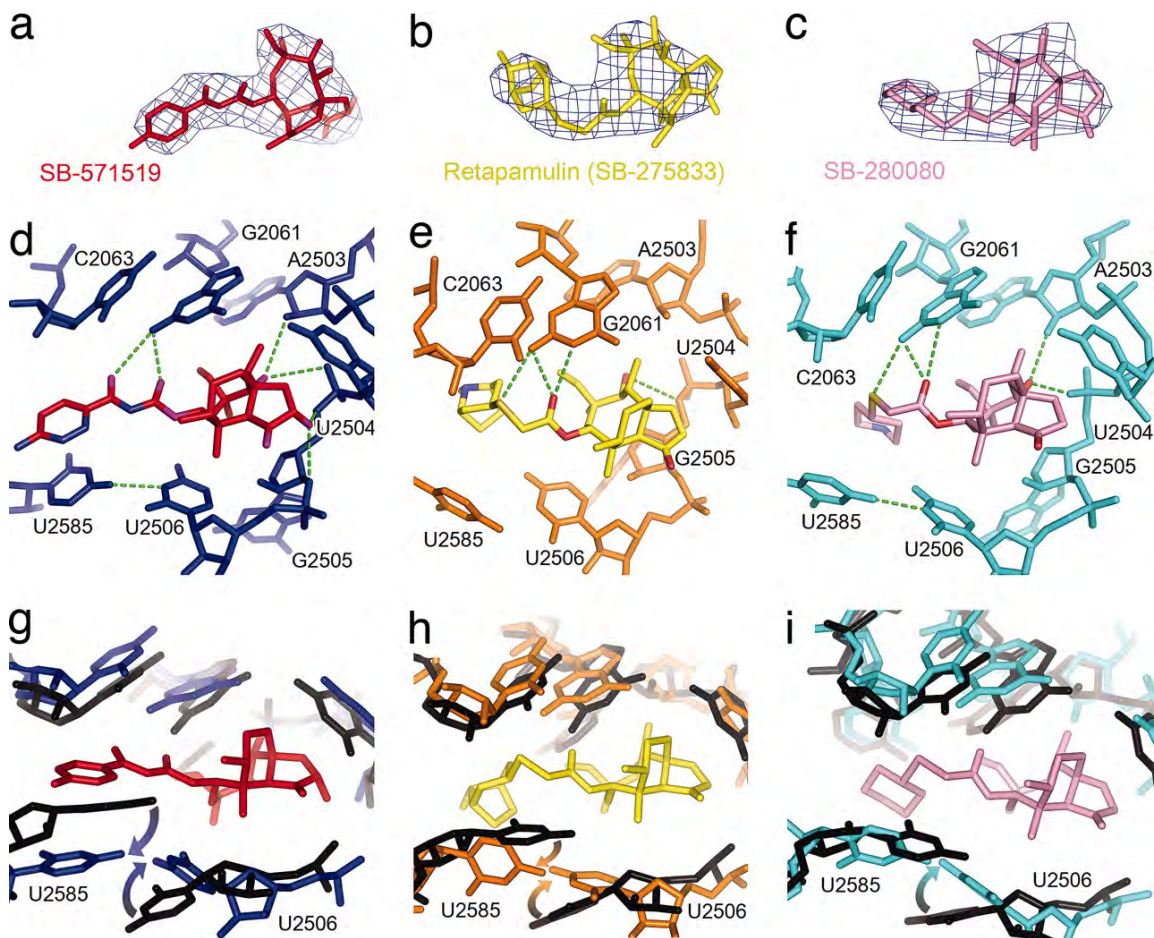
Figure F4 – Induced fit binding of pleuromutilin antibiotics to the PTC. Selected regions from the crystal structures of the large ribosomal subunit from D. radiodurans complexed with pleuromutilin acyl-carbamate derivative SB-571519 (in red: a, d, and g) and two sulfanyl-acetate derivatives retapamulin (SB-275833) (in yellow: b, e, and h) and SB-280080 (in pink: c, f, and i) at 3.50, 3.66, and 3.56-Å resolution, respectively. **Panels a–c**: 2Fo − Fc electron density maps, contoured at 1.5 σ level. **Panels d–f:** Interactions between pleuromutilin derivatives and 23S rRNA (the 23S rRNA bound conformation is shown in dark blue for SB-571519, orange for SB-275833, and cyan for SB-28008). All show H-bonds between G2061 and pleuromutilins' C14 extension and the possibility of H-bond between C11 hydroxyl and G2505 phosphate. In SB-571519 and SB-280080 complexes, C11 hydroxyl may serve as acceptor in an additional H-bond with the OH group of A2503 O2′, and a nontypical H-Bond is observed between U2585 and U2506. **Panels g–i:** Induced-fit mechanism promotes pleuromutilins binding (colour code as in d–f). In all, the unbound 23S rRNA (PDB ID code 1NKW) is black, and the pleuromutilin-bound conformations are colure. On binding, U2585 translates away from the C14 extension and U2506 rotates toward the pleuromutilin and thus closes tightly the binding pocket. H-bonds (d and f) or other interactions (e) between the two shifted nucleotides may further stabilize the rRNA conformation at the bound state.

74
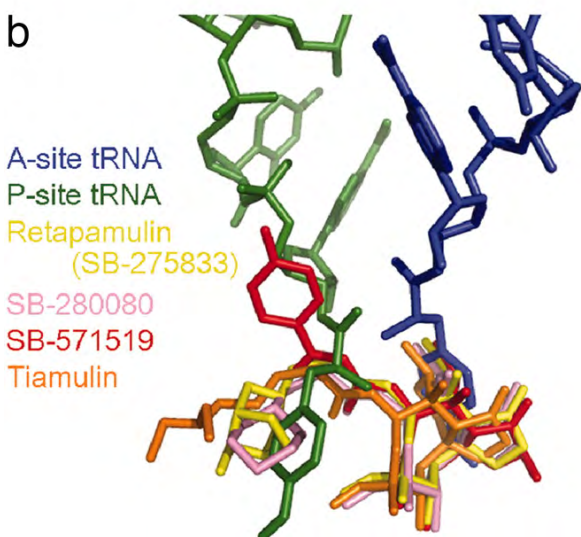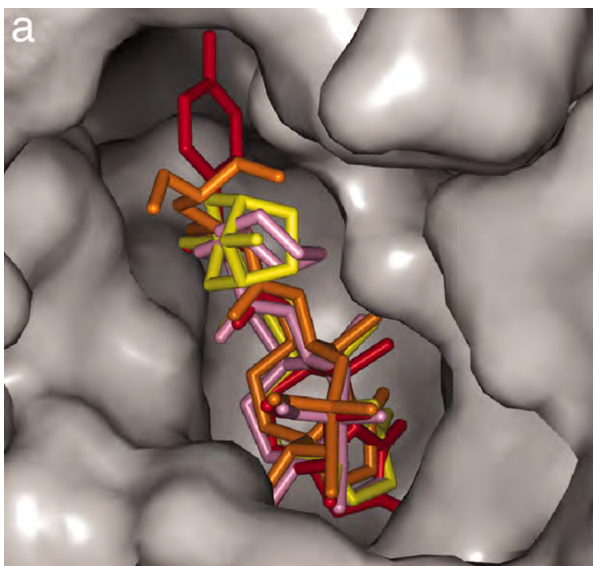
Figure F7 - Four pleuromutilin derivatives superimposed in the binding pocket. (a) A surface representation of the binding pocket. Several nucleotides have been removed to permit a clear view of the binding site. The structure of D50S/SB-517519 was used for surface representation. (b) A side view of pleuromutilins with the 3′ ends of an A-site tRNA mimic and the derived P-site tRNA. All pleuromutilin derivatives presented here are located at the PTC, with their tricyclic core oriented similar to tiamulin and their C14 extensions placed within the PTC.
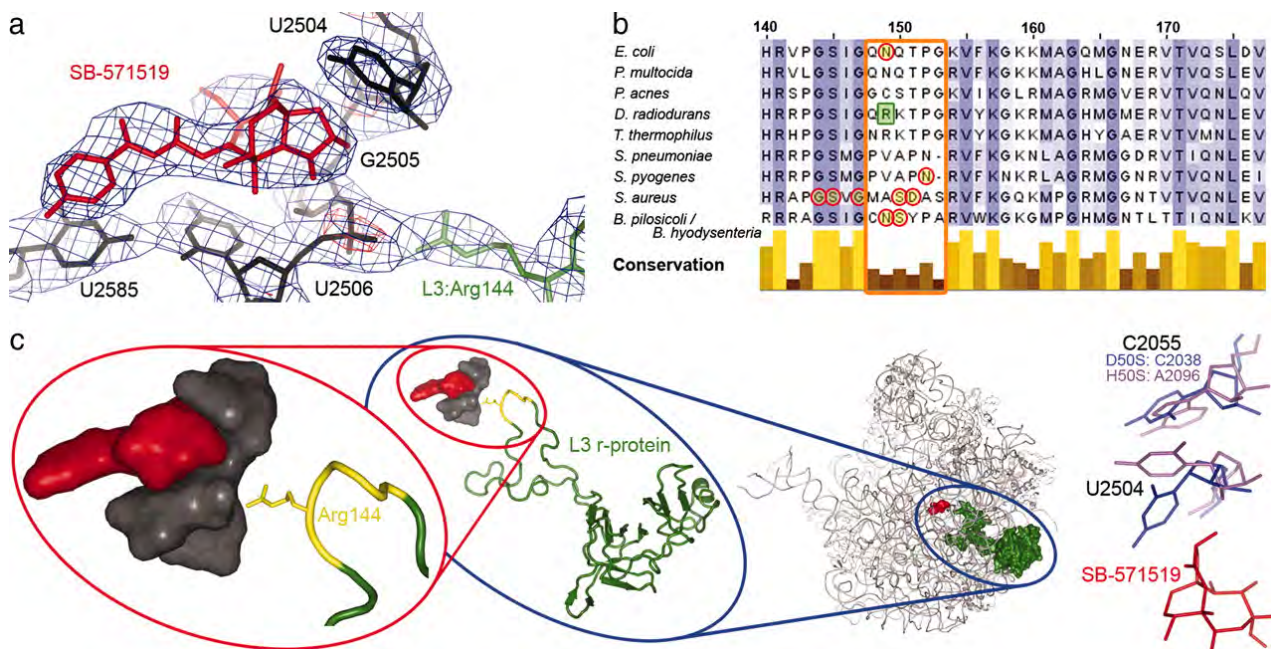
Figure F6 - Remote factors acquiring resistance and selectivity. Panels a–c: Possible contribution of L3 to pleuromutilin resistance. (a) 2 Fo – Fc electron density map of the carbamate-derivative (red) SB-571519. 23S rRNA nucleotides are shown in black, and protein L3 Arg144 in green. Blue mesh is contoured at 1.0 σ. The red meshes (contoured at 5.0 σ) indicate phosphate locations. (b) Multiple sequence alignment of protein L3 from selected bacteria. Top numbering according to *E. coli* (where Arg144 of *D. radiodurans* is Asn149), bottom bars indicate conservation among these strains, and yellow circles indicate mutations with reduced pleuromutilin susceptibility. Most of these mutations are located in a highly diverse six amino acids window (orange box). In *D. radiodurans*, this window includes Arg144 (green square). **Panel c:** L3 protein penetrates from the surface of the ribosome deeply toward the vicinity of the PTC (right image, L3 in green, SB-571519 in red). The L3 nonconserve loop-like region (consisting of six amino acids, shown in b in the orange box) is colured yellow in the center and left image. In *D. radiodurans*, Arg144 electrostatically interacts with U2506 phosphate (a). 23S rRNA nucleotides 2504 to 2506 (left, gray surface representation) define a large portion of induced-fit binding pocket (see text), obtained mainly by conformational change of U2506. (d) Differences in remote nucleotides acquire pleuromutilin selectivity. An example is U2504, which is among the nucleotides that define pleuromutilins binding site. In eubacteria it points toward the PTC, whereas in the Archaeon H50S, this nucleotide stacks with 2055, which is A in eukarya and archaea but C in eubacteria. This stacking seems to stabilize U2504 position away from the binding pocket. SB-571519 is red; nucleotides 2504 and 2055 are blue in its complex with D50S and purple in H50S.
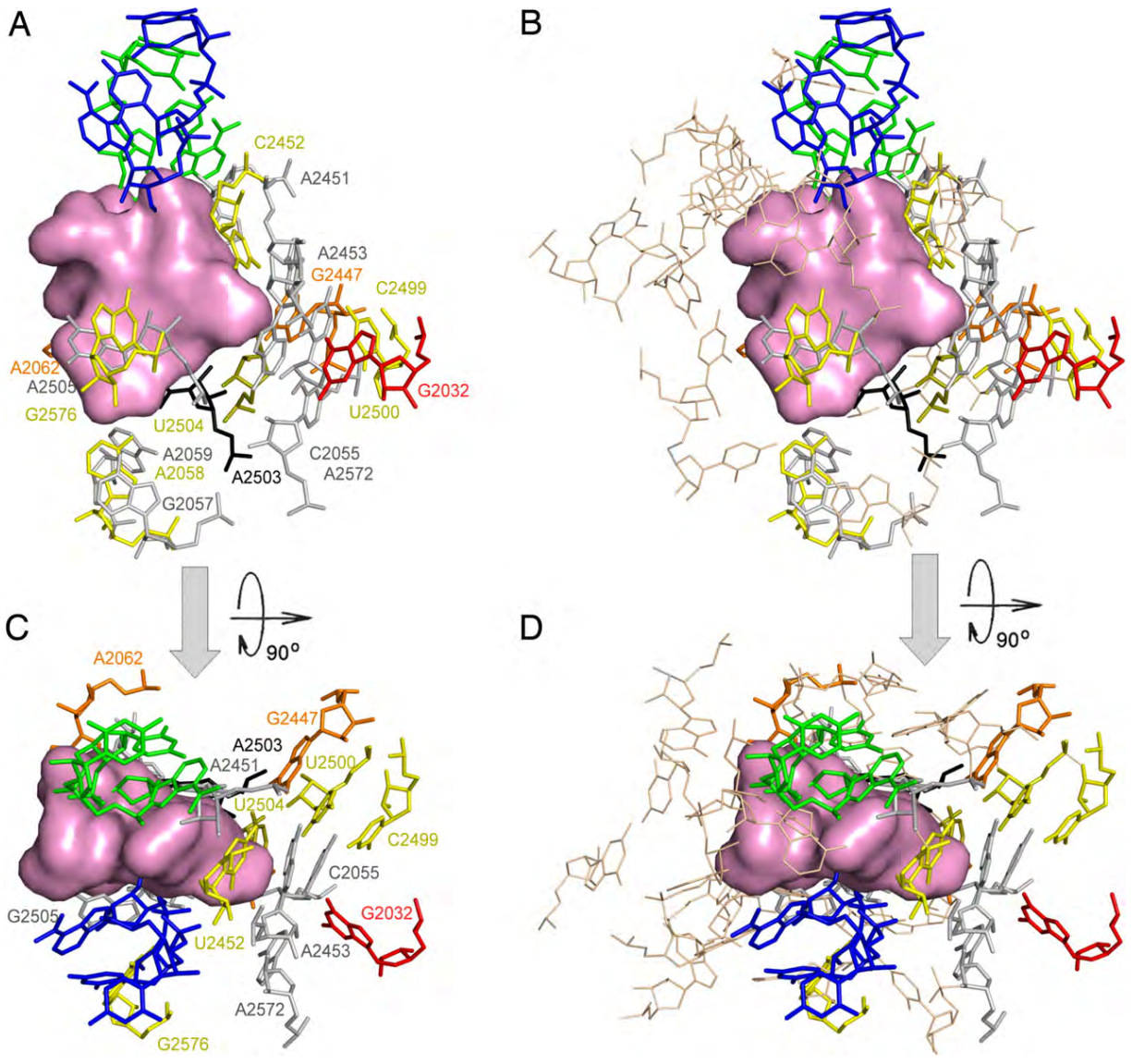
Figure F7 - Nucleotides shown to undergo mutations or methylations that confirm PTC antibiotic resistance or reduce susceptibility. Nucleotides are colored according to the number of affected classes (one, two, three, four, and five classes are represented by gray, yellow, orange, red, and black, respectively). The pink surface shows the total volume occupied by the PTC antibiotics: clindamycin (lincosamides), dalfopristin (streptograminsA), retapamulin (pleuromutilins), chloramphenicol (phenicols), and linezolid (oxazolidinones). For orientation, the A site tRNA 3′ end and the derived P site tRNA 3′ end are shown in blue and green, respectively. Images were taken from the direction of the L7/12 stalk (A and B) and from the top of the cavity leading to the PTC (C and D). Nucleotides located in the vicinity of the PTC within a distance <8 Å from the corresponding antibiotic, and are not involved in known resistance determinants, are either shown as wheat-colored lines (B and D) or excluded (A and C).
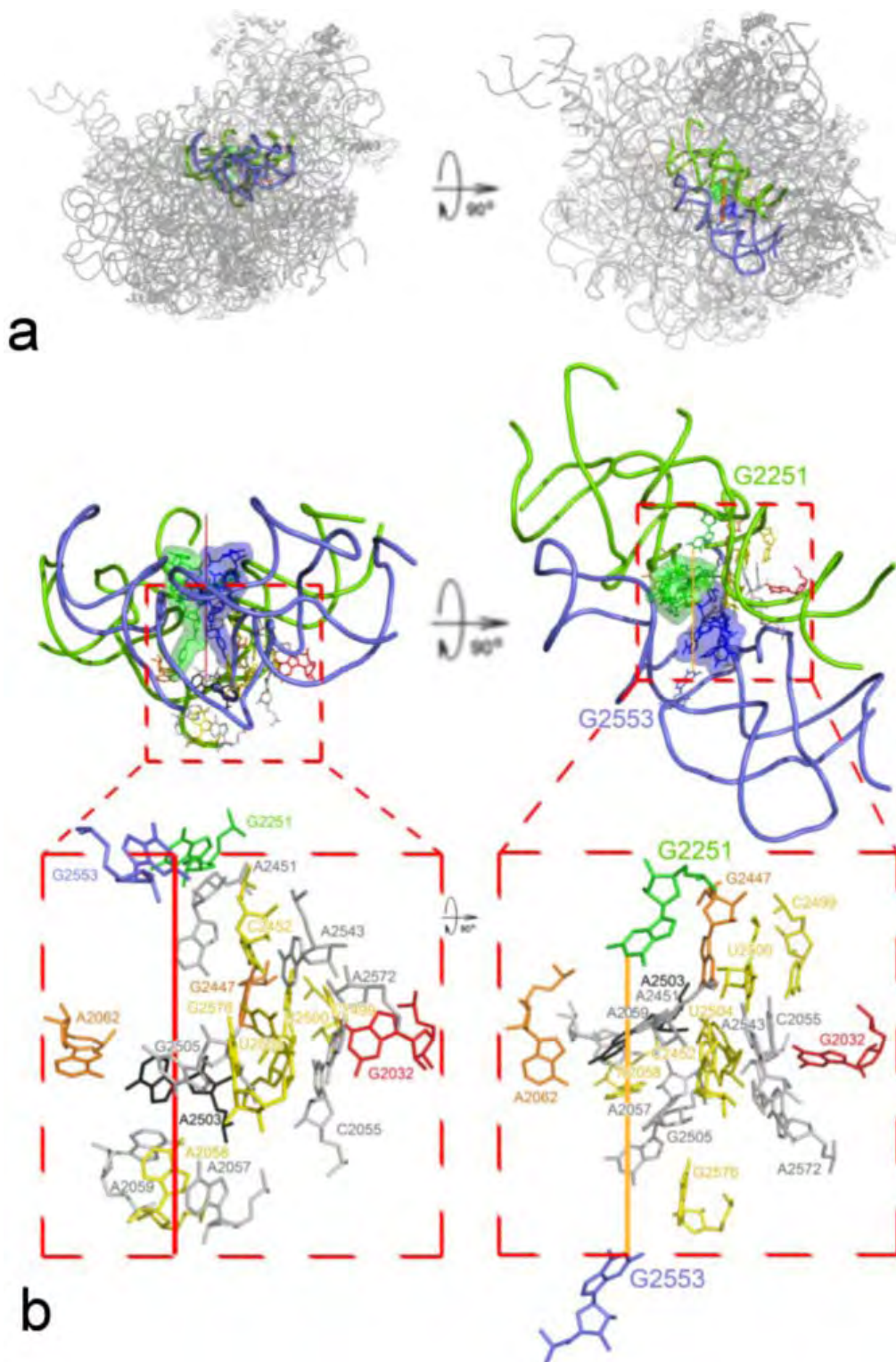
Figure F8 - The centrality of the symmetrical region and the 2 perpendicular axes that define the planes confining the PTC regions that participate in antibiotic

resistance. In all: images were captured perpendicular to the 2-fold symmetry axes (**right panels**) and to the axes defined by the line connecting G2553 to G2251 (**left panels**). The rRNA backbone is shown in gray, except for the symmetrical region, where the subregion containing the A loop (called A region), is colored blue and that containing the P-loop (the P-region) is shown in green. The imaginary 2-fold rotation axis is shown in red. Nucleotides are colored according to the number of affected classes (one, two, three, four, and five classes are represented by gray, yellow, orange, red, and black, respectively). CCA 3' ends of tRNA in the A and the P sites colored blue and green, respectively. (*a*) Two views of the large ribosomal subunit showing the centrality of the internal 2-fold symmetry region. The left side shows the large subunit as seen from its interface surface, and the right side is a view taken into the PTC. (*b*) The symmetrical region with the two imaginary axes relevant to cross-resistance. **Left panels:** the 2-fold symmetry axis colored red. **Right panels:** The line connecting G2553 to G2251, which divides the front and back walls of the PTC, colored orange. The two fold pseudo-symmetry regions of the PTC, including the A loop and the P loop, are pale blue and green, respectively. Zooms into these views, in which the nucleotides involved in resistance or reduced susceptibility are depicted, are shown in the **lower panels**.
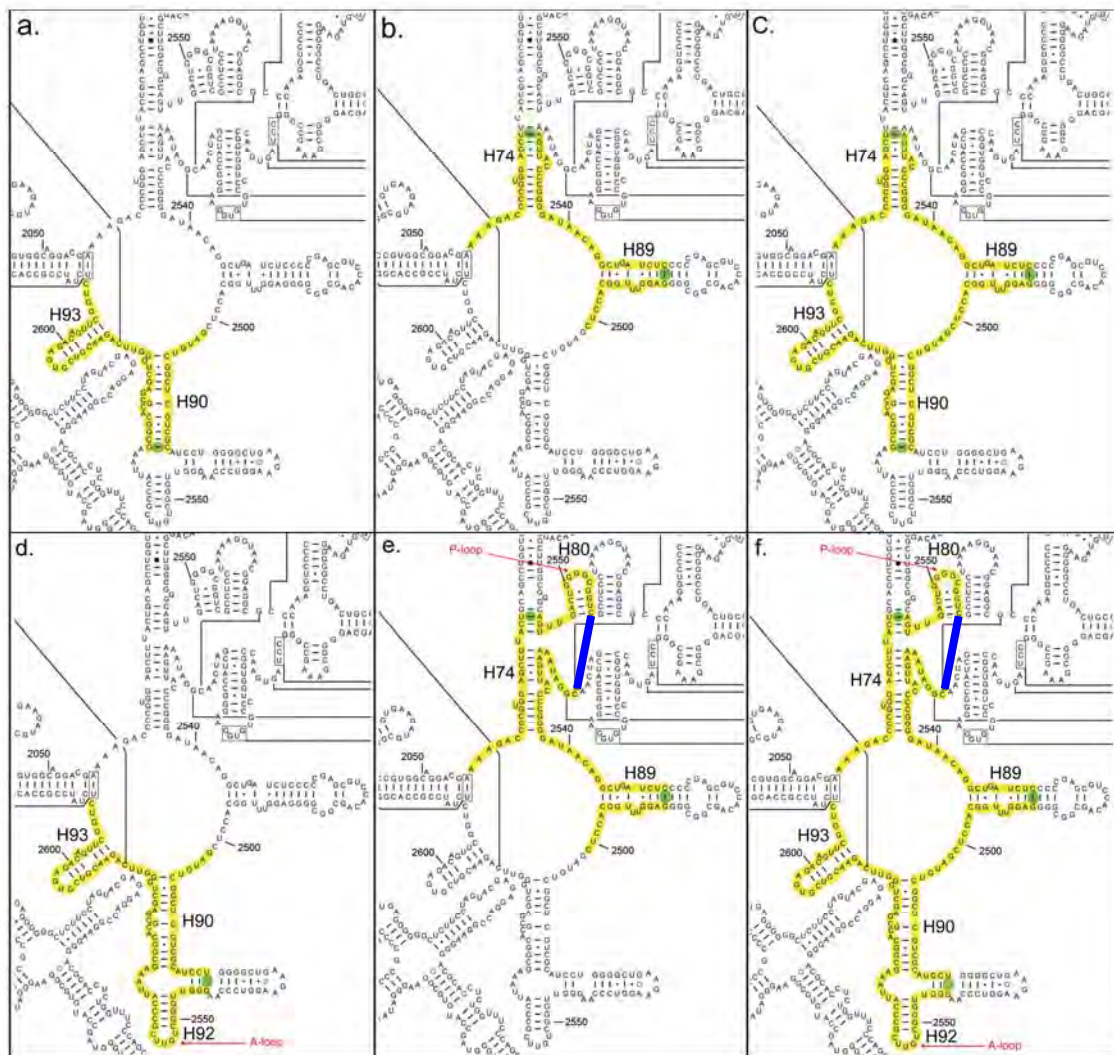
Figutre F9: Two-dimensional representation of 23 rRNA of *T. thermophilus* from the surroundings of the PTC. Nucleotides highlighted yellow in **panels a-f** were used to design the sequences of RNA constructs A1, P1, AP1, A2, P2 and AP2, respectively. Blue stretches indicate direct connection between nucleotides and green dots represents positions where the hyper stable CUUCGG hairpin was inserted. This was done in order to avoid rRNA sequences that perturbing from the A- or P-regions and do not obey the two fold symmetry within the surroundings of the PTC, according to the three dimensional structure. rRNA helices and nucleotide numbers (*E. coli* numbering) are designated in black. A-loop and P-loop are pointed by red arrows.

80
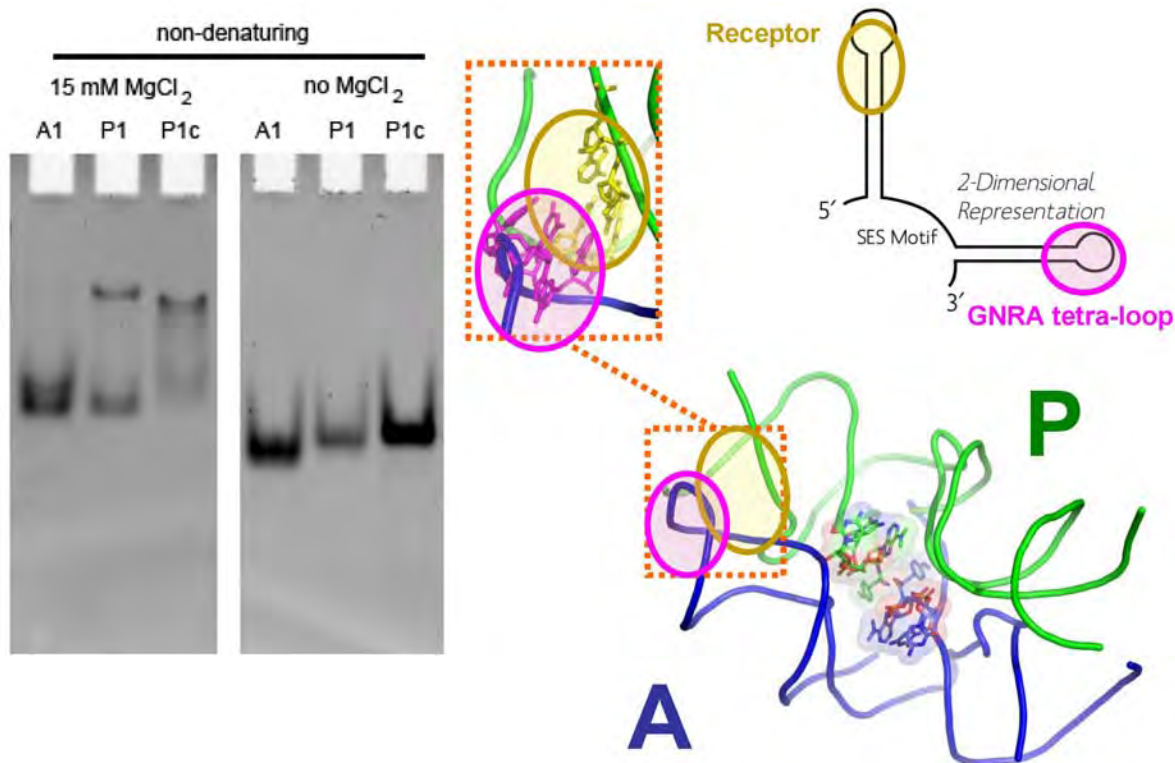
Figure F10: Incorporation of GNRA tetra-loop to P1 RNA sequence resulted with enhanced dimerization. Bottom right: Three dimensional backbone representation of the minimal component of the two-fold symmetry region from the surroundings of the PTC, within the crystal structure of the large ribosomal subunit from the eubacteria *D. radiodurans*. A-region and P-region marked accordingly and colored blue and green, respectively. Coordinates of CCA 3' ends in the PTC are surrounded with transparent surface representation and colored as CPK, with carbon atoms in blue and green for substrates located in the A- and the P-site, respectively. Dashed orange box highlights the location of A-minor interactions between the GNRA (GUGA) tetra-loop located in H93 (purple circle) and the receptor at H74 (yellow circle). **Top middle dashed box:** Zoom into the residues involved in A-minor interactions, in sticks representation. The four nucleotides in the GUGA tetraloop are colored purple and nucleotides forming the receptor are colored yellow. **Top right:** Two dimensional representation of P1c construct. The construct was designed to form two helices baring the sequence of nucleotides of the P-region, as shown at the bottom right panel. Yellow circle indicates location of the receptor, designed based on the corresponding H74 within the contemporary ribosome. Purple circle indicates the location of the GNRA tetra-loop that was taken from H93 within the sequence of contemporary 23S rRNA and inserted into P1c within the helix corresponding to H89. **Left:** Non-denaturing PAGE

of A1, P1 and P1c (lanes marked accordingly) in the presence (left gel) and absence (right gel) of magnesium ions (see methodology and results sections for full description).
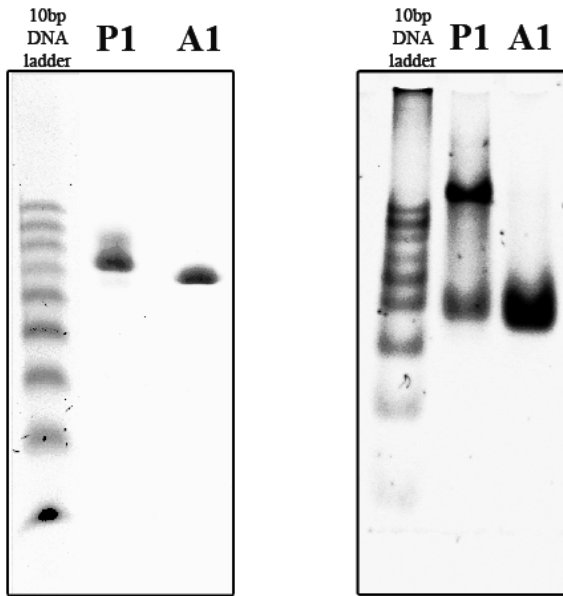
Figure F11: **Denaturing and Non-denaturing Polyacrylamide Gel Electrophoresis of RNA constructs A1 and P1. Left**: 15% polyacrylamide gel under denaturing conditions. Both A1 and P1 migrate according to their molecular weight. The 10 bp DNA ladder composes of 10 to 100 bp DNA segments. **Right**: 12% polyacrylamide under non-denaturing conditions. Each loaded sample contained RNA in 2 μM concentration (see methodology for full description). While A1 migrates with only one band, two bands were clearly observed for P1, indicating a fast migrating monomer and a slow migrating dimer.
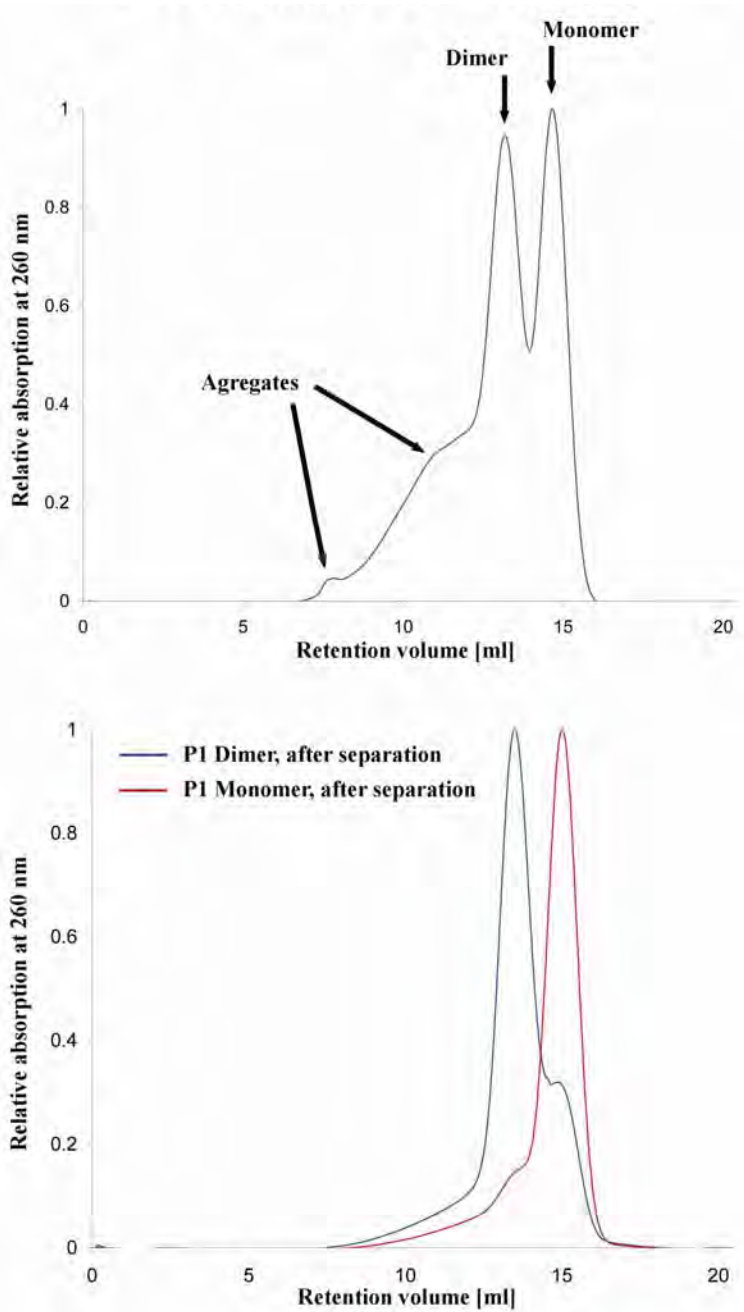
Figure F12: Separation of P1 dimer and monomer by Size Exclusion Chromatography. Top: Chromatogram obtained following injection of 100 μg P1 RNA in 300 μM concentration after incubation in conditions that permit dimerization. Fractions including the dimer and monomer (indicated) were collected and injected for a second run (see text for full details). **Bottom:** Chromatograms obtained in the second run, after injection of the monomer (red) and the dimer (blue) fractions.
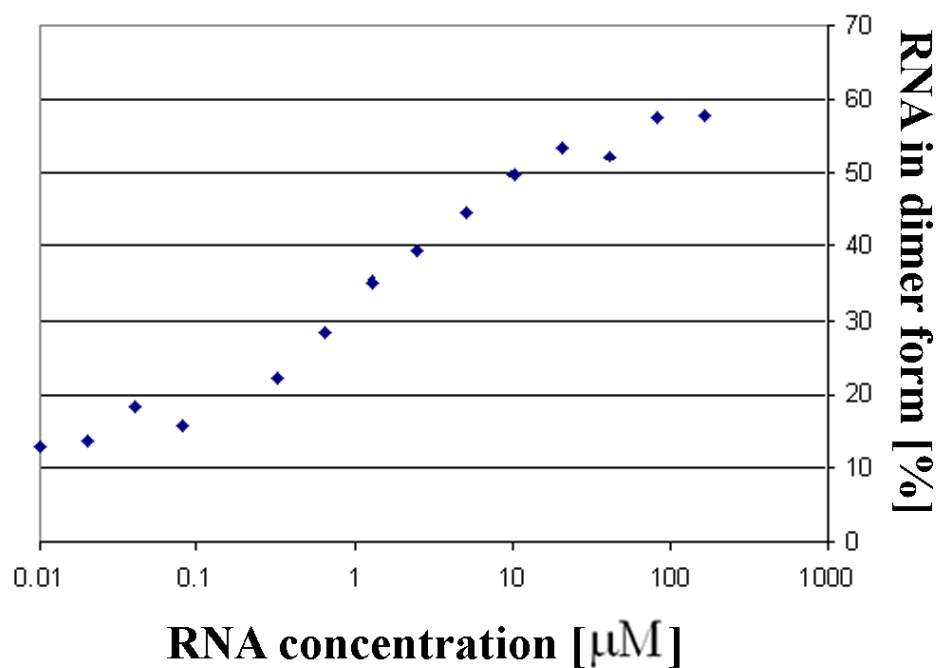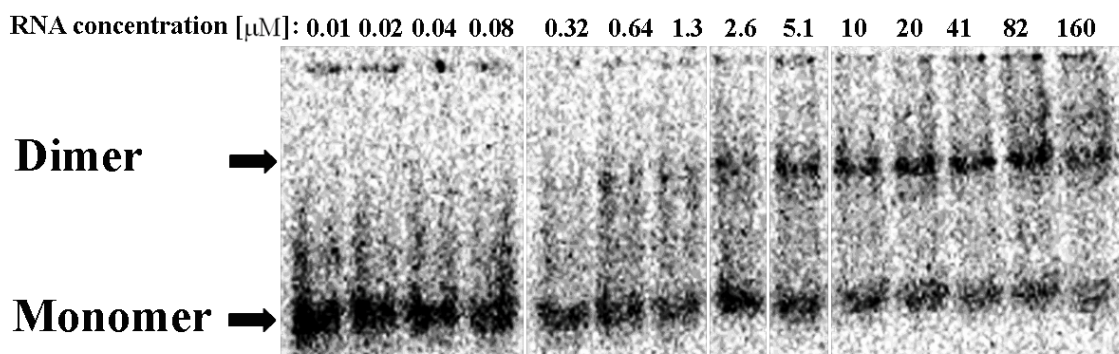
RNA concentration [μM]: 0.01 0.02 0.04 0.08   0.32 0.64 1.3   2.6   5.1   10   20   41   82   160

Dimer ➡

Monomer ➡

Figure F13: RNA concentration dependent P1 homodimer formation. Top: EMSA performed using ^{33}P labeled P1 RNA (see text for further details). **Bottom:** The amount of the low migrating band is concentration dependent, indicating for a homo-dimer with K_d of the order of 10^{-5} M.
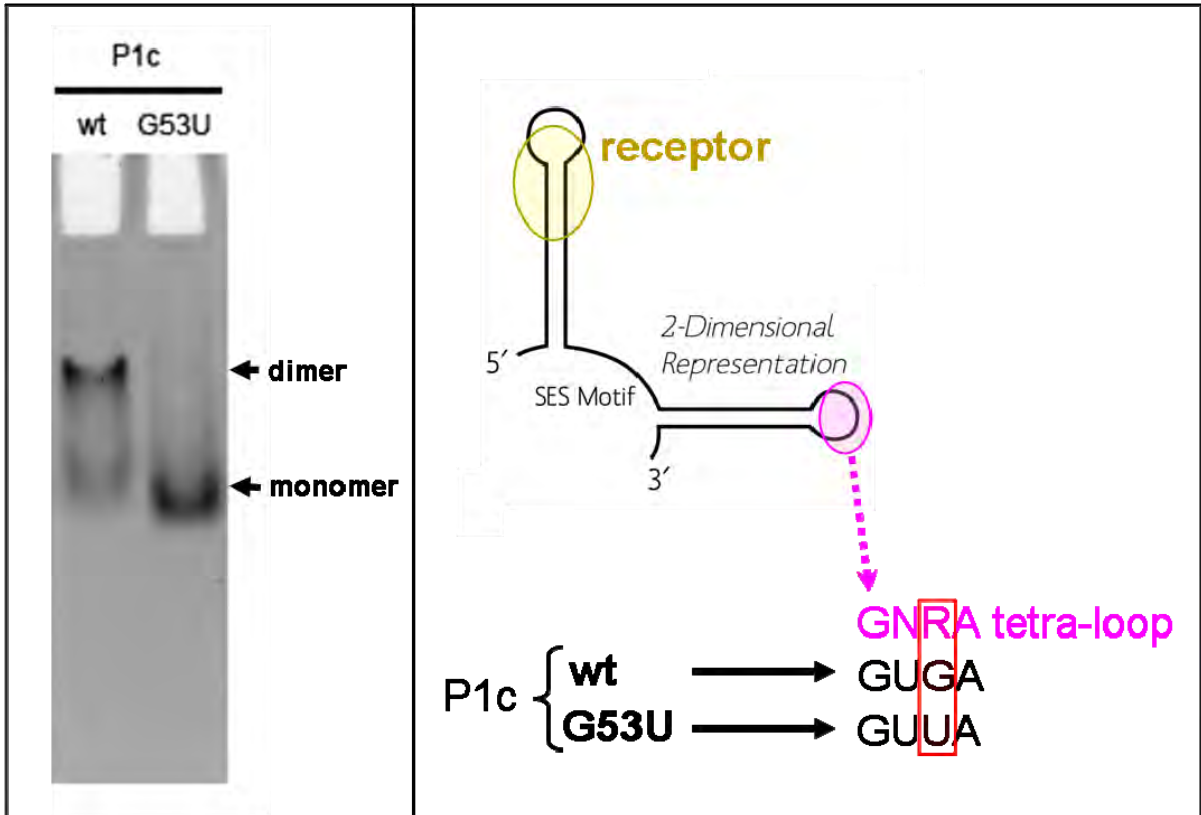
Figure F14: Point mutation in P1c to abolish the GNRA motif resulted with loss of dimerization. Right panel: two dimensional representation of P1c design includes the location of the receptor (yellow circle) and the GNRA tetra-loop (purple circle). The mutation G53U is highlighted with a red box. **Left panel:** non-denaturing PAGE of P1c wild type and G53U mutant. Bands of dimer and monomer are indicated.
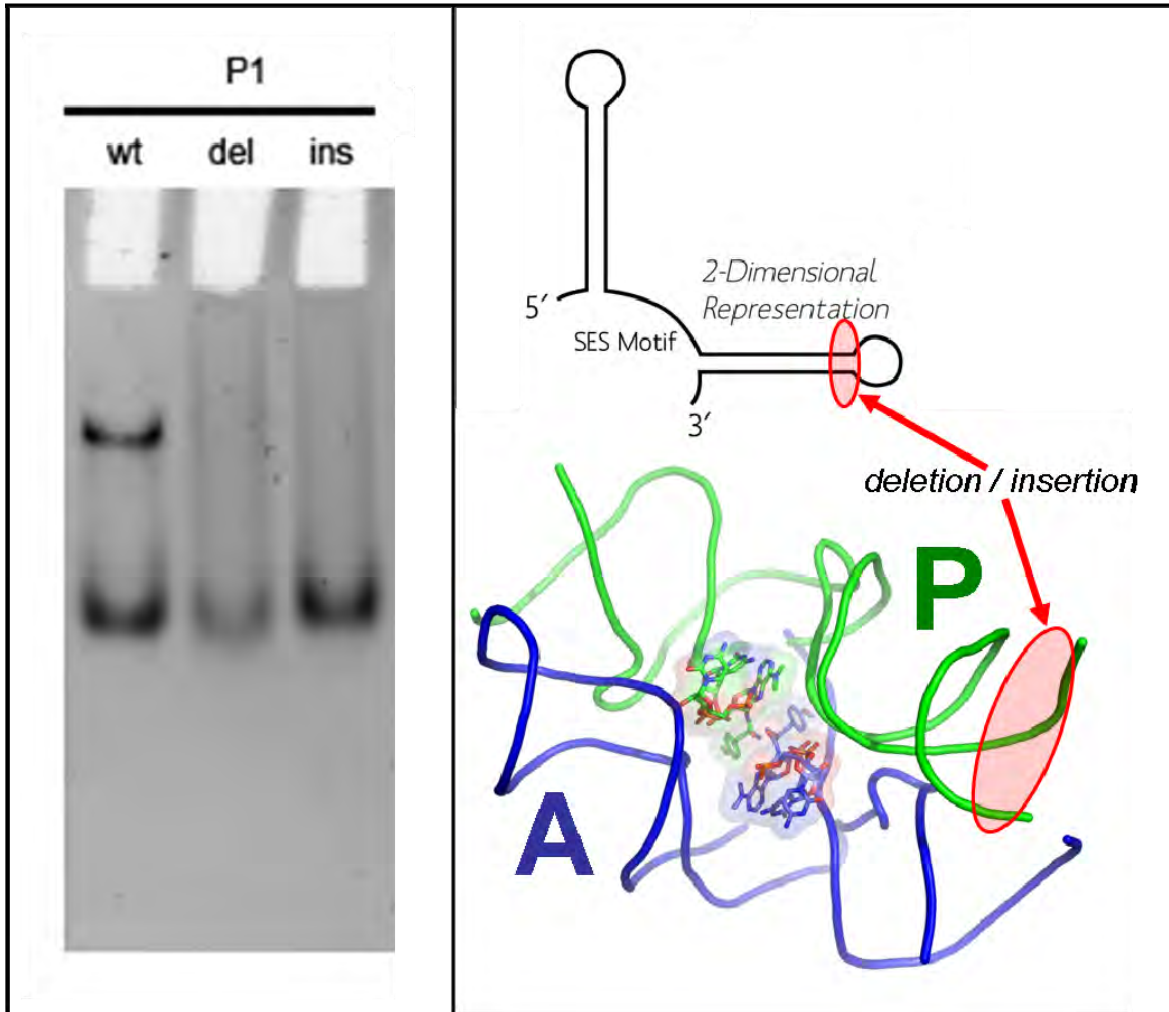
Figure F15 - Dimerization of P1 RNA abolished following either insertion or deletion of two nucleotides designed to form a single base-pair. Right Three-dimensional representation of rRNA at the surroundings of the PTC includes the minimal components within the A-region and the P-region required for the formation of the interface between the two symmetrical regions and the PTC catalytic center (**bottom**) and two-dimensional representation of these constructs, as designed (**top**). Sequences of A1 and P1 RNA were designed based on the sequence of 23S rRNA nucleotides represented here in blue and green, respectively. Coordinates of CCA 3' ends in the PTC are surrounded with transparent surface representation and colored as CPK, with carbon atoms in blue and green for substrates located in the A- and the P-site, respectively. Ellipsoids represent for the location where a single base-pair was either inserted or deleted. **Left panel:** Non-denaturing PAGE for P1 (designated "wt") and the two double

mutants including either base-pair deletion or insertion (designated "del" and "ins", respectively).
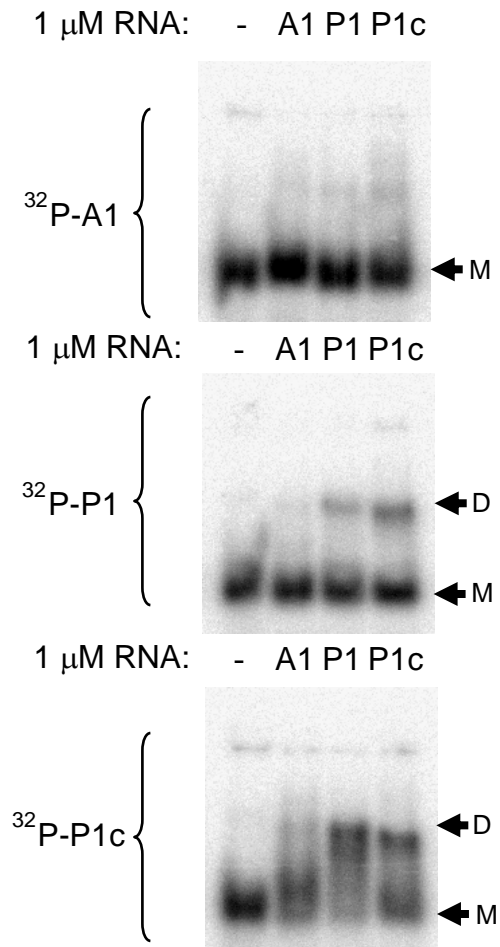
Figure F16 - EMSA for the detection of heterodimerization between A1, P1 and P1c.
Experiments performed as described in methodology above. Non-labeled RNA
concentration in all samples was 1 uM. Non-labeled RNA construct used in each sample
is indicated above each lane and ^{32}P radio-labeled used for each experiment is indicated
at the left of the corresponding gel scan. "D" and "M" are for dimer and monomer,
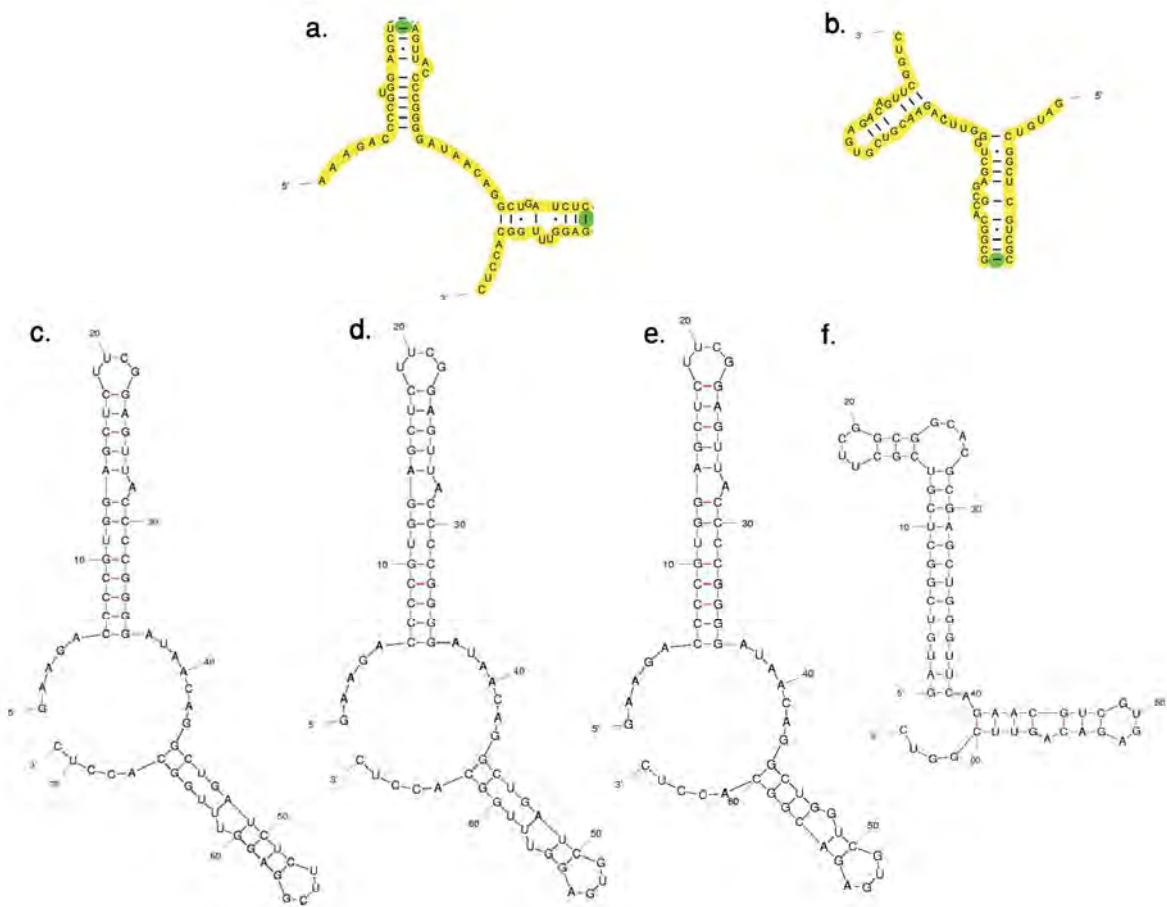respectively.

Figure F17 - Two dimensional structure of RNA constructs P1, P1c and A1 as predicted by mFold. Top: Two dimensional representation of nucleotides sequence within 23S rRNA that were used to design RNA constructs P1, P1c, P1d (**panel a** for all) and A1 (**panel b**). **Bottom:** Two dimensional structures for P1, P1c, P1d and A1, as predicted by mFold, are in **panels c-f**, respectively.
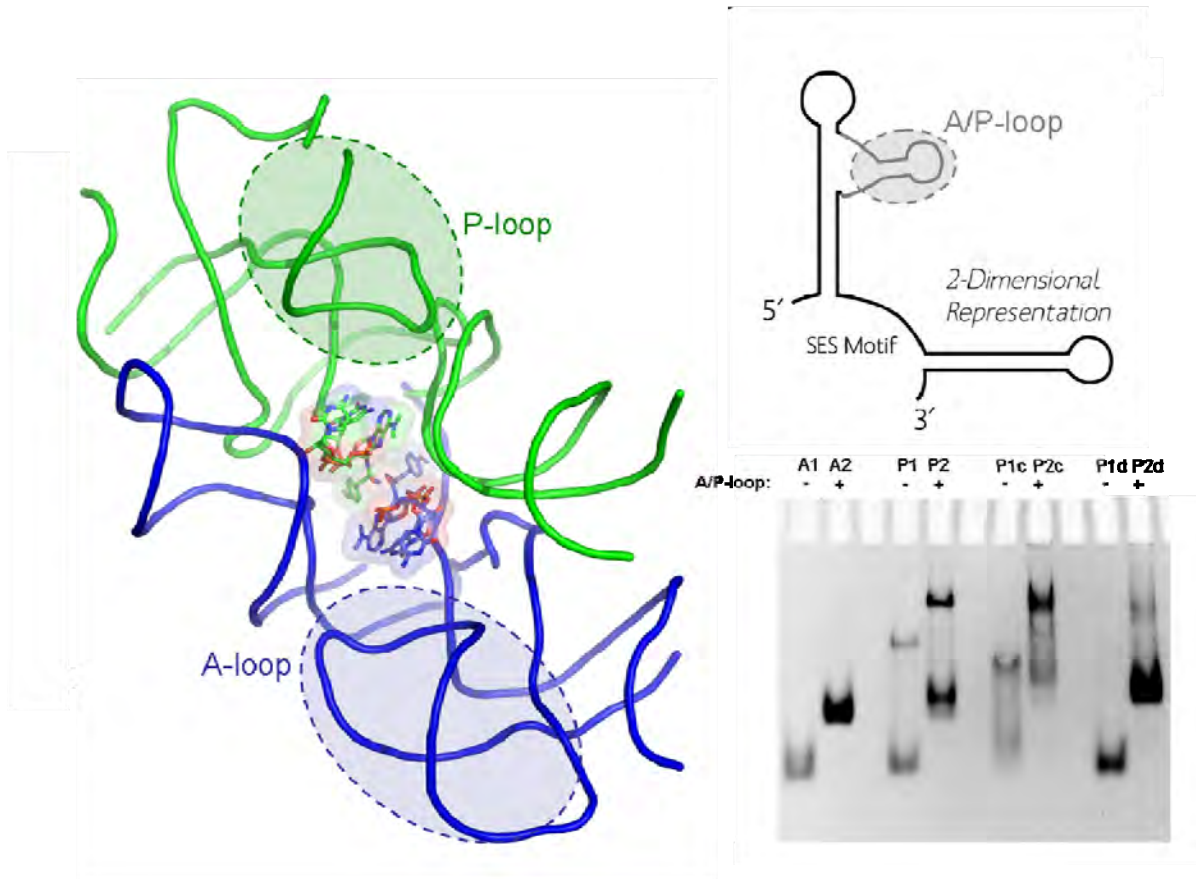
Figure F18 - **Incorporation of the P-loop into P1 and P1c RNA did not prevent dimerization. Left:** Three-dimensional structure of nucleotides from the surroundings of the PTC, as determined within the crystal structure of the large ribosomal subunit of the eubacteria *D. radiodurans*. A-region and P-region are colored blue and green, respectively. Coordinates of CCA 3' ends in the PTC are surrounded with transparent surface representation and colored as CPK, with carbon atoms in blue and green for substrates located in the A- and the P-site, respectively. Blue and green dashed ellipsoids highlight the location of the A- and P-loops, including the helices that carry them respectively. **Top right:** Two-dimensional schematic representation of the RNA constructs A2, P2 P2c and P2d as designed with the location of the A- or P-loops, including the helix carries it, highlighted by dashed gray ellipsoid. **Bottom right:** Non-denaturing PAGE of various RNA constructs, as indicated above each lane, that including ("+") or excluding ("-") the sequences of A- and P-loops and sequences of helices that carry them within the contemporary ribosome.
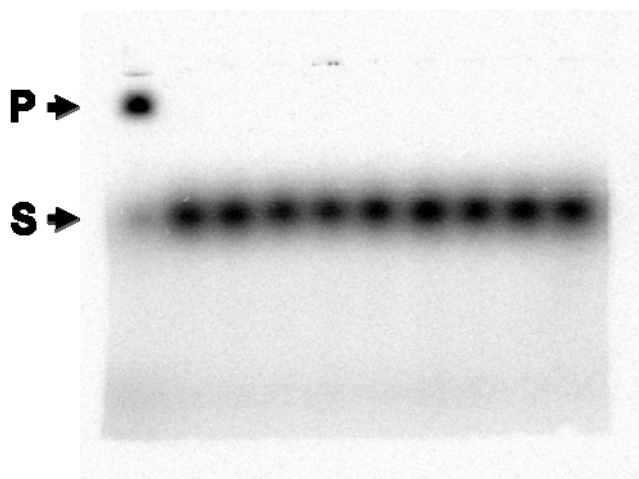
Figure F19 - Gel scan revealing results of a typical peptidyl transferase assay. Fast migrating band carries the unconsumed radiolabeled substrate (marked "S") ^{33}P-CCPmn. Slow migrating band including the streptavidin retarded product (marked "P"), ^{33}P-CCPmn-phenyl alanine-caproic acid-biotin. Product was generated by large ribosomal subunits from *E. coli* that served as a control throughout all experiments.
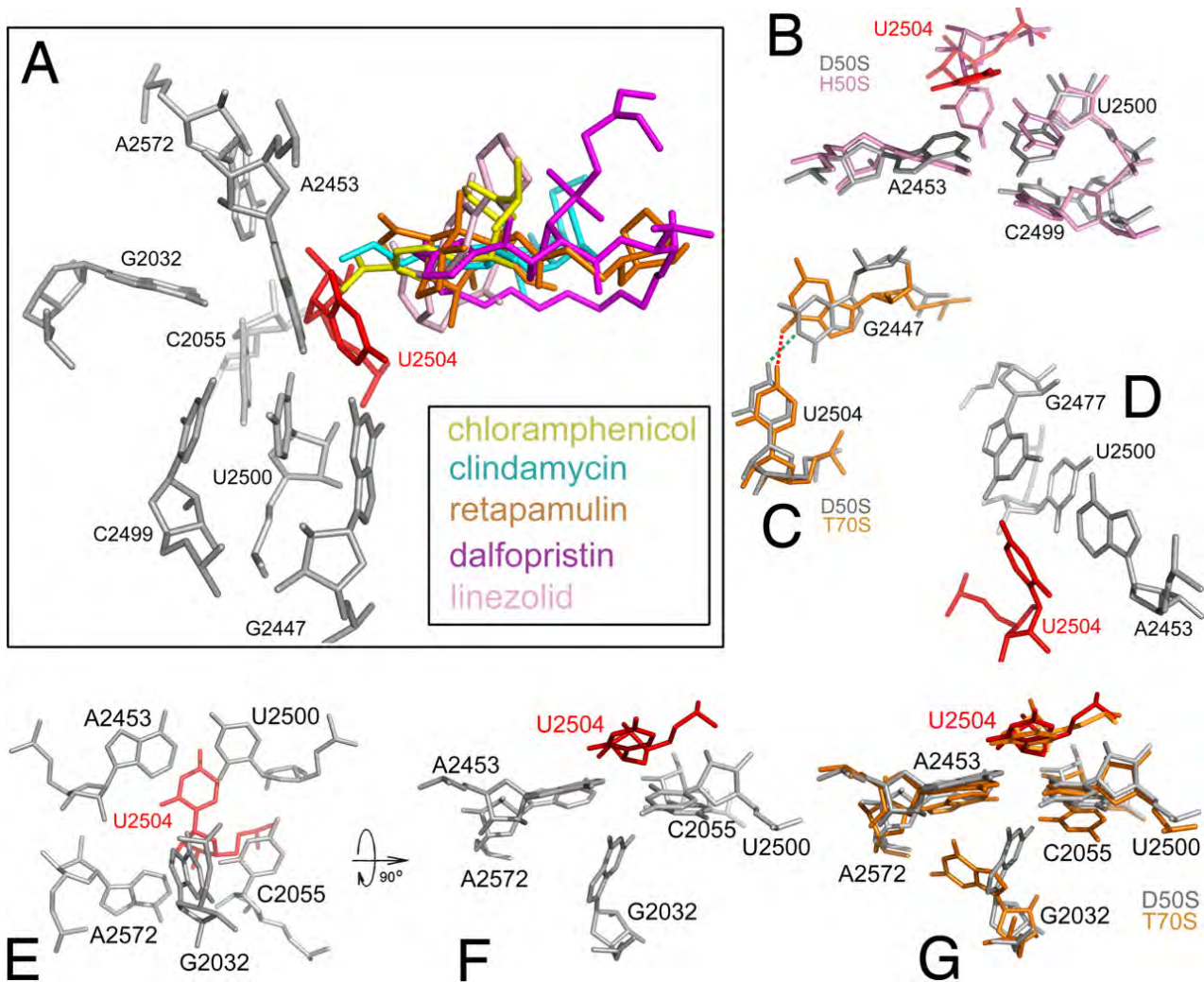
Figure F20 - Remote mutations that affect the conformation and/or the flexibility of U2504 by a network of interactions. Panels A: PTC antibiotics chloramphenicol (yellow), clindamycin (cyan), retapamulin (orange), dalfopristin (magenta) and linezolid (pink) bind in close proximity to U2504 (red). **Panels B–G:** Selected interactions within the networks around U2504. rRNA is gray, pink, or orange for D50S, H50S, or T70S, respectively. Wherever drawn, U2504 of D50S is red. Images of D50S, T70S, and H50S were generated from their coordinates (PDB ID codes 1NKW, 2J01, and 1S72, respectively).
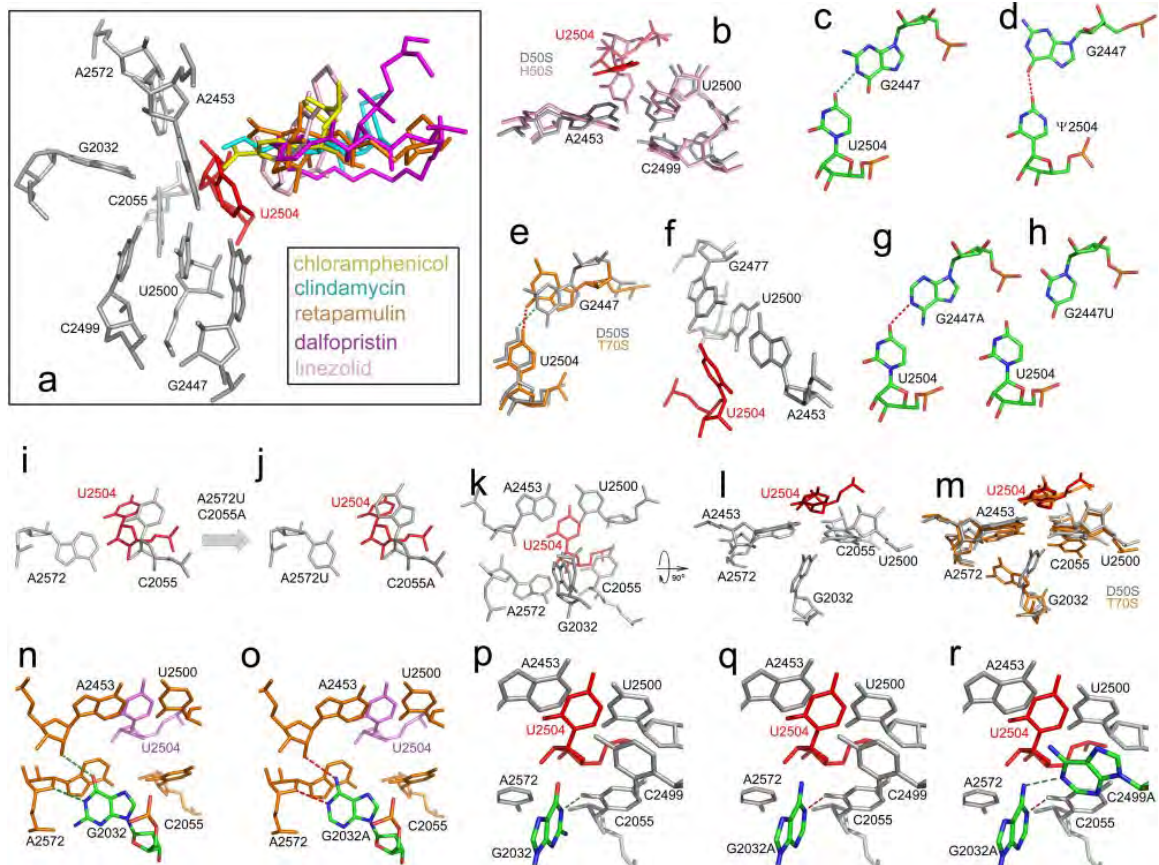
Figure F21 - Remote mutations that affect the conformation and/or the flexibility of U2504 by a network of interactions. Panel a: PTC antibiotics chloramphenicol (yellow), clindamycin (cyan), retapamulin (orange), dalfopristin (magenta), and linezolid (pink) bind in close proximity to U2504 (red). **Panels b–r:** The interactions network around U2504. rRNA is gray, pink, or orange for D50S, H50S, or T70S, respectively. Wherever indicated U2504 is red for D50S or purple for T70S. When applicable, different atoms are colored according to CPK color code to emphasize the chemical differences occurring by the mutagenesis. CPK colored nucleotides in **panels n and o** are of T70S, **panel d** shows E70S nucleotides after in silico modification from U to pseudo uracil at position 2504. All other images colored according to CPK are of D50S. Images of D50S, T70S, E70S, and H50S were generated from their coordinates (PDB ID codes 1NKW, 2J01, 2AWD, and 1S72, respectively).
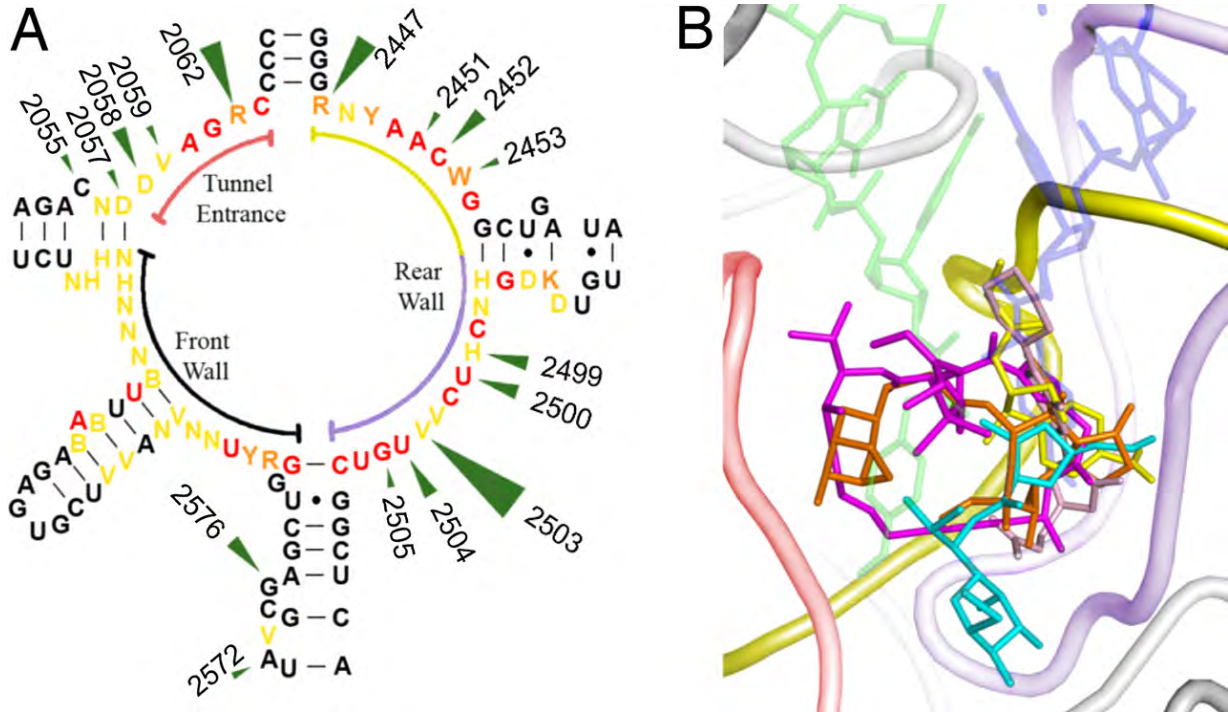
94

Figure F22 - Antibiotics binding pockets within the PTC. Panel A: 2D diagram of the 23S RNA at the vicinity of the PTC. Green arrows indicate nucleotides mediating resistance to PTC antibiotics. Arrow size is proportional to the number of different classes of antibiotics that are being affected. Relations between *E. coli* cell vitality and nucleotide alterations (Sato et al., 2006) are color coded. Absolutely essential nucleotide, which cannot be mutated are shown in red. Nucleotides that can be replaced by a single nucleotide are shown in orange. Nucleotides that can be replaced by 2 or 3 other nucleotides are shown in yellow. Nomenclature for Nucleotide Code Base is according to IUPAC (Cornish-Bowden, 1985). Specific sections of the 2D diagram have colors identical to the colors of their corresponding regions in the 3D structure shown in **panel B**. **Panel B:** The 3-dimensional positions of PTC antibiotics showing their overlapping positions. The antibiotics chloramphenicol, clindamycin, retapamulin, dalfopristin, and linezolid are shown in yellow, cyan, orange, magenta, and pink, respectively. A site tRNA 3′ end and the derived P site tRNA are shown in transparent blue and green, respectively. The 23S rRNA is shown in red, yellow, and blue, as their corresponding sections in the 2D representation (in **panel A**). 23S rRNA segments not shown in **panel A** are colored gray. The black arc in **panel A** is not shown in **panel B** because the latter is shown from the front wall direction.

c
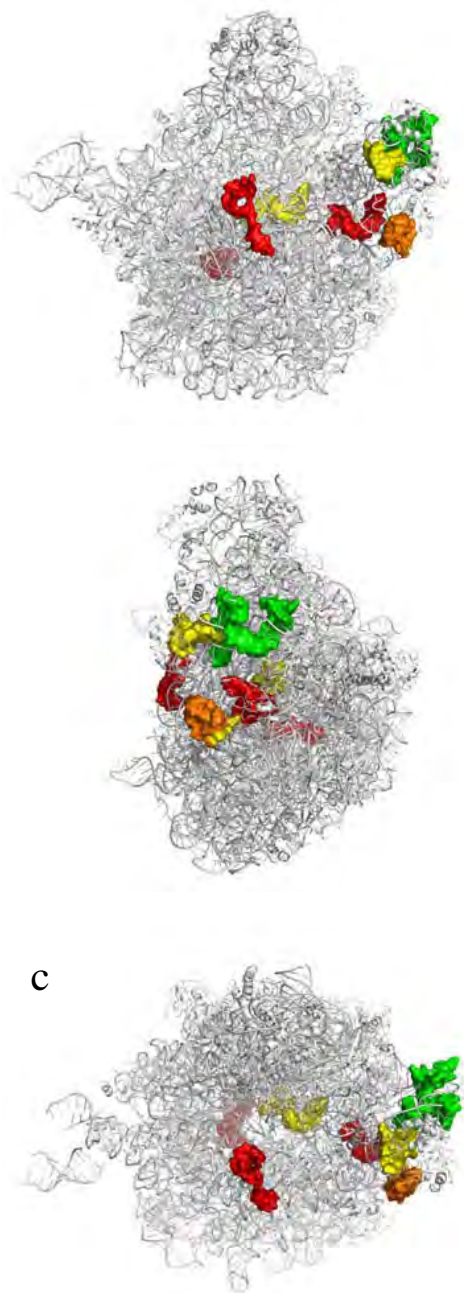
Figure F23: Location of the short target sites on the ribosome and activity of their complimentary ODNs. Target sites are presented as space filling models and are colored according to the IC_{50} of their corresponding ODNs (green: $IC_{50} < 40$ μM, yellow: 40 μM $\leq IC_{50} \leq 80$ μM, red: $IC_{50} > 80$ μM, hybrid colors are representing overlapping target sites). (a) Front ("crown") view, (b) side view and (c) top view.
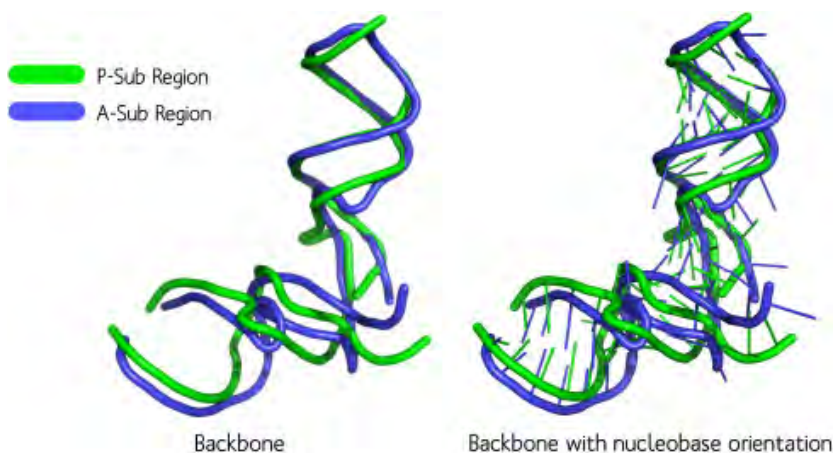
Figure F24 - Superposition of the rRNA in the A- and the P-subregions (in blue and green, respectively). The striking overlap of the backbones of the two subregions, indicating the high level of symmetry, is shown on the left. Deviations from the symmetrical arrangements, indicated by the differences in the orientations of the non base-paired bases of the two subregions, are suggestive of the optimization that each half of the PTC underwent in order to fit the specific task of each site.

Tables

Compound	SB-571519	SB-280080	Retapamulin (SB-275833)
Crystal information			
Space group	I222	I222	I222
a [Å]	170.4	170.5	170.1
b [Å]	405.8	412.7	405.9
c [Å]	703.8	696.7	695.2
Diffraction data statistics			
X-ray source	ID19, SBC/APS	ID19, SBC/APS	ID19, SBC/APS
Wavelength [Å]	1.033201	0.97933757	0.979290
Number of crystals	1	7	9
Crystal oscillation [°]	0.3–0.8	0.3–0.4	0.3–0.5
Resolution [Å]	30–3.50 (3.62–3.50)	30–3.56 (3.69–3.56)	30–3.66 (3.79–3.66)
Unique reflections	284,085	263,433	243,598
Observed reflections	1,400,909	1,541,408	1,973,738
Redundancy	4.9 (4.1)	5.9 (3.2)	8.1 (3.7)
Completeness [%]	92.7 (84.9)	90.7 (70.2)	93.1 (70.0)
$\langle I \rangle / \langle \sigma \rangle$	6.3 (1.5)	7.2 (1.5)	9.1 (1.4)
R-merge [%]	18.4 (79.7)	16.8 (70.2)	19.0 (79.1)
Refinement			
R-factor [%]	27.5	27.6	26.0
R-free (5%) [%]	33.4	33.8	33.4
rmsd bonds [Å]	0.008	0.008	0.008
rmsd angles [°]	1.4	1.4	1.4

Table T1 – Data statistics.

Nucleotide	Appeared clinically [Y/N]	Antibiotic (family)	Bacterial strain	References (full list is following)
2032	N	Chloramphenicol (phenicol)	*E. coli*	[1]
			B. hyodysenteriae	[2]
		Clindamycin (lincosamide)	*E. coli*	[1]
		Linezolid (oxazolidinine)	*E. coli*	[3]
		Tiamulin (pleuromutilin)	*B. hyodysenteriae*	[2]
2055	N	Tiamulin (pleuromutilin)	*B. pilosicoli*	[2]
2057	N	Chloramphenicol (phenicol)	*E. coli*	[1,4]
2058	Y	Chloramphenicol (phenicol)	*E .coli*	[1]
		Clindamycin (lincosamide)	*E. coli*	[1]
2059	N	Virginiamycin M1 and Pristinamycin II (streptogramins A)	*H. halobium*	[5]
2062	Y	Chloramphenicol (phenicol)	*H. halobium*	[6]
		Linezolid (oxazolidinone)	*H. halobium*	[7]
		Pristinamycin II (streptogramins A)	*S. pneumoniae*	[8]
		Pristinamycin I together with pristinamycin II or dalfopristin together with quinupristin (streptogramins A and B)	*S. pneumoniae*	[8]
2447	N	Linezolid (oxazolidinone)	*E. coli*	[3]
			M. smegmatis	[9]
		Tiamulin (pleuromutilin)	*B. hyodysenteriae*	[2]
			E. coli	[10]
		Chloramphenicol (phenicol)	*E. coli* and *B. stearothermophilus*	[11]
2451	N	Chloramphenicol (phenicol)	*E. coli* and *B. stearothermophilus*	[11]
2452	N	Chloramphenicol (phenicol)	*H. halobium*	[6]
		Linezolid (oxazolidinone)	*H. halobium*	[7]
2453	N	Linezolid (oxazolidinone)	*H. halobium*	[7]
2499	N	Linezolid (oxazolidinone)	*H. halobium*	[7]
		Tiamulin (pleuromutilin)	*B. hyodysenteriae*	[2]
2500	Y	Linezolid (oxazolidinone)	*S. aureus* (MRSA)	[12]
			H. halobium	[7]
			E. coli	[10]
		Tiamulin (pleuromutilin)	*E. coli*	[10]
2503	Y	Chloramphenicol and florfenicol (phenicols)	*E. coli*	[13]
			S. aureus and *E. coli*	[14,15]
			S. aureus	[16]
		Clindamycin (lincosamide)	*S. aureus* and *E. coli*	[14,15]
			S. aureus	[16]
		Linezolid (oxazolidinones)	*S. aureus* and *E. coli*	[14,15]
			S. aureus	[16]
		Tiamulin and Valnemulin (pleuromutilins)	*S. aureus* and *E. coli*	[14,15]
		virginamycin M$_1$ (streptogramins A) and	*S. aureus* and *E. coli*	[14,15]
		dalfopristin/quinupristin (streptogramins A and B)	*H. halobium*	[5]

2504	N	Linezolid (oxazolidinone)	*H. halobium*	[7]
		Tiamulin (pleuromutilin)	*Brachyspira pilosicoli*	[2]
			B. hyodysenteriae	[2]
2505	N	Linezolid (oxazolidinone)	*Enterococcus*	[17]
			E. faecalis	[18]
2572	N	Tiamulin (pleuromutilin)	*B. hyodysenteriae*	[2]
2576	Y	Linezolid (oxazolidinone)	*Enterococcus*	[17]
			Enterococcus	[19]
			S. aureus	[20]
			E. faecium	[21]
			S. aureus	[22]
			S. aureus	[23]
			E. faecium	[24]
		Tiamulin (pleuromutilin)	*S. aureus*	[10]

Table T2 – Resistance determinants in the PTC. Nucleotides are according to *E. coli* numbering system, references for this table are following below.

References for table T2:

1.   Douthwaite, S., Functional interactions within 23S rRNA involving the peptidyltransferase center. J Bacteriol, 1992. 174(4): p. 1333-8.

2.   Pringle, M., et al., Mutations in ribosomal protein L3 and 23S ribosomal RNA at the peptidyl transferase centre are associated with reduced susceptibility to tiamulin in Brachyspira spp. isolates. Mol Microbiol, 2004. 54(5): p. 1295-306.

3.   Xiong, L., et al., Oxazolidinone resistance mutations in 23S rRNA of Escherichia coli reveal the central region of domain V as the primary site of drug action. J Bacteriol, 2000. 182(19): p. 5325-31.

4.   Ettayebi, M., S.M. Prasad, and E.A. Morgan, Chloramphenicol-erythromycin resistance mutations in a 23S rRNA gene of Escherichia coli. J Bacteriol, 1985. 162(2): p. 551-7.

5.   Porse, B.T. and R.A. Garrett, Sites of interaction of streptogramin A and B antibiotics in the peptidyl transferase loop of 23 S rRNA and the synergism of their inhibitory mechanisms. J Mol Biol, 1999. 286(2): p. 375-87.

6.   Mankin, A.S. and R.A. Garrett, Chloramphenicol resistance mutations in the single 23S rRNA gene of the archaeon Halobacterium halobium. J Bacteriol, 1991. 173(11): p. 3559-63.

7.   Kloss, P., et al., Resistance mutations in 23 S rRNA identify the site of action of the protein synthesis inhibitor linezolid in the ribosomal peptidyl transferase center. J Mol Biol, 1999. 294(1): p. 93-101.

8.   Depardieu, F. and P. Courvalin, Mutation in 23S rRNA responsible for resistance to 16-membered macrolides and streptogramins in Streptococcus pneumoniae. Antimicrob Agents Chemother, 2001. 45(1): p. 319-23.

9.   Sander, P., et al., Ribosomal and non-ribosomal resistance to oxazolidinones: species-specific idiosyncrasy of ribosomal alterations. Mol Microbiol, 2002. 46(5): p. 1295-304.

10.   Miller, K., et al., Linezolid and tiamulin cross-resistance in Staphylococcus aureus mediated by point mutations in the peptidyl transferase center. Antimicrob Agents Chemother, 2008. 52(5): p. 1737-42.

11.   Thompson, J., et al., Analysis of mutations at residues A2451 and G2447 of 23S rRNA in the peptidyltransferase active site of the 50S ribosomal subunit. Proc Natl Acad Sci U S A, 2001. 98(16): p. 9002-7.

12.   Meka, V.G., et al., Linezolid resistance in sequential Staphylococcus aureus isolates associated with a T2500A mutation in the 23S rRNA gene and loss of a single copy of rRNA. J Infect Dis, 2004. 190(2): p. 311-7.

13.   Vester, B. and R.A. Garrett, The importance of highly conserved nucleotides in the binding region of chloramphenicol at the peptidyl transfer centre of Escherichia coli 23S ribosomal RNA. Embo J, 1988. 7(11): p. 3577-87.

14.   Long, K.S., et al., The Cfr rRNA methyltransferase confers resistance to Phenicols, Lincosamides, Oxazolidinones, Pleuromutilins, and Streptogramin A antibiotics. Antimicrob Agents Chemother, 2006. 50(7): p. 2500-5.

15.   Kehrenberg, C., et al., A new mechanism for chloramphenicol, florfenicol and clindamycin resistance: methylation of 23S ribosomal RNA at A2503. Mol Microbiol, 2005. 57(4): p. 1064-73.

16.   Toh, S.M., et al., Acquisition of a natural resistance gene renders a clinical strain of methicillin-resistant Staphylococcus aureus resistant to the synthetic antibiotic linezolid. Mol Microbiol, 2007. 64(6): p. 1506-14.

17.   Prystowsky, J., et al., Resistance to linezolid: characterization of mutations in rRNA and comparison of their occurrences in vancomycin-resistant enterococci. Antimicrob Agents Chemother, 2001. 45(7): p. 2154-6.

18.   Lobritz, M., et al., Recombination proficiency influences frequency and locus of mutational resistance to linezolid in Enterococcus faecalis. Antimicrob Agents Chemother, 2003. 47(10): p. 3318-20.

19.   Auckland, C., et al., Linezolid-resistant enterococci: report of the first isolates in the United Kingdom. J Antimicrob Chemother, 2002. 50(5): p. 743-6.

20.   Wilson, P., et al., Linezolid resistance in clinical isolates of Staphylococcus aureus. J Antimicrob Chemother, 2003. 51(1): p. 186-8.

21.   Rahim, S., et al., Linezolid-resistant, vancomycin-resistant Enterococcus faecium infection in patients without prior exposure to linezolid. Clin Infect Dis, 2003. 36(11): p. E146-8.

22.   Pillai, S.K., et al., Linezolid resistance in Staphylococcus aureus: characterization and stability of resistant phenotype. J Infect Dis, 2002. 186(11): p. 1603-7.

23.   Tsiodras, S., et al., Linezolid resistance in a clinical isolate of Staphylococcus aureus. Lancet, 2001. 358(9277): p. 207-8.

24.   Herrero, I.A., N.C. Issa, and R. Patel, Nosocomial spread of linezolid-resistant, vancomycin-resistant Enterococcus faecium. N Engl J Med, 2002. 346(11): p. 867-9.

Compound	K_d [nM]
SB-275833 (retapamulin)	2.0 ± 0.05
SB-280080	7.5 ± 1.4
SB-571519	11.1 ± 3.2

Table T3 - Affinities of pleuromutilin derivatives in binding to *E. coli* ribosomes.

Values are results ± standard error from two independent experiments.

ODN	IC50 [μM]	n
463-10	148 ± 32	3
570-17	33 ± 0	2
713-17	21 ± 6	4
817-20	41 ± 10	4
1042-14	24 ± 4	3
1067-22	47 ± 10	3
1064-15	46 ± 12	4
1064-12	56 ± 11	4
1082-15	75 ± 25	4
1082-12	18 ± 4	4
1655-17	57 ± 13	3
1681-15	28 ± 6	2
1909-18	46 ± n.a.	1
1923-12	116 ± 47	4
1989-17	11 ± 2	2
2306-15	113 ± 29	4
2444-14	54 ± 26	4
2515-14	94 ± 27	4
2653-15	40 ± 3	3
2654-13	50 ± 14	4
2655-11	94 ± 11	3

Table T4 - IC$_{50}$ of the various ODNs. IC$_{50}$ assayed based on the activity of *E. coli* (BL21(DE3) strain, Stratagene) cell-free transcription translation system in the presence of ODNs, with firefly luciferease as reporter. Standard deviation was derived based on the number of independent experiments as indicated on the right column.

Name	Sequence
A1	GAUGUCGGCUCGUCGCUUCGGCGGCACGCGAGCUGGGGUUCAGAACGUCGUGAGACAGUUCGGUC
A2	GAUGUCGGCUCGUCGCAUCCUUCGGGUUGGGCUGUUCGCCCAUUAAAGCGGCACGCGAGCUGGGUUCAGAACGUCGUGAGACAGUUCGGUC
AP1	GAAGACCCCGUGGAGCUCUUCGGAGUUACCCCGGGGAUAACAGGCUGAUCUCUUCGGAGGUUUGGCACCUCGAUGUCGGCUCGUCGCUUCGGCGGCACGCGAGCUGGGUUCAGAACGUCGUGAGACAGUUCGGUC
AP2	GAAGACCCCGUGGAGCUUUACUCUUCGGAGUUUGACUGGGGCGGUCCGGAUAAAAGUUACCCCGGGGAUAACAGGCUGAUCUCUUCGGAGGUUUGGCACCUCGAUGUCGGCUCGUCGCAUCCUUCGGGUUGGGCUGUUCGCCCAUUAAAGCGGCACGCGAGCUGGGUUCAGAACGUCGUGAGACAGUUCGGUC
P1	GAAGACCCCGUGGAGCUCUUCGGAGUUACCCCGGGGAUAACAGGCUGAUCUCUUCGGAGGUUUGGCACCUC
P1.del	GAAGACCCCGUGGAGCUCUUCGGAGUUACCCCGGGGAUAACAGGCUGAUCCUUCGGGGUUUGGCACCUC
P1.ins	GAAGACCCCGUGGAGCUCUUCGGAGUUACCCCGGGGAUAACAGGCUGAUCUGCUUCGGCAGGUUUGGCACCUC
P1c	GAAGACCCCGUGGAGCUCUUCGGAGUUACCCCGGGGAUAACAGGCUGAUCGUGAGGUUUGGCACCUC
P1c.G53U	GAAGACCCCGUGGAGCUCUUCGGAGUUACCCCGGGGAUAACAGGCUGAUCGUUAGGUUUGGCACCUC
P1d	GAAGACCCCGUGGAGCUCUUCGGAGUUACCCCGGGGAUAACAGGCUGGUCGUGAGACGGCACCUC
P2	GAAGACCCCGUGGAGCUUUACUCUUCGGAGUUUGACUGGGGCGGUCCGGAUAAAAGUUACCCCGGGGAUAACAGGCUGAUCUCUUCGGAGGUUUGGCACCUC
P2c	GAAGACCCCGUGGAGCUUUACUCUUCGGAGUUUGACUGGGGCGGUCCGGAUAAAAGUUACCCCGGGGAUAACAGGCUGAUCGUGAGGUUUGGCACCUC
P2d	GAAGACCCCGUGGAGCUUUACUCUUCGGAGUUUGACUGGGGCGGUCCGGAUAAAAGUUACCCCGGGGAUAACAGGCUGGUCGUGAGACGGCACCUC

Table T5 - RNA sequences. Construct names appear as referred within the text and figures.

Parameter	regression coefficient	units	p-value
Average base-to-base distance (see text)	-61.2817 ± 13.4477	Å/base	0.001372
Sequence conservation (mean Rseq)	-154.5816 ± 43.5188	$base^{-1}$	0.006196
Duplex formation energy	6.9786 ± 2.3291	[kcal/mol]	0.015047
Target structure energy	-0.035185 ± 0.01048	[kcal/mol]	0.008425
Intercept estimate	899.7343	μM	

Table T6 - Multiple linear regression model for the prediction of IC$_{50}$ values of short ODNs (10 ≤ length ≤ 15). The Model is based on all ODNs with length ≤ 15 (n=14). Presented are regression coefficients and their standard error, as well as p-values for testing whether a given regression coefficient is equal to zero. Overall p-value for the model is 0.011445.

Plots
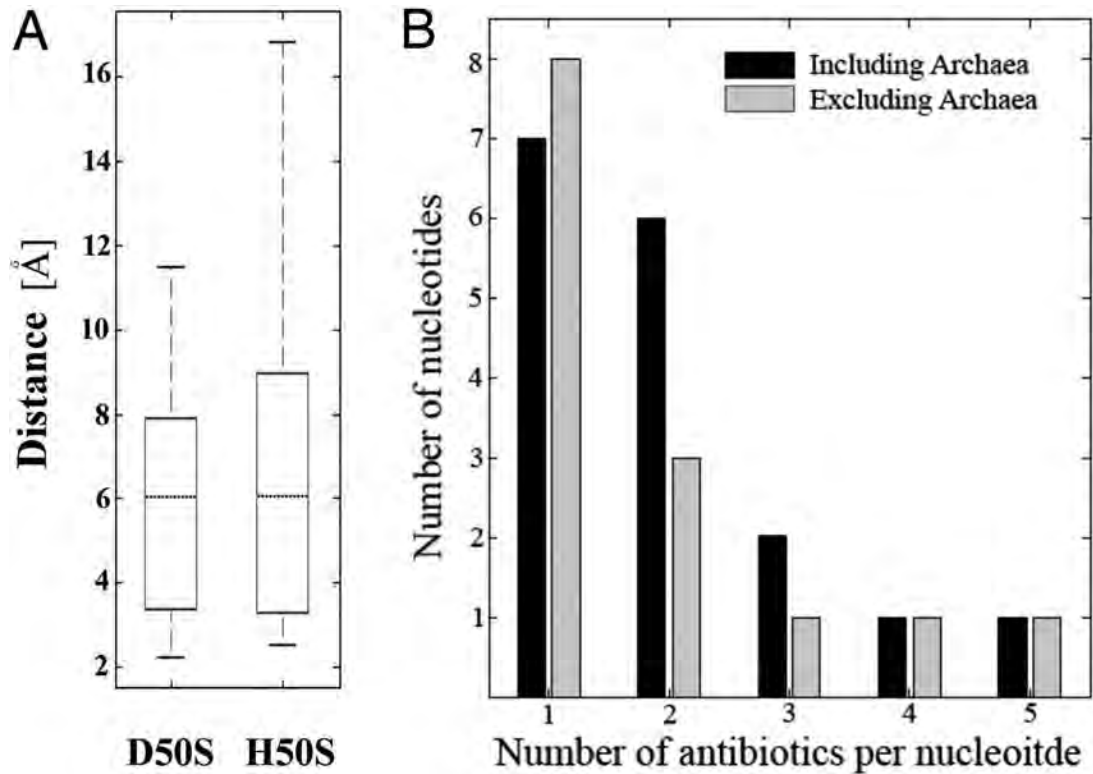
Plot P1 - Overlaps of resistance determinants and distances between antibiotics binding sites and nucleotides mediating resistance. (A) Boxplot representation of nucleotide-antibiotic distances determined for D50S and H50S complexes. Dotted lines show medians; the upper and lower horizontal lines of the boxes stand for upper and lower quartiles (namely cutoffs for 25% and 75% of the data). Top and bottom external horizontal lines show the maximal and minimal values. (B) Resistant mutations or methylations observed in bacterial strains including (black bars) or excluding (gray bars) archaea. x axis indicates the number of different classes of antibiotics that are being affected. y axis stands for the number of nucleotides characterized for this observation.
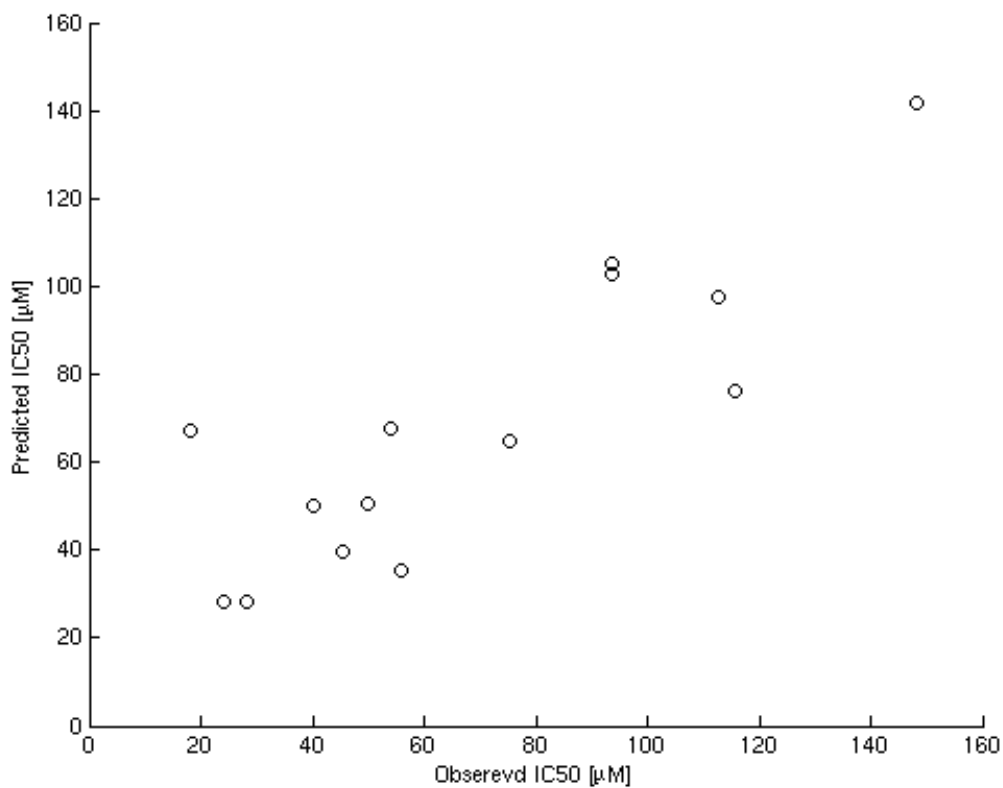
Plot P2 - Predicted vs. Observed IC50 values. Predicted values were calculated according to the multiple linear regression model suggested in **table T6**. Observed values are as presented in **table T4**.